LBL-34894
UC-331

Lawrence Berkeley Laboratory

UNIVERSITY OF CALIFORNIA

ENERGY & ENVIRONMENT DIVISION

Methanol Electrooxidation on Well-Characterized Pt-Ru Alloys

H.A. Gasteiger,* P.N. Ross, Jr., and E.J. Cairns
*(Ph.D. Thesis)

November 1993

ENERGY & ENVIRONMENT DIVISION

REFERENCE COPY
Does Not
Circulate
Bldg. 50 Library.
LBL-34894
Copy 1

Prepared for the U.S. Department of Energy under Contract Number DE-AC03-76SF00098

DISCLAIMER

This document was prepared as an account of work sponsored by the United States Government. While this document is believed to contain correct information, neither the United States Government nor any agency thereof, nor The Regents of the University of California, nor any of their employees, makes any warranty, express or implied, or assumes any legal responsibility for the accuracy, completeness, or usefulness of any information, apparatus, product, or process disclosed, or represents that its use would not infringe privately owned rights. Reference herein to any specific commercial product, process, or service by its trade name, trademark, manufacturer, or otherwise, does not necessarily constitute or imply its endorsement, recommendation, or favoring by the United States Government or any agency thereof, or The Regents of the University of California. The views and opinions of authors expressed herein do not necessarily state or reflect those of the United States Government or any agency thereof, or The Regents of the University of California.

Available to DOE and DOE Contractors
from the Office of Scientific and Technical Information
P.O. Box 62, Oak Ridge, TN 37831
Prices available from (615) 576-8401

Available to the public from the
National Technical Information Service
U.S. Department of Commerce
5285 Port Royal Road, Springfield, VA 22161

Lawrence Berkeley Laboratory is an equal opportunity employer.

DISCLAIMER

This document was prepared as an account of work sponsored by the United States Government. While this document is believed to contain correct information, neither the United States Government nor any agency thereof, nor the Regents of the University of California, nor any of their employees, makes any warranty, express or implied, or assumes any legal responsibility for the accuracy, completeness, or usefulness of any information, apparatus, product, or process disclosed, or represents that its use would not infringe privately owned rights. Reference herein to any specific commercial product, process, or service by its trade name, trademark, manufacturer, or otherwise, does not necessarily constitute or imply its endorsement, recommendation, or favoring by the United States Government or any agency thereof, or the Regents of the University of California. The views and opinions of authors expressed herein do not necessarily state or reflect those of the United States Government or any agency thereof or the Regents of the University of California.

LBL-34894

METHANOL ELECTROOXIDATION ON WELL-CHARACTERIZED Pt-Ru ALLOYS

by

Hubert A. Gasteiger, Philip N. Ross, Jr. and Elton J. Cairns

Energy & Environment Division
Lawrence Berkeley Laboratory
University of California
Berkeley, California 94720

November 1993

This work was supported by the Assistant Secretary for Energy Efficiency and Renewable Energy, Office of Transportation Technologies, Electric and Hybrid Propulsion Division of the U.S. Department of Energy under Contract No. DE-AC03-76SF00098.

recycled paper

Abstract

Methanol Electrooxidation on Well-Characterized Pt-Ru Alloys

by

Hubert Andreas Gasteiger

Doctor of Philosophy in Chemical Engineering

University of California at Berkeley

Professor Elton J. Cairns, Chair

The electrooxidation of methanol in sulfuric acid electrolyte on well-characterized Pt-Ru alloy electrodes was studied over a temperature range from 25 to 60°C. The functionality between bulk and surface composition of annealed and sputter-cleaned alloy electrodes was determined definitively in ultra high vacuum (UHV) *via* low energy ion scattering (LEIS) and Auger electron spectroscopy (AES). Equilibrated, *i.e.* annealed, alloy surfaces were strongly enriched in platinum consistent with ideal solution thermodynamics, whereas the non-equilibrium process of sputtering produced surfaces which closely resembled the bulk structure of the alloys.

The rate-limiting step in the electrooxidation of methanol on sputter-cleaned Pt-Ru electrodes at 25°C was shown to be the initial adsorption/dehydrogenation of methanol on Pt surface atom ensembles, resulting in an optimum Ru surface composition of 10 atomic%; conversely, Ru-rich surfaces poison the methanol oxidation reaction since Ru

is inactive towards the dissociative adsorption of methanol. However, the nucleation of oxygen-containing species on bare Ru atoms at low electrode potentials promotes the oxidative removal of methanol dehydrogenation fragments, thereby preventing the long-term deactivation of Pt-Ru electrodes. This bifunctional character of Pt-Ru alloys was verified in measurements on their electrocatalytic activity towards the electrooxidation of CO: the nucleation of oxygen-containing species on Ru surface atoms significantly enhanced the oxidation of adsorbed CO, producing a catalytic shift of 0.25 V for an alloy with the optimum Ru surface composition of ≈50 atomic%. The same optimum Ru surface composition was observed in the electrooxidation of formic acid, which similar to CO interacts with both Pt and Ru surface atoms.

For the methanol electrooxidation reaction it was found that the activity of Ru towards the dissociative adsorption of methanol is a strong function of temperature. This change in the adsorptive nature of the Ru sites with temperature produced a variation in the optimum surface composition with temperature, from ≈7 at 25°C to ≈33 atomic% at 60°C. The shift in optimum composition with temperature was attributed to a shift in the rate-determining step from methanol adsorption/dehydrogenation at room temperature to the surface reaction between the dehydrogenated intermediate and surface oxygen at 60°C.

Table of Contents

Table of Contents i

List of Figures iv

List of Tables vi

Acknowledgements vii

Introduction 1
1. Background 1
2. Objectives 4

Chapter 1: UHV Characterization of Pt-Ru Alloys 7
1. Introduction 7
2. Experimental Procedures 9
2.1. Pt-Ru Alloy Preparation 9
2.2. UHV Measurements 9
3. Results 13
3.1. LEIS Measurements 13
3.2. AES Measurements 23
4. Discussion 29
4.1. Comparison with Literature Data 29
4.2 Thermodynamic Equilibrium Model 31
5. Conclusions 36

Chapter 2: CH_3OH Oxidation on Pt-Ru Alloys at 25°C 37
1. Introduction 37
2. Experimental Procedures 40
2.1. Electrochemical Measurements 40
2.2. Sample Transfer Test 43
3. Results 44
3.1. UHV Characterization 44
3.2. Electrochemical Measurements 46
4. Discussion 58
4.1. Accumulated Surface "Poisons" 60
4.2. UHV *vs* Electrochemistry on Pt and Ru 61
4.3. Formulation of a Major Reaction Pathway 62

4.4. Characteristics of Pt-Ru Alloys 64
4.5. Statistical Interpretation of Bifunctional Pt-Ru Electrodes 65
5. Conclusions 71

Chapter 3: CO Oxidation on Pt-Ru Alloys at 25°C 72
1. Introduction 72
2. Experimental Procedures 75
2.1. Electrochemical Measurements 75
2.2. Sample Transfer Test from CO- to Stripping-Cell 77
3. Results 79
3.1. CO Stripping Voltammetry on Pt and Ru 79
3.2. CO Stripping Voltammetry on Pt-Ru Alloys 82
3.3. Potentiostatic Oxidation of Adsorbed CO 87
3.4. CO Oxidation on Sputtered *vs* Annealed Pt-Ru Electrodes 93
4. Discussion 94
4.1. CO Electooxidation on Pt-Ru Alloys 95
4.2. Gas Phase Oxidation of CO on Pt and Ru 98
4.3. Origin of the Synergistic Behavior of Pt-Ru in CO Electrooxidation 100
4.4. Comparison of Methanol and CO Oxidation on Pt-Ru Alloys 101
5. Conclusions 102

Chapter 4: HCOOH Oxidation on Pt-Ru Alloys at 25°C 104
1. Introduction 104
2. Experimental Procedures 105
3. Results 105
3.1. Potentiodynamic Experiments 105
3.2. Potentiostatic Experiments 112
4. Discussion 116
4.1. Pure Pt and Ru Electrodes 116
4.2. Pt-Ru Alloys 119
5. Conclusions 122

Chapter 5: CH_3OH Oxidation at Elevated Temperatures 124
1. Introduction 124
2. Experimental Procedures 126
3. Results 128
3.1. CH_3OH Electrooxidation at 25°C 128
3.2. CH_3OH Electrooxidation at Elevated Temperatures 130
4. Discussion 141
4.1. Formulation of the Reaction Pathway on Pt-Ru Alloy Surfaces 142
4.2. Interpretation of Activity Data 144
4.3. Interpretation of Activation Energies 147
4.4. Comparison With Fuel Cell Electrodes and Performance Projections 150
5. Conclusions 151

Conclusions 153

References 157

List of Figures

Figure 1-1. UHV chamber and system electronics. 11

Figure 1-2. UHV chamber with surface analysis tools 12

Figure 1-3. $^4He^+$ LEIS on pure Pt and pure Ru. 15

Figure 1-4. $^4He^+$ LEIS on a Pt-Ru alloy. 16

Figure 1-5. Surface composition of sputtered Pt-Ru alloys 18

Figure 1-6. Equilibration time for Pt segregation at 800°C 21

Figure 1-7. Surface composition of annealed Pt-Ru alloys 22

Figure 1-8. Pt-Ru phase diagram 23

Figure 1-9. AES spectra of Pt-Ru alloys 24

Figure 1-10. Second-layer composition from AES 28

Figure 2-1. UHV sample holder with sample protected by water 41

Figure 2-2. Meniscus between sample surface and electrolyte 42

Figure 2-3. Transfer test of a UHV-cleaned Pt electrode 44

Figure 2-4. Surface composition of sputtered and annealed alloys 45

Figure 2-5. Cyclic voltammetry of Pt, Ru and Pt-Ru in H_2SO_4 47

Figure 2-6. Cyclic voltammetry of Pt in CH_3OH 50

Figure 2-7. Cyclic voltammetry of Ru in CH_3OH 51

Figure 2-8. Cyclic voltammetry of Pt-Ru alloys in CH_3OH 52

Figure 2-9. Potentiodynamic activities of Pt and Pt-Ru alloys 55

Figure 2-10. Potentiostatic CH_3OH oxidation at 0.5 V 57

Figure 5-7. Arrhenius plot at 0.4 V for various $x_{Ru,s}$ 141

Figure 5-8. Short-time methanol oxidation currents..... 144

Figure 5-9. CO stripping voltammetry on surfaces with ≈7 and ≈33 atomic% Ru 149

List of Tables

Table 1-1. Composition and crystal structure of Pt-Ru samples 10

Table 1-2. LEIS sensitivity factors for Pt and Ru 17

Table 1-3. Surface composition data for sputtered Pt-Ru alloys 19

Table 1-4. Surface composition data for annealed Pt-Ru alloys 20

Table 1-5. Molar surface areas of low-index Pt and Ru faces 34

Table 2-1. Relative CH_3OH oxidation currents on Pt and Pt-Ru alloys 58

Acknowledgements

According to a good friend of mine, it is said that good research never goes on in a vacuum. And while, to a large extent, my data were collected in a vacuum, I am grateful to acknowledge here that I never found myself working in one. Quite the contrary: my professors, colleagues and friends at the Lawrence Berkeley Laboratory and the University guided and encouraged my every step along this bumpy trail towards a Ph.D.

Professor Elton Cairns has been patient with me since my arrival at Berkeley in January 1989, and generously entrusted me with freedom to develop my own ideas while guiding me through the long sequence of years, many of which I have spent in the laboratory of Phil Ross. Phil assisted me in getting my "feet wet" in surface science and was constantly available to share the up and downs of my research; he was an invaluable teacher who accompanied me along its avenues with both his enthusiasm and his professional expertise. Facing the daily technical obstacles so common in ultra high vacuum technology would have been impossible without the knowledgeable help of Lee Johnson, with whom it was even fun to take apart the most intricate instruments, while Bob Wright initiated me into the miraculous procedure of tightening copper gaskets and finally convinced me that epoxy is not compatible with good UHV practice. Troubleshooting of flaws with the electronic instrumentation was never much trouble thanks to Jim Severns, whom I could always bribe with a cup of coffee into coming over to the lab at 8 am, given, of course, that he was not on a cruise. The other kind of "electronic" problems, *viz.* the crashing of computer programs as well as other computer related nightmares would always be solved easily by calling Jim Rudnicki, without whom

this thesis would certainly not have been printed in time for the final deadline. Throughout my stay at the Lawrence Berkeley Laboratory I have not had to deal with any of the generally encountered administrative hurdles set up by the lab, for which I have to thank Susan Lauer, Frank McLarnon, Kim Kinoshita and Garth Burns, although Garth refused to invest his tax-dollars in my thesis paper.

In spite of all the professional help I received from my colleagues above, the long journey to earn a Ph.D. is inconceivable without the support I have had from my friends at Berkeley. Aldean Wingfield kept me awake during many days by dragging me out from my office for a cigarette break, Kathryn Striebel and Jeff Weaver showed me the beautiful jogging trails and bicycle routes around Berkeley, and Ian Tidswell skillfully organized many trips to rainy Hawaii and snowy Yosemite. My house mate Martin Strell helped me to survive the long nights in the laboratory by providing freshly baked bread in the early morning hours, whereas my old friend David Engel taught me how to indulge in cigars and Cognac, while we commiserated on his Heraklites studies and the failure of my early experimental work; also, without Dave's help I would have missed many of the deadlines imposed by the Graduate Division. "Mon amie" Gessie Brisard, my soul-mate and companion in the opera and the symphony, never failed to patiently listen to both my happy tidings and my grouchy complaints.

Last, but certainly not least, there are Nenad Marković and his wife Mila. Nenad was my mentor in every aspect of life over the past few years and there is not much in my work which I have not learned from him. His enthusiasm for research in general was very inspiring, although it made me do much more work than would have been necessary. The friendship of Nenad and Mila, who often fed me, as well as the unrestricted support I found in my mother and my dearest friend Sepp made the process of research and writing a doctoral dissertation endurable and memorable. It was this "Wunder" of friendship which allowed me to pursue Graduate School to its very end, much in the spirit of Schiller's

words : "...Du mußt glauben, du mußt wagen/Denn die Götter leihn kein Pfand/ Nur ein Wunder kann dich tragen/ In das schöne Wunderland." - As Dave would say: sine quibus non.

Of course, I could not end with acknowledging the support of this work by the Assistant Secretary for Conservation and Renewable Energy, Office of Energy Storage and Distribution, Energy Storage Division, of the United States Department of Energy under contract number DE-AC03-76SF00098.

Introduction

1. Background 1
2. Objectives 4

1. BACKGROUND

On the first few of some hundred pages devoted to the electrooxidation of methanol on Pt-Ru alloy electrodes in sulfuric acid electrolyte, it will be instrumental to briefly examine the relevance of this reaction in the broader context of electrochemical energy conversion, particularly by means of fuel cells.

The discovery of the basic principles of a fuel cell dates back to W. Grove, who in 1842 described an electrochemical system capable of converting oxygen and hydrogen directly into electric energy. It consisted of two separate platinized electrodes partially immersed in electrolyte, one being in contact with hydrogen, the other with oxygen gas, so that the half-cell reactions could be formulated as:

$$H_2 \longrightarrow 2H^+ + 2e^-;\ E_- \qquad \text{(I-1)}$$

$$\tfrac{1}{2}O_2 + 2H^+ + 2e^- \longrightarrow 2H_2O;\ E_+ \qquad \text{(I-2)}$$

The standard half-cell potentials, E_- and E_+, are related to the free energy change of the system and can be assessed by means of tabulated values for the standard free energy of formation, according to:

$$E_{+,-} = -\Delta G_R/nF \tag{I-3}$$

where ΔG_R represents the free energy change for the reaction, F refers to the Faraday constant and n are the number of electrons as written in the half-cell reaction. For Equations I-1 and I-2, if evaluated under standard conditions $E_-=0$ V and $E_+=1.23$ V. The overall fuel cell reaction is then the summation of Equations I-1 and I-2:

$$\tfrac{1}{2}O_2 + H_2 \longrightarrow H_2O;\ E_{\pm} \tag{I-4}$$

The difference between the two half-cell potentials, $E_{\pm} \approx 1.23$ V at 25°C, is constant for all values of the hydronium ion concentration in solution (*i.e.* the pH), and it is common in the fuel cell literature to refer to the reversible hydrogen potential in the same solution (RHE) as a measure of activity, a reference scale for which the half-cell potentials of both hydrogen oxidation (Equation I-1) and oxygen reduction (Equation I-2) remain unchanged at 0 and 1.23 V, respectively. On the RHE scale which was used throughout the following 5 Chapters, thermodynamic equilibrium is approached (thereby increasing the overall efficiency of the energy conversion) as the anode potential (the negative electrode in a fuel cell) decreases towards E_- and as the cathode potential (the positive electrode) increases towards E_+ .

Theoretically, the difference in thermodynamic half-cell potentials, $E_{\pm}$, reflects the complete conversion of chemical into electric energy, without the Carnot-cycle limitations encountered with heat engines. Therefore, a reversibly operating fuel cell would allow a 100% conversion of chemically stored free energy into electric energy. This rather promising comparison between heat engines and fuel cells has been the major driving force in trying to develop a commercially viable fuel cell. Unfortunately, kinetic resistances of both electrode reactions (Equations I-1 and I-2) make it impossible to reach the reversible electrode potential and large overpotentials (*i.e.* differences between the

reversible and the measured half-cell potential) result from drawing reasonable current densities from a fuel cell. Therefore, unacceptably large electrode surfaces would be required to reduce the current density, resulting in a low utilization of electrocatalysts. Unfortunately, since very little has changed since the days of Grove, the most active single-component electrocatalyst for the above fuel cell reactions is platinum, thereby imposing exorbitant costs on the manufacture of fuel cell electrodes. Kinetic resistances (*i.e.* overpotentials) for the hydrogen/oxygen fuel cell reaction are somewhat alleviated in alkaline electrolytes, which led to the development of the flagship of fuel cell research, *viz* the alkaline hydrogen/oxygen fuel cell for the space-shuttle space program; undoubtedly, cost was not an important factor in this application.

The difficulty of storing hydrogen efficiently is the prime disadvantage of its use in fuel cells, particularly if one were to envisage the development of fuel cell powered vehicles. A fuel cell, on the other hand, which would electrochemically "burn" a liquid organic fuel could be re-fueled in close analogy to internal combustion engines, and the most promising choice is methanol, which can be converted to electric energy in a direct methanol/air fuel cell (DMFC), where the oxygen necessary for the cathode reaction would be supplied by air. While the corresponding half-cell reaction for oxygen is again Equation I-2, the half-cell reaction for methanol can be formulated as:

$$CH_3OH + H_2O \longrightarrow CO_2 + 6H^+ + 6e^-;\ E_- \qquad \text{(I-5)}$$

with a half-cell potential of $E_- \approx 0.03$ V *versus* RHE, very close to the hydrogen half-cell potential (Equation I-1). The overall cell reaction of a DMFC would then be:

$$CH_3OH + 1.5O_2 \longrightarrow CO_2 + 2H_2O;\ E_{\pm} \qquad \text{(I-6)}$$

with an overall reversible potential difference of $E_{\pm}\approx 1.2$ V. A difficulty associated with a DMFC is that the evolution of CO_2 (Equation I-5) necessitates the use of acidic electrolytes in order to maintain an invariant electrolyte composition by rejecting CO_2 from the solution. Both methanol oxidation and oxygen reduction are significantly more facile in alkaline solutions, in which, however, the evolution of CO_2 leads to the carbonation of the electrolyte.

The most active electrocatalysts for methanol electrooxidation in acidic electrolytes are alloys of platinum and ruthenium, which have been known for decades. Their electrocatalytic activity enhancement over pure Pt is significant, ranging from one to two orders of magnitude; nevertheless, activity expressed in terms of achievable power per mg of noble metal is still too low to offer a viable commercial development of direct methanol air fuel cells. As will be shown in Chapter 5, very little room remains for further optimizing the electrocatalytic activity of Pt-Ru alloys for DMFC's, at least in acidic electrolytes. Nevertheless, these alloy electrodes may be utilized for fuel cells running on reformed methanol, since, in contrast to pure Pt, Pt-Ru electrocatalysts are less susceptible towards deactivation by small concentrations of CO present in the H_2/CO_2 mixture derived from reformed methanol. Additional improvement, however, may be possible in carbonate/bicarbonate electrolytes, which allow the application of higher reaction temperatures on account of their comparably low vapor pressure, and which under certain conditions are invariant with CO_2 .

2. OBJECTIVES

Why then to devote a dissertation to the study of the activity of Pt-Ru alloys towards methanol electrooxidation in sulfuric acid electrolyte? - an obvious question coming to mind at this point. It is true that numerous research efforts have already been

expended on measuring the performance of this same catalyst system under very similar conditions. The question which was to be answered by this dissertation, however, was directed towards the more fundamental aspects of the electrocatalysis of methanol on alloy electrodes, hoping to learn more about the origin of the large kinetic resistences of this reaction, even entertaining the vague hope of being able to attain the facility to put forth an "educated" guess as to how one might "design" an improved electrocatalyst.

The premise for pursuing this goal was to first understand the interplay of alloy surface *versus* bulk composition in order to distinguish the various well-known catalytic effects in alloy catalysis, *viz* electronic interactions between the elements constituting an alloy, blocking of surface sites by one alloy component leading to different reaction pathways, and the bifunctional action observed in many alloy systems in gas-phase catalysis. The surface characterization of Pt-Ru alloys is the subject of Chapter 1 and was carried out in ultra high vacuum (UHV), employing standard surface analytical tools like low energy ion scattering (LEIS) in conjunction with Auger electron spectroscopy (AES) as well as sputtering and annealing to prepare clean sample surfaces.

The transfer of UHV-prepared, well-characterized samples into an electrochemical cell to measure their activity towards methanol electrooxidation (Equation I-5) at room temperature is the topic of Chapter 2, together with a discussion of the fundamental reaction pathways.

Chapter 3 and 4 deal with the activity of Pt-Ru alloy electrodes towards carbon monoxide and formic acid oxidation, both of which are reaction intermediates proposed in the literature. Measured activities were then correlated with the observations made for methanol electrooxidation. In addition, the activity of Pt-Ru electrocatalysts is of interest in fuel cells with reformed methanol.

Finally, Chapter 5 focuses on the changes in the methanol electrooxidation rate with temperature on different alloy surfaces. This last part was especially important in view of the fact, that possible applications of a direct methanol fuel cell would require elevated temperatures, and that measurements at room temperature do not always yield a proper basis for an extrapolation to higher temperatures. Thus, since the majority of the literature data for methanol electrooxidation on Pt-Ru alloy catalysts were conducted at temperatures in the vicinity of 60°C, experiments at this temperature were crucial in resolving the question whether electrocatalytic activities measured on the model-catalysts of this study are in correspondence with the literature data on supported, high-surface area fuel cell catalysts or whether metal-support interactions and particle-size effects invalidate this comparison.

Chapter 1:
UHV Characterization of Pt-Ru Alloys

1. Introduction 7
2. Experimental Procedures 9
   2.1. Pt-Ru Alloy Preparation 9
   2.2. UHV Measurements 9
3. Results 13
   3.1. LEIS Measurements 13
      3.1.1. Calibration and signal deconvolution 13
      3.1.2. Surface composition of sputtered alloys (0.5 keV Ar^+) 18
      3.1.3. Surface compositions of annealed alloys (800°C in UHV) 20
   3.2. AES Measurements 23
4. Discussion 29
   4.1. Comparison with Literature Data 29
   4.2 Thermodynamic Equilibrium Model 31
5. Conclusions 36

1. INTRODUCTION

Thermodynamic modelling of surface enrichment has become progressively more refined [*e.g.* 1-5], as experimental methods have evolved to assess the composition of the outermost surface layers in contrast to the bulk composition of homogeneous alloys. This outermost surface layer composition was soon recognized to be an important factor in determining the activity of alloy catalysts in gas-phase catalysis [6] as well as in electrocatalysis [7]. Auger electron spectroscopy (AES) was one of the first methods applied to the study of surface enrichment phenomena. To quantify Auger signals in terms of atomic percent, calibration spectra are usually taken on elemental standards and

in order to account for significant matrix effects in electron backscattering, *in-situ* fracturing of alloys in ultra high vacuum (UHV) has been employed [8]. Rather long, and not easily measurable attenuation lengths of Auger electrons (several monolayers), however, still seriously hamper the quantitative analysis of AES data in terms of top-layer compositions [9], rendering angle-resolved AES an important part of signal quantification. The same problem, even more pronounced due to commonly larger attenuation lengths applies to X-ray photoelectron spectroscopy (XPS). Low energy ion scattering spectroscopy (LEIS), discovered in its present form in the late sixties [10], overcomes the difficulties associated with the signal averaging over several atomic layers in AES and XPS. Experiments with monolayers of bromine on silicon [11] as well as many other adsorption studies have established the outstanding sensitivity in LEIS towards the outermost atomic layer. The large cross-section for neutralization of rare gas ions by itinerant electrons in metals is responsible for the excellent surface sensitivity of LEIS [12]. The energy loss due to the elastic scattering of low energy noble gas ions from a clean surface in UHV can easily be measured with standard electrostatic ion/electron analyzers and is well described by the classical equations for the conservation of energy and momentum.

The present study is aimed at assessing surface and near-surface concentrations of sputtered and annealed platinum-ruthenium alloys by means of AES and LEIS. These alloys are utilized in hydrogenation catalysis [13] and are also the most promising electrocatalysts in the anodic oxidation of methanol . Besides our interest in conjunction with their catalytic activity towards the electrooxidation of small organic molecules which will be the subject of Chapters 2 to 5, Pt-Ru is an alloy system which serves as an interesting test case for thermodynamic models of surface segregation due to the large difference in the heat of sublimation of platinum and ruthenium but very similar atomic radii [14, 15].

2. EXPERIMENTAL PROCEDURES

2.1. Pt-Ru Alloy Preparation

Five polycrystalline platinum-ruthenium bulk alloys and specimens of the pure elements were prepared in an arc-melting furnace under argon atmosphere from 99.95% pure materials (Johnson Matthey). They were homogenized by at least 10 melt cycles, followed by homogenization under vacuum at 1600°C for 24 hours. All alloys were shown to consist of a single phase *via* X-ray diffraction and their chemical composition was verified by X-ray fluorescence spectroscopy (±0.5 atomic%), calibrated with mixtures of platinum and ruthenium black powders (Johnson Matthey). The chemical composition and the lattice constants of the alloys employed in this study are listed in Table 1-1. All alloy specimens were polished with emery paper and mirror-finished with a ¼ μm diamond paste (Buehler); before introduction into the UHV they were ultrasonically cleaned in detergent, in pyro-distilled water, and in methanol.

2.2. UHV Measurements

LEIS and AES data were collected in a PHI UHV system with a base pressure of $5 \cdot 10^{-10}$Torr, equipped with an angular-resolving double pass cylindrical mirror analyzer (DPCMA Φ15-255GAR) with an electron source at its center axis. AES data were recorded in a derivative mode with a modulation width of 3 eV selected *via* a Φ20-805 analyzer control at an electron beam energy of 3 keV; no angular resolved AES measurements were recorded. A digitally controlled Φ32-100 electron multiplier supply in combination with a Φ20-810 analyzer control and an IBM PC were employed for LEIS data acquisition. For the recording of both AES and LEIS data the DPCMA was operated in the constant retard ratio mode. Using the 90° slit in the angular resolving drum of the

Table 1-1. Prepared specimens: composition in atomic% based on X-ray fluorescence measurements, crystal structure and lattice parameters for fcc (a) and hcp (a and c) lattices measured by X-ray diffraction.

	Pt	PtRu-3	PtRu-5	PtRu-4	PtRu-2	PtRu-6	Ru
% Pt	100.0	90.3	70.2	48.3	39.4	9.5	0.0
Structure	fcc	fcc	fcc	fcc	fcc	hcp	hcp
a in Å	3.9231	3.9166	3.8907	3.8624	3.8486	2.7178	2.7058
c in Å	--	--	--	--	--	4.3140	4.2819

DPCMA, the signal count rate could be maximized without compromising its resolution, requiring an acquisition time of only one minute per spectrum. A Φ04-303A differentially pumped ion gun was used to raster a 2 keV $^4He^+$-ion beam over an area of approximately 3 mm by 3 mm. Ion beam currents were measured at a positive bias of 95 V and were always less than 20 nA/cm^2 at a residual He pressure of $2 \cdot 10^{-8}$ Torr in the UHV chamber. The angle of incidence (angle between the surface and the ion beam) of the $^4He^+$ ions was 45° and the take-off angle was 87° to avoid shadowing effects; the average backscattering angle was 127°. Figure 1-1 shows the UHV chamber together with the electronics and Figure 1-2 is a close-up on the UHV chamber itself; a more detailed description of the instrumentation can be found in Reference 16. Samples were prepared in the UHV *via* cycles of sputtering with argon ions at an incidence angle of 63° and a beam energy of 0.5 keV, and of annealing at 800°C by means of a resistively heated tungsten filament. For some of the alloy specimens a more elaborate preparation method had to be devised in order to attain UHV annealed surfaces without surface active contaminants (Cu, P and S). These specimens were sputtered with 0.5 keV Ar^+ while being maintained at a temperature of 900°C over a period of several days; this cleaning

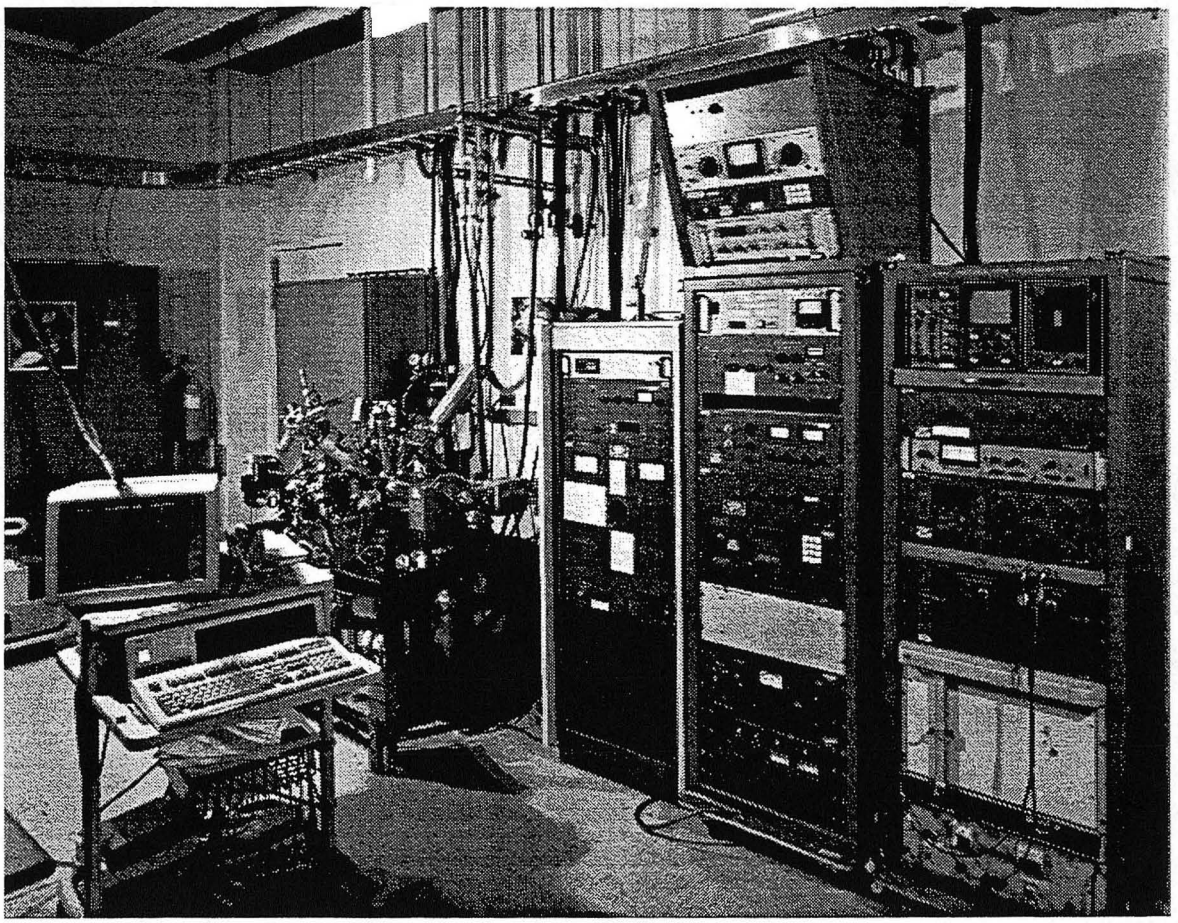

Figure 1-1. UHV chamber for surface preparation and analysis, including the electronics to control the various system components and a IBM-compatible PC for data acquisition.

procedure was successful with all samples. Prior to any sample analysis, all specimens introduced into UHV were sputter-cleaned (2 keV Ar^+) followed by annealing at 800°C in UHV for 15 minutes in order to minimize possible effects of sputter etching. AES spectra from 40 to 540 eV were then recorded before each experiment to verify the absence of surface active contaminants.

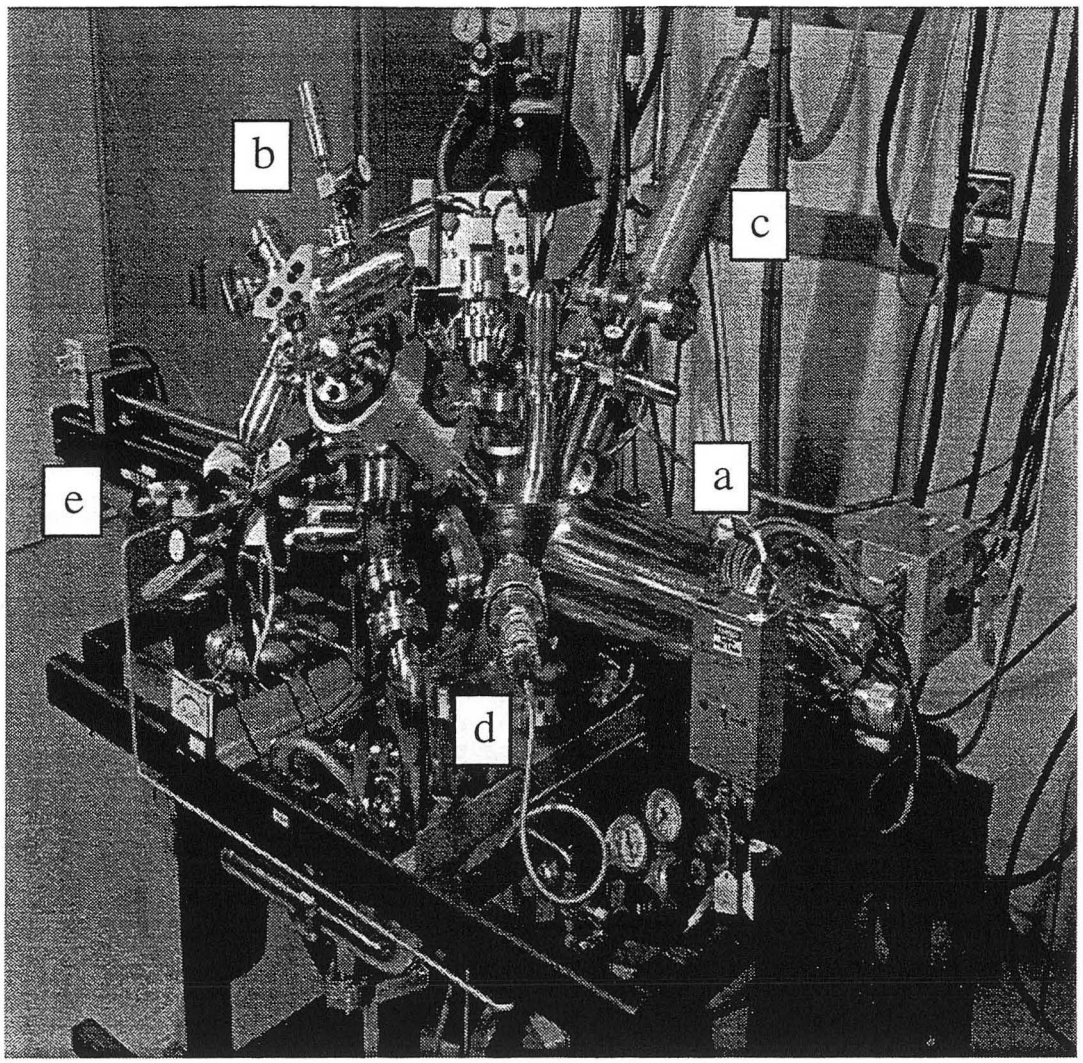

Figure 1-2. UHV chamber with surface analysis tools: **(a)** DPCMA with AES electron source on its center axis; **(b)** differentially pumped LEIS source with He, Ne, and Ar gas capsules; **(c)** X-ray source; **(d)** sputter gun; **(e)** sample transfer system.

3. RESULTS

3.1. LEIS Measurements

3.1.1. Calibration and signal deconvolution

Calibration of the ion scattering signals was carried out on pure platinum and pure ruthenium at a total beam current of 100 nA and a He background pressure of $2 \cdot 10^{-8}$ Torr, at room temperature. These LEIS signals were carefully maximized by moving the sample across the focal point of the analyzer and the beam current was measured at a sample bias of +95 V in order to supress the emission of secondary electrons. The scattering peaks of Pt and Ru agreed to within ±0.5% with the value predicted by the classical equation for elastic collisions [17]:

$$\frac{E_1}{E_0} = \frac{1}{\left[1+(M_2/M_1)\right]^2} \cdot \left(\cos\theta + \sqrt{(M_2/M_1)^2 - \sin^2\theta}\right)^2 \qquad (1\text{-}1)$$

where M_1 and M_2 are the mass of the incident ion and the target atom, respectively, E_0 is the energy of the incoming ion beam, E_1 is the energy of scattered He ions and θ is the backscattering angle. For our experimental parameters the relative energy loss, E_1/E_0, for ion scattering from platinum and ruthenium is 0.936 and 0.881, respectively. To attain a more accurate agreement with Equation 1-1, one would need to consider that the average scattering angle of 127° in our experimental arrangement has a deviation of ±6°, based on the use of the 90° slit in the angle resolving aperture of the DPCMA.

In our LEIS experiments we have chosen $^4He^+$ ions because of their extremely low sputtering rates as compared to Ne^+ or Ar^+ ions (approximately a factor of 20 [18, 19]), ensuring us of a sputter damage of less than 0.5% of a monolayer during data

acquisition. However, with He^+ there is more overlap of the Pt and Ru scattering peaks than with the heavier gases. It was necessary to devise a method to numerically fit the LEIS signals of Pt and Ru to deconvolute the signals. Although several examples of LEIS peak fitting can be found in the literature, *e.g.* exponentially decaying tails [20, 21], we have sought to develop our own fitting equation. This equation outlined in the following has the advantage over, *e.g.* the fitting with exponentially decaying tails, in that the initial input parameters are very well defined and easily extracted from a recorded spectrum, whereas it is rather tedious to establish initial guesses for the referenced fitting equations in the literature. Ion scattering signals with $^4He^+$ ions in particular are characterized by a pronounced low energy tail due to inelastic losses to metal electrons [12], therefore we have based our model equation on the assumption that most of the inelastic losses occur by means of surface plasmon excitations. A free electron gas model can predict the energy of volume and surface plasmons [22] and numerical results for Pt and Ru volume plasmons are cited in the literature to be 30.2 eV and 28.5 eV, respectively [23]. Neither of the two metals is a good example of a free electron material, but inelastic electron beam scattering experiments (1 keV) in our laboratory have yielded values of the volume plasmons for Pt and Ru of 30 eV and 29 eV, respectively. Since LEIS signals originate from the outermost surface layer, surface plasmons rather than volume plasmons were used in our fitting. In the following, we have approximated the energy of surface plasmons for Pt-Ru alloys, ω_s, with an average value of 20.8 eV, corresponding to $1/\sqrt{2}$ times the value of the measured and averaged bulk plasmons. The expression to fit the measured LEIS spectra of Pt and Ru is then a summation of a main signal at the elastic peak position, E_1, and a decaying series of plasmon modes, all characterized by a gaussian profile:

$$Y(E) = c_1 \left(e^{-\frac{1}{2}\left[\frac{E-E_1}{c_2}\right]^2} + c_3 \sum_{i=1}^{20} \frac{1}{i + c_4\sqrt{i}} \cdot e^{-\frac{1}{2}\left[\frac{E-(E_1 - i\cdot\omega_s)}{c_2}\right]^2} \right) \tag{1-2}$$

where Y(E) is the measured ion yield at energy E, c_1 is the overall signal amplitude, c_2 is the width of the gaussian as determined mainly by the angular resolution of the analyzer (see Equation 1-1), c_3 is the tail amplitude and c_4 is an additional tail parameter. The limit on the index i was chosen to be sufficiently large as to extend over the entire energy range, E, where data were acquired. For spectra of pure Pt and pure Ru, a numerical least-square fitting routine was utilized [24] to evaluate the parameters c_1, c_2, c_3, c_4 and E_1. Results of these fits are shown in Figure 1-3.

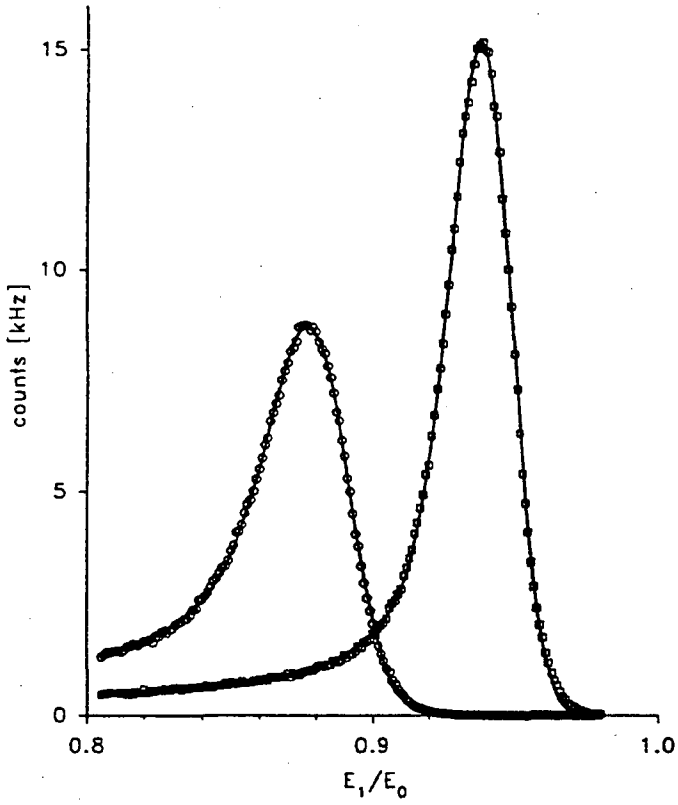

Figure 1-3. $^4He^+$ LEIS (2 keV) on pure Pt (□) and pure Ru (O) at a beam current of 15 nA/cm^2. The beam was rastered over an area of 3 mm by 3 mm. The solid lines are least-square fits according to Equation 1-2 in the text.

The deviation between the numerical fit and the data at the high energy end of the respective spectra most likely derives from multiple scattering events, which have not been considered, but whose effect is negligible for our purposes. LEIS spectra on the alloys were then deconvoluted by fitting Equation 1-2 to the ion scattering data, with all parameters remaining fixed to their values as assessed above except for c_1 and E_1 for both Results of metals and c_3 for platinum. The numerical values for E_1 did vary by approximately ±0.2%, based on the accurate positioning of the sample. Figure 1-4 shows a typical fit on an annealed alloy sample with a Pt surface composition of 91.8±3 atomic%.

Sensitivity factors, $S_{Pt/Ru}$, were derived from the fitted peak height ratios, H_{Pt}/H_{Ru}, extracted from Y(E) (Equation 1-2). Values of $S_{Pt/Ru}$ for three independent

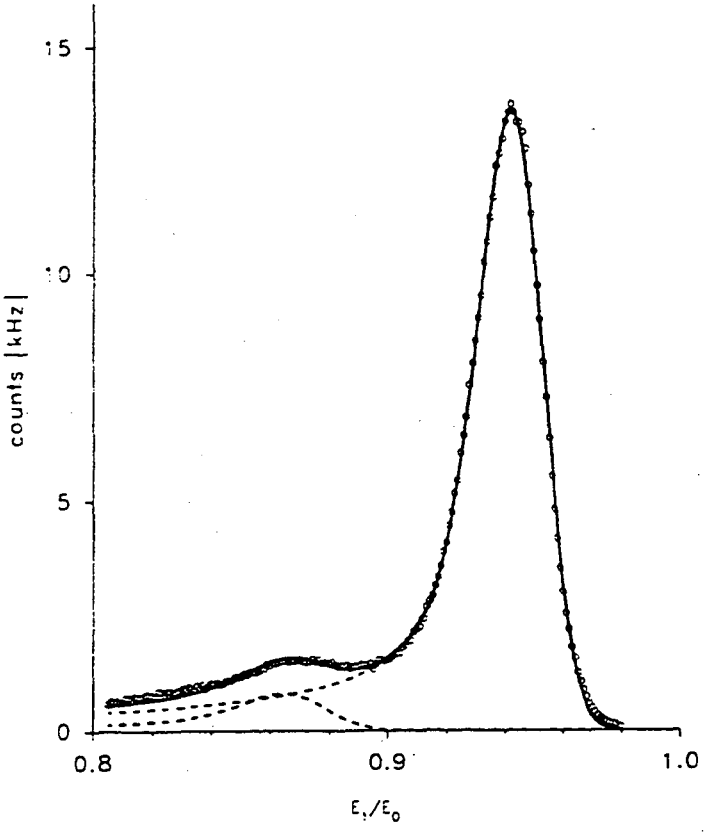

Figure 1-4. $^4He^+$ LEIS (2 keV) on an annealed Pt-Ru alloy (PtRu-5) at a beam current of 18 nA/cm^2. The beam was rastered over an area of 3 mm by 3 mm: (O) raw data; (———) least-squares fit.

experiments over the course of three months are shown in Table 1-2, based on [25]:

$$S_{Pt/Ru} = \left(H_{Pt} / H_{Ru}\right)_{pure} \cdot \left(\frac{\sqrt{3/4} \cdot a_{Ru}^2}{\sqrt{3/16} \cdot a_{Pt}^2} \right) \tag{1-3}$$

where H_{Pt}/H_{Ru} is the intensity ratio measured for the pure elements and a_{Ru} and a_{Pt} are the lattice constants of the elements as listed in Table 1-1 (*i.e.* molar surface areas are approximated for a (111) surface). Their variance is significantly less than reported in a recent LEIS study on Pt-Cu alloys [25] and results in an average absolute error of ±2 atomic% in assigning atomic fractions to LEIS signals, according to:

$$x_{Pt}^{surf} = \frac{S_{Pt/Ru}}{S_{Pt/Ru} + \left(H_{Pt} / H_{Ru}\right)_{exp}} \tag{1-4}$$

Ackermans *et al* [26] have reported a different method to attain sensitivity factors in LEIS analysis, based on absolute signal counts rather than intensity ratios. Since, however, we have worked with extremely low ion beam currents (≈1 nA) in order to avoid sputtering effects, our beam current measurements were accurate only to within ±30%, necessitating the use of intensity ratios.

If, as is commonly assumed, matrix effects in LEIS signals are negligible, the ratio of the differential cross-sections of Pt and Ru should correspond to the ratio found in the above calibration, if the analyzer transmission function is accounted for. Differential

Table 1-2. Sensitivity factors, $S_{Pt/Ru}$, for three independent experiments on Pt and Ru standards (see equation 2): 2keV $^4He^+$ ion beam, 100.0 nA/cm^2, room temperature, θ=127°.

	$S_{Pt/Ru}$		average $S_{Pt/Ru}$
1.52	1.64	1.38	1.51±0.13

cross-sections for LEIS can be calculated classically by assuming a potential energy function for the colliding atoms, *e.g.* a screened Coulomb potential [27, 28]. For the parameters in our experiment, we have calculated the ratio of differential cross-sections of Pt to Ru to be 1.36. By approximating the DPCMA transmission function for the constant retard ratio mode by a $\sqrt{E_1}$ functionality, the LEIS sensitivity factor for Pt and Ru, $S_{Pt/Ru}$, is calculated to be 1.41, which is very close to the measured values (see Table 1-2).

3.1.2. Surface composition of sputtered alloys (0.5 keV Ar^+)

It is well established that sputtering of bimetallic surfaces in UHV may produce surface enrichment in one of the components if the atomic sputtering yields (number of sputtered surface atoms per sputtering ion) are significantly different from each other (e.g., in the Cu-Ni system). In conjunction with our research on the electrocatalytic activity of sputtered Pt-Ru alloys towards the oxidation of methanol, we investigated here the relationship between bulk and surface concentration for sputter-cleaned Pt-Ru alloys. Alloy specimens were bombarded with 0.5 keV Ar+ ions at an angle of incidence of 63°

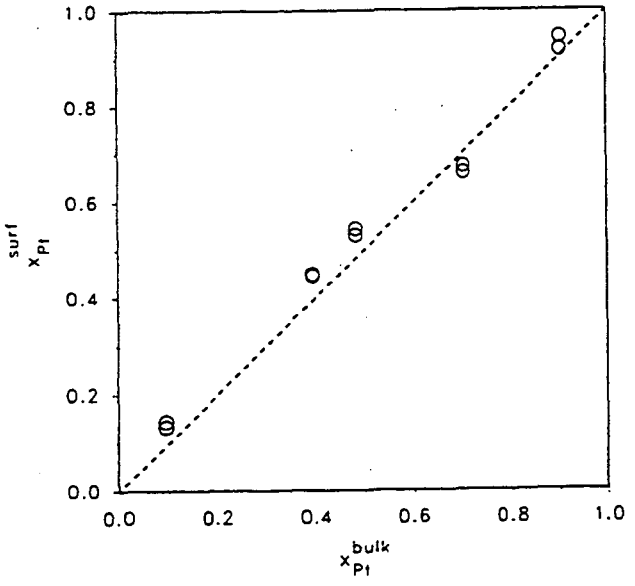

Figure 1-5. Pt surface and bulk compositions of sputtered Pt-Ru alloys as determined by LEIS. Sputtering conditions: 0.5 keV Ar^+ at 63° angle of incidence.

and at a current density of approximately 10 mA/cm^2 for 15 minutes. Sputtering over longer periods of time did not affect the results of LEIS and AES experiments. The cleanliness of the prepared surfaces was verified *via* AES for each measurement in two independent sets, listed in Table 1-3 and summarized in Figure 1-5 which exhibit excellent reproducibility. The amount of oxygen present on the two alloys with a high Ru bulk concentration is estimated to be at most 10% of the Ru atomic fraction, as inferred from AES peak-to-peak ratios of Ru and oxygen [29]. No reduction in ion scattering yields was observed in these cases. It is clear from Figure 1-5 that, under the above conditions, surface and bulk composition of sputtered Pt-Ru alloys are essentially identical within the accuracy of the measurement. Published data on the sputter yields of pure platinum and pure ruthenium at normal incidence of 0.5 keV Ar+ ions [19] would predict a slight enrichment of Ru based on a sputter yield ratio of Pt to Ru of 1.3. Sputter yields at approximately 60° incidence, however, are up to 100% larger than those at normal incidence [30] and sputter yield ratios are expected to change significantly with

Table 1-3. Surface compositions (atomic%) of sputtered alloys (0.5 keV Ar^+) as determined by LEIS for two independent sets of experiments, and AES peak-to-peak ratios based on Auger transition energies as indicated by the subscripts.

	PtRu-3	PtRu-5	PtRu-4	PtRu-2	PtRu-6
Data set 1:					
x_{Pt}^{surf}	94.4	67.5	54.4	44.5	14.4
$(Pt_{64} / Ru_{273})_{AES}$	12.2	2.88	1.26	0.78	0.105
$(Ru_{273} / O_{503})_{AES}$	---	---	---	60	50
Data set 2:					
x_{Pt}^{surf}	91.7	66.1	53.1	44.9	13.3
$(Pt_{64} / Ru_{273})_{AES}$	12.2	3.11	1.24	0.81	0.095
$(Ru_{273} / O_{503})_{AES}$	---	---	---	55	65

the angle of incidence.

3.1.3. Surface compositions of annealed alloys (800°C in UHV)

After sputter-cleaning Pt-Ru alloys were annealed in UHV at 800°C for periods of 15 or 30 minutes and data for two independent sets of experiments are listed in Table 1-4. In studying the surface segregation of these alloys it was imperative to ascertain whether equilibrium was attained under the conditions of the experiment. Starting out with the equilibrium sputtered surface of one alloy sample (PtRu-6, which has the highest melting point) at 25°C, we raised the temperature to 800°C and recorded its surface composition at various times. Although the sensitivity factor, $S_{Pt/Ru}$, is based on room temperature measurements, it is not expected to significantly change with temperature (this is assumption based on theoretical considerations is confirmed in a study on Pt-Rh alloys by Beck *et al* [31]). The experimental data in Figure 1-6 verify the establishment of equilibrium within 10 minutes for the highest-melting alloy in our study. All other segregation measurements reported here were recorded after sample cooling to room

Table 1-4. Surface compositions (atomic%) of annealed alloys (800°C) as determined by LEIS for two independent sets of experiments, and AES peak-to-peak ratios based on Auger transition energies as indicated by the subscripts.

	PtRu-3	PtRu-5	PtRu-4	PtRu-2	PtRu-6
Data set 1:					
x_{Pt}^{surf}	>96	92.1	88.4	84.8	90.6
$(Pt_{64} / Ru_{273})_{AES}$	26.7	6.18	3.66	2.46	0.98
$(Ru_{273} / O_{503})_{AES}$	---	---	---	---	---
Data set 2:					
x_{Pt}^{surf}	>96	91.8	88.3	84.6	90.3
$(Pt_{64} / Ru_{273})_{AES}$	30.9	6.45	3.36	2.54	0.96
$(Ru_{273} / O_{503})_{AES}$	---	---	---	---	---

temperature, at initial cooling rates of 200°C/min, reaching 500°C in less than two minutes. For temperatures below 500°C, the equilibration is very slow (>1hour) and so the error introduced by cooling the samples prior to analysis was expected to be negligible, as confirmed by Figure 1-6. The slight increase in surface enrichment for the cooled sample is consistent with predictions of theoretical equilibrium models presented in Section 4.2.

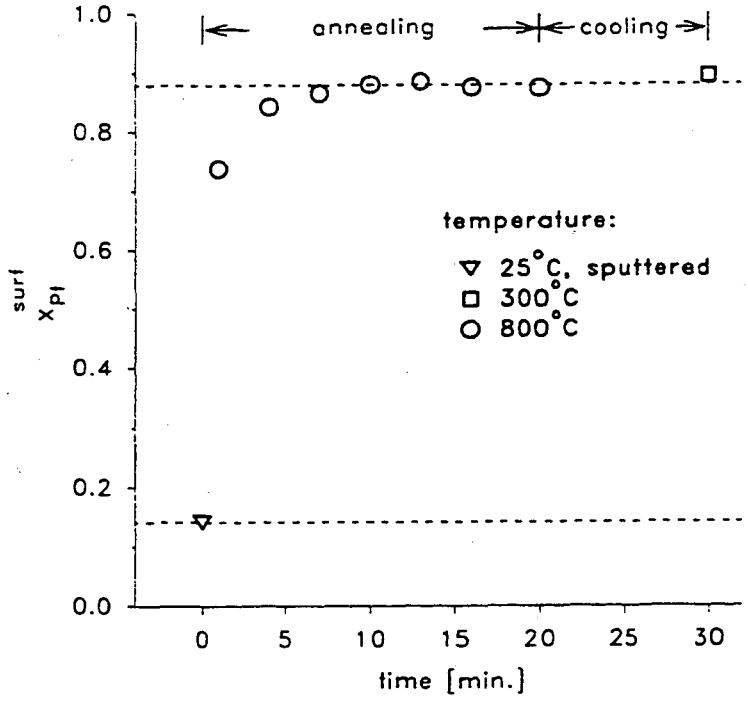

Figure 1-6. Surface composition of the PtRu-6 alloy sample as a function of annealing time at 800°C, and after sample cooling. Prior to this experiment the surface was sputtered with 0.5 keV Ar^+ ions. The average surface compositon of annealed and sputtered alloys is indicated by dashed lines.

The equilibrium surface compositions of four Pt-Ru alloys are plotted in Figure 1-7 together with theoretical predictions which will be discussed later. The surface enrichment in platinum is quite significant and does behave in a systematic fashion for the fcc structure alloys. The alloy with the largest platinum content (PtRu-3) yielded a surface composition above 96 atomic% and since we could not assign a more definite numerical value it is

indicated by a plain error bar in Figure 1-7. Apparently different behavior is exhibited by the alloy with the hexagonal crystal structure (hcp) at a bulk composition of 9.5 atomic% platinum, where the platinum surface enrichment seems too large in comparison with the other alloy samples. According to the bulk phase diagram of the platinum-ruthenium system (reproduced from Hutchinson [33]), Figure 1-8, the hcp alloy (PtRu-6) reaches a surface composition which, in the bulk would correspond to a fcc lattice. The additional driving force for segregation established by this crystal structure mismatch may be responsible for the very strong enrichment observed in this alloy. Embedded atom calculations for the Co-Ni system (Ni has a fcc structure and Co crystallizes in a fcc

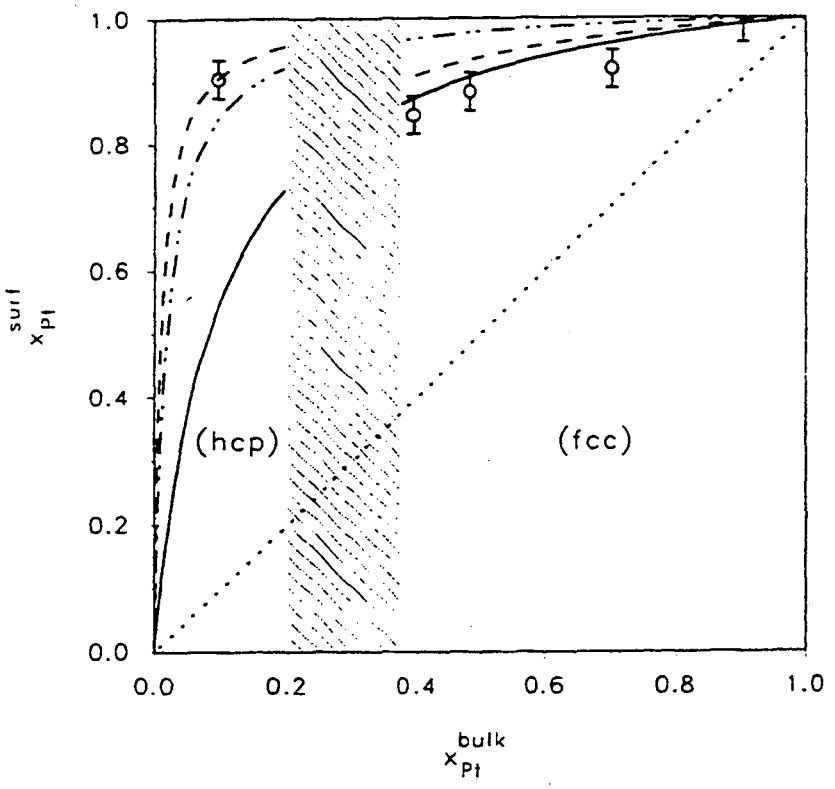

Figure 1-7. Experimental data of Pt-Ru alloys annealed at 800°C in UHV (O). Thermodynamic monolayer model by King *et al* [32] for different low-index planes: (———) fcc(111) and hcp(0001) ; (– ·· – ·· –) fcc(110) and hcp($11\bar{2}0$); (- - - - -) fcc(100) and hcp($10\bar{1}0$); (· · · · · ·) diagonal; (\\\\\\\\\\) indicates the two-phase region of the bulk alloy.

lattice) have predicted a very strong surface enrichment in Ni, although heats of sublimation and atomic radii of these two elements are very nearly identical [34]. This will be discussed in more detail in Section 4.2.

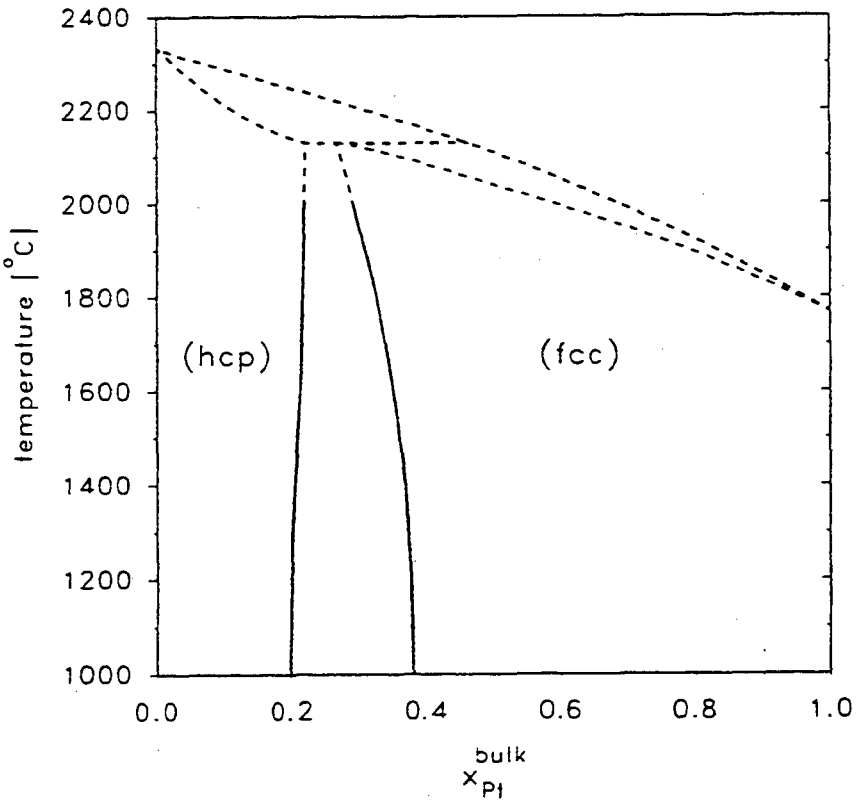

Figure 1-8. Phase diagram of the platinum-ruthenium system (reproduced from J.M. Hutchinson [33]).

3.2. AES Measurements

In contrast to the outermost-layer information provided by LEIS, AES signals incorporate information from several atomic layers with a depth-distribution along the surface normal (z-axis) characterized by the mean free path of Auger electrons, $\lambda(E)$, at

energy E. Typical AES spectra of an annealed and a sputtered Pt-Ru alloy are compared in Figure 1-9.

The overall intensity is a well-defined function of the depth-distribution of the electron emitting element, $N_A(z)$, the impinging electron beam current, I_0, with energy

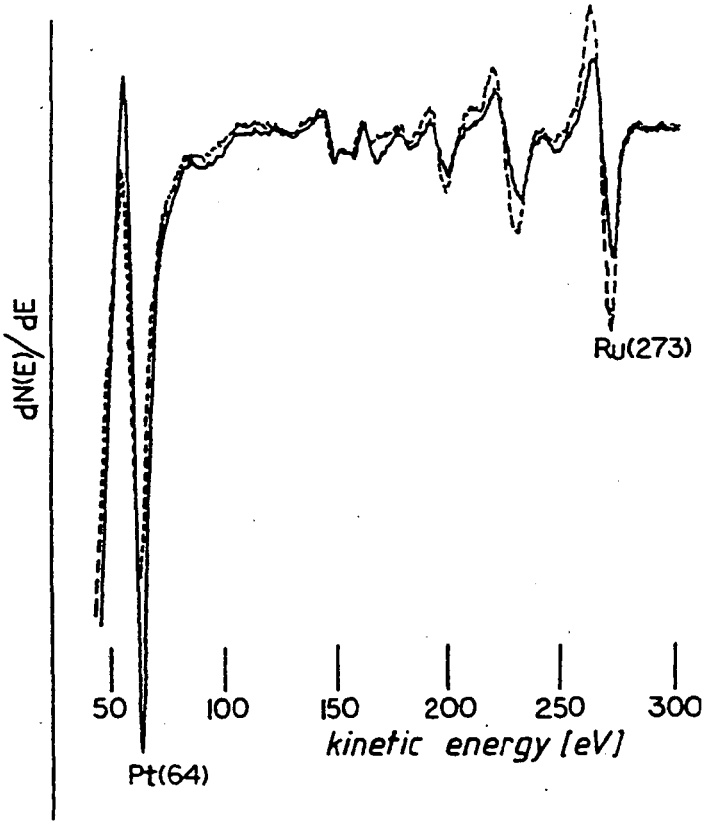

Figure 1-9. AES spectra of PtRu-5 recorded in the derivative mode: (——) annealed at 800°C in UHV; (- - - -) sputtered with 0.5 keV Ar^+ ions.

E_p, the roughness factor of the specimen, ρ, the Auger cross-section, $\sigma(E_p)$, the matrix-dependent backscattering factor, R_M, the transmission function of the analyzer, T(E), and the detector efficiency, D(E). The attenuation length of Auger electrons is defined by the product of their mean free path and the cosine of the angle of emission with respect to the

surface normal, α. The mathematical description (*e.g.* see Rivière [17]) of an Auger signal from element A, I_A, is then:

$$I_A = I_0\, \rho\, \sigma_{A(E_p)}\, R_M\, T_{(E)}\, D_{(E)} \int_\phi \int_\beta \int_0^\infty N_{A(z)} \exp\left(\frac{-z}{\lambda_A \cos\alpha}\right) dz \sin\beta\, d\beta\, d\phi, \qquad (1\text{-}5)$$

where β is the acceptance angle of the analyzer (42.3°±6° for the DPCMA) and ϕ is the rotation angle about the analyzer axis. For our experimental set-up, with the sample being mounted at 45° with respect to the analyzer axis, $\cos\alpha$ is defined as:

$$\cos\alpha = \frac{1}{\sqrt{2}} \cdot (\cos\phi \cdot \sin\beta + \cos\beta) \qquad (1\text{-}6)$$

Since neither Auger cross-sections nor backscattering factors can be calculated from first principles with sufficient accuracy, signal calibration is of essential importance in AES. The most accessible calibration method is based on elemental standards while recording Auger peaks at different energies to attain depth-distribution information [35]. Here it is crucial to reproduce precisely the sample alignment, electron beam current and surface roughness for each sample. A more cumbersome, yet very powerful procedure is the *in-situ* fracturing of an alloy specimen in order to create a homogeneous distribution of its components along the z-axis [8]. In our experiments we have attempted to employ a very similar calibration method based on the LEIS results on sputtered alloy surfaces (see section 3.1.2.), which were shown to have identical bulk and surface concentrations within the accuracy of the measurement. Knowing that N_{Pt} and N_{Ru} are independent of z for sputtered alloys, Equations 1-5 simplifies to:

$$\frac{I_{Pt}}{I_{Ru}} = \frac{\sigma_{Pt(E_p)}\, R_{M(E_{Pt})}\, T_{(E_{Pt})}\, D_{(E_{Pt})}\, \lambda_{(E_{Pt})}}{\sigma_{Ru(E_p)}\, R_{M(E_{Rut})}\, T_{(E_{Rut})}\, D_{(E_{Ru})}\, \lambda_{(E_{Ru})}} \cdot \frac{x_{Pt}}{x_{Ru}}, \tag{1-7}$$

This may be rewritten as:

$$\frac{I_{Pt}}{I_{Ru}} = K \cdot \frac{x_{Pt}}{x_{Ru}} \tag{1-8}$$

Since the bulk atomic fractions are known, the Auger intensity ratios in Table 1-3 will facilitate the evaluation of the calibration factor K, varying by approximately ±5% for each sample. The only matrix dependent variables in K are the backscattering factors, R_M, and the electron mean free paths. The former characterizes the enhancement of the impinging electron beam *via* elastic backscattering of high energy electrons ($\approx E_p$) and is to a very good approximation a function of the bulk matrix composition only [36]. The inelastic mean free path of electrons is most commonly evaluated using the "universal curve" compiled by Seah *et al* [37]. Based mainly on overlayer experiments, a functional relationship between λ and electron energy was established for the elements, ignoring matrix effects and resulting in a root mean square scatter factor of 1.59. Recent inelastic mean free path (IMFP) calculations [23] for electrons by means of optical data provide a more accurate assessment of the mean free path of electrons as it is applicable to AES experiments . From these calculations we have derived the IMFP at 64 eV kinetic energy (corrected for the work function of the analyzer) in platinum and ruthenium to be 4.34 Å and 4.33 Å, respectively; the values at a kinetic energy of 273 eV are 5.80 Å and 6.32 Å, respectively. The matrix effect in the IMFP is quite small considering the precision claimed by Tanuma *et al* [23] and we have applied arithmetic averages at each electron energy for our calculations. The values at 273 eV are markedly lower than the prediction given by the "universal curve", significantly affecting AES model calculations. It should

be noted that because of the contribution of elastic electron scattering the IMFP should be considered as the upper limit for the electron mean free path [38].

UHV annealed Pt-Ru alloys exhibit a first layer composition strongly enriched in platinum, as evidenced by our ion scattering analysis. Therefore, the composition of near surface layers is a function of their position along the z-axis, expressed as $N_A(z)$ in Equation 1-5, which may be integrated layer by layer:

$$\frac{I_{Pt}}{I_{Ru}} = K \frac{x_{Pt}^{(1)} \int_{\phi}\int_{\beta} \cos\alpha \, \sin\beta \, d\beta \, d\phi + \sum_{i=1}^{\infty}\left(x_{Pt}^{(i+1)} - x_{Pt}^{(i)}\right) \int_{\phi}\int_{\beta} \exp\left(\frac{-i\,d}{\lambda_{Pt}\cos\alpha}\right) \cos\alpha \, \sin\beta \, d\beta \, d\phi}{x_{Ru}^{(1)} \int_{\phi}\int_{\beta} \cos\alpha \, \sin\beta \, d\beta \, d\phi + \sum_{i=1}^{\infty}\left(x_{Ru}^{(i+1)} - x_{Ru}^{(i)}\right) \int_{\phi}\int_{\beta} \exp\left(\frac{-i\,d}{\lambda_{Ru}\cos\alpha}\right) \cos\alpha \, \sin\beta \, d\beta \, d\phi} \quad (1\text{-}9)$$

Here, the mole fractions of platinum and ruthenium are expressed for each layer, i (i=1 is the outermost surface layer, i=∞ refers to the bulk compositon), and the average distance between crystal planes of a poly-crystalline specimen, d, derived from molar volumes is 2.34 Å. Assuming the above values for the mean free paths of Auger electrons emitted from platinum (64 eV) and from ruthenium (273 eV, also see Figure 1-9), the angular integrals in Equation 1-9 in conjunction with Equation 1-6 are easily evaluated by numerical integration.

Thus, we find that 79% of the platinum Auger signal and 67% of the ruthenium Auger signal stem from the first and the second layer. Given the large signal contribution from the two outermost atomic layers, we have extracted second layer compositions from our Auger data by fixing the first layer composition to the values found by LEIS (see Table 1-4) and by assigning the sample's bulk composition from the third layer on. The

latter assumption is based on the fact that nearly ideal solutions will approach bulk composition within a few atomic layers; that the Pt-Ru system behaves very closely to an ideal solution will be shown in Section 4.2. Thus, Equation 1-9 simplifies to:

$$\frac{I_{Pt}}{I_{Ru}} = K \cdot \frac{0.4604\, x_{Pt}^{(1)} + 0.2034\left(x_{Pt}^{(2)} - x_{Pt}^{(1)}\right) + 0.1008\, x_{Pt}^{(\infty)}}{0.4604\, x_{Ru}^{(1)} + 0.2513\left(x_{Ru}^{(2)} - x_{Ru}^{(1)}\right) + 0.1492\, x_{Ru}^{(\infty)}}, \tag{1-10}$$

where K, as discussed above is a constant evaluated for each alloy sample, depending on its bulk composition only. Second layer compositions of annealed alloys derived from Equation 1-10 are plotted together with the LEIS data in Figure 1-10.

The error bars are based on the estimated accuracy of K (±5%), the precision of Auger peak-to-peak intensities (±5% experimentally observed scatter), the variation of the

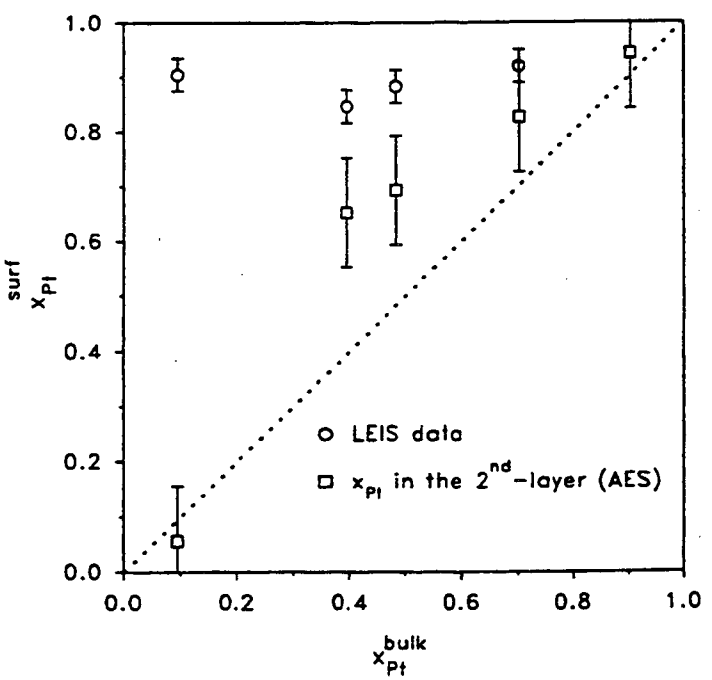

Figure 1-10. First and second layer platinum surface composition of annealed Pt-Ru alloys: (O) LEIS data; (□) second layer composition derived from AES; (· · · · · ·) diagonal.

distance between different atomic planes (±15% for low index planes), and the uncertainty in the mean free paths of Auger electrons (±13%, Reference 23). Figure 1-10 indicates the second layer composition to still be significantly different from the bulk composition and our previous assumption, *viz* that the third layer would already be very close to the bulk compositon may not be correct. Nevertheless, the error introduced by this factor is expected to be small because the main contribution to the Auger signals does originate from the first two atomic layers as outlined above. In principle, measuring Auger transitions at different energies, Equation 1-9 can be utilized to solve for more than two atomic layers [*e.g.* see 35]. Unfortunately, all other Pt and Ru Auger transitions below 1000 eV overlap and we did not use the high energy transition of platinum at 1967 eV [39] because of its long IMFP of approximately 20 Å.

4. DISCUSSION

4.1. Comparison with Literature Data

The literature on surface segregation phenomena of Pt-Ru bulk alloys is very scarce and even for supported bimetallic clusters not much has been published. A photoemission study of Pt-Ru bulk alloys with up to 55 atomic% ruthenium was reported by Hilaire *et al* [40]. Its results, which show very little platinum surface enrichment, are in stark contrast to our data. A major error in attempting to quantify their measurements in terms of atomic%, is their approach of plainly using sensitivity factors in their XPS (X-ray photoelectron spectroscopy) signal analysis. The inelastic mean free paths of Pt and Ru photoelectrons (Al anode) are 17 Å [23], and signals will be averaged over approximately 10 atomic layers, which clearly invalidates their assumption of attaining first layer information without more refined signal processing or angle-resolved measurements. Ticanelli *et al* [41] report $^{20}Ne^{+}$ ion scattering on a 50 atomic% Pt-Ru

bulk alloy subjected to voltammetric cycling, but no attempt was made to quantify LEIS signals. A recent time-of-flight (TOF) atom-probe analysis by Tsong et *al* [42] investigated the (001) face of a Pt-Ru alloy (17.7 atomic% Ru), which had been annealed in UHV at 700°C for 15 minutes. The reported first layer platinum composition of approximately 93 atomic% is in very good agreement with our findings (see Figure 1-7). In their study, the bulk composition is reached in the third layer, but the reported second layer composition (≈76%) would imply an oscillatory behavior which is at variance with our AES data analysis (see Figure 1-10). However, it is very likely that 5 minutes at 700°C were not sufficient to warrant the establishment of equilibrium over several atomic layers, so that their measurement would reflect a transient state rather than equilibrium. In support of this, we refer to Figure 1-6 which shows that equilibration even at 800°C requires approximately 5 minutes. Diffusivities of solids change very drastically with temperature, *e.g.* the diffusivity of platinum in platinum at 700°C is more than a factor of 20 smaller than the value at 800°C [15], decreasing its diffusion length by a factor of 4.5, and so we believe that complete equilibration has not been achieved in this study by Tsong and coworkers. In an older study by the same author [43] "equilibration" of a Pt-Ru alloy had been carried out at 800°C for 15 seconds and no segregation was observed.

Bimetallic supported catalysts are the very basis of industrial catalysis. Very common support materials are *e.g.*, carbon, alumina and silica. Surface enrichment of Pt-Ru clusters on either alumina or silica was investigated by Miura *et al* [44]. Support materials were coimpregnated with Pt and Ru salts, reduced in hydrogen and annealed in vacuum at 450°C. All samples, over the entire compositional range exhibited surface enrichment of platinum as measured by O_2-CO surface titration (≈80% Pt for a 50% bulk composition on both alumina and silica). For clusters diluted in one of the components, the authors report different behavior depending on the nature of the support, which they

rationalize by metal-support interaction. It is stated that dispersions (ratio of the number of surface atoms to the number of bulk atoms) of catalysts supported on silica are larger than of those supported on alumina, with the dispersion for bimetallics ranging from 17% to 60%. At high dispersion, a large fraction of the atoms in a particle (≈10 to 25 Å) are located on the surface and the internal composition, *i.e.* "bulk composition", changes significantly if surface segregation occurs, necessarily leading to cherry-model like structures. Thus, one would expect large differences in the surface compositions of clusters on different substrates when there is a large variation in the dispersion. The dispersion of metals on supports is a strong function of the reducing conditions during cluster preparation, the nature of the metal precursors, and the substrate [45, 46], and in our view it is the effect of the substrate on dispersion that is the cause of the difference in surface composition for Pt-Ru on silica *vs.* alumina. In order to be able to compare platinum enrichment found in the supported clusters with that found here, the comparison should only be made at a sufficiently low dispersion and at sufficiently small surface enrichment such that segregation is not effecting a large fractional change in the cluster's bulk composition. Bulk and surface compositions of Pt-Ru clusters were reported by Miura *et al* [44]; for samples for which the above conditions were satisfied the agreement with our data is excellent.

4.2 Thermodynamic Equilibrium Model

The first thermodynamic models to assess the compositonal difference between a surface monolayer and the bulk of a binary ideal solution were developed by Butler [47] and Schuchowitzky [48]. Guggenheim [49] extended their formalism to incorporate regular solution behavior, but Defay *et al* [50] proved this approach to be at variance with the Gibbs adsorption isotherm and showed that more than one surface layer was necessary to thermodynamically account for non-ideal solutions. The "quasichemical" approach [51] to model surface segregation is based on bond-breaking considerations and Williams

et al [1] have derived a formalism accounting for four surface layers. For non-ordering binary alloys they have shown the monolayer model to be sufficient, if ideal solution behavior is assumed. If, however, enthalpy of mixing data are utilized to approximate regular solution behavior, the composition varies through more than one layer, in agreement with Reference 50. In either case, the extent of surface enrichment is strongly dependent on the exposed crystal face, *viz* the number of broken bonds at the surface. For ordering alloys, the entropy of mixing must be evaluated differently as was outlined by Santen *et al* [52]. Effects of lattice strain due to different atomic radii of the components in a binary were discussed by Wynblatt *et al* [53]. A monolayer model for binary transition metal alloys, incorporating surface free energies, enthalpies of mixing and atomic size differences was proposed by Miedema [54]. More recently Strohl *et al* [32] have developed a thermodynamic multilayer, multi-component model applicable to non-random, non-regular solutions, provided the alloy's mixing properties are known. Besides these, the most important input parameters for both, the thermodynamic and the bond-breaking models are surface free energies whose measurement is very difficult for solids and prone to large errors [2]. Therefore, Overbury *et al* [55] devised a method for estimating these parameters from enthalpy of sublimation data (*e.g.* [14]). Based on more refined thermodynamic considerations, Tyson *et al* [56] have predicted temperature-dependent surface free energies for a large number of solid elements for which the surface tension of the liquid at the melting point was available. Their evaluations are based on estimating surface entropies and they were able to show very good agreement of extrapolated surface free energies at 0 K with bond strengths assessed from enthalpies of sublimation at 0 K; a slightly different approach was taken by Mezey *et al* [57]. The variations in surface segregation calculations depending on both the selection of the model and on the parameters were investigated by Kelley [58]. A very recent development in the calculation of the thermodynamics of surface segregation is the embedded atom method. This mathematically quite elaborate treatment makes use of a

Monte Carlo simulation method and is thus able to yield configurational distributions on an alloy surface rather than merely net surface compositions [*e.g.* 34]. Excellent reviews of surface segregation modelling are provided in References 3 and 5.

In calculating the equilibrium surface composition of annealed Pt-Ru alloys we have employed the thermodynamic model proposed by Strohl *et al* [32]. Surface free energies at 800°C were estimated according to Reference 56; their numerical values for platinum and ruthenium are 2.38 J/m^2 and 2.93 J/m^2, respectively. Molar areas of both elements were evaluated from molar volumes and structure factors according to Tyson [59], and are summarized in Table 1-5 for different low-index faces of fcc and hcp lattices. Surface areas for different crystal faces derived from lattice parameters of pure platinum and pure ruthenium (see Table 1-1) are identical to those based on molar volumes and structure factors. Enthalpy of mixing data have never been measured for the Pt-Ru system. A semi-quantitative estimate of the enthalpy of mixing for PtRu was given by Miedema [60] to be -2 kJ/mole. His predictions for all binary transition metal alloys lie within a range of approximately ±100 kJ/mole and he claims that values close to zero would imply the absence of intermetallic phases and good miscibility, which is congruent with the Pt-Ru phase diagram (see Figure 1-8). Miedema showed that large predicted values of the enthalpy of mixing agreed well with measurements, whereas values close to zero could not be assessed very precisely. For this reason and since the estimated enthalpy of mixing for our system is very small compared to the difference in molar surface free energies of platinum and ruthenium, we have decided to simulate surface segregation with an ideal solution model. The extent to which Vegard's Law is obeyed by the fcc structure Pt-Ru alloys (see Table 1-1) is indeed indicative of a closely ideal solution.

Table 1-5. Molar surface areas of platinum and ruthenium for different low-index surfaces of hcp and fcc structures (in m^2/mole). Numerical values are based on structure factors [59] and molar volumes.

	platinum	ruthenium
fcc(111)	$4.01 \cdot 10^4$	$3.75 \cdot 10^4$
fcc(100)	$4.64 \cdot 10^4$	$4.33 \cdot 10^4$
fcc(110)	$6.55 \cdot 10^4$	$6.12 \cdot 10^4$
hcp(0001)	$4.01 \cdot 10^4$	$3.75 \cdot 10^4$
hcp($11\bar{2}0$)	$6.55 \cdot 10^4$	$6.12 \cdot 10^4$
hcp($10\bar{1}0$)	$7.58 \cdot 10^4$	$7.08 \cdot 10^4$

With these assumptions, the equilibrium condition according to Strohl *et al* does predict only the outermost layer composition, $x_{Ru}^{(1)}$ and $x_{Pt}^{(1)}$, to be different from the bulk composition, $x_{Pt}^{(\infty)}$ and $x_{Ru}^{(\infty)}$:

$$\gamma^{(1)} = \gamma_{Pt}^{(1)} \frac{A_{Pt}^{(1)}}{\overline{A}_{Pt}^{(1)}} + \frac{RT}{\overline{A}_{Pt}^{(1)}} \ln\left(\frac{x_{Pt}^{(1)}}{x_{Pt}^{(\infty)}}\right) = \gamma_{Ru}^{(1)} \frac{A_{Ru}^{(1)}}{\overline{A}_{Ru}^{(1)}} + \frac{RT}{\overline{A}_{Ru}^{(1)}} \ln\left(\frac{x_{Ru}^{(1)}}{x_{Ru}^{(\infty)}}\right), \tag{1-11}$$

where $A_i^{(1)}$ and $\overline{A}_i^{(1)}$ represent molar and partial molar areas of Pt and Ru, and $\gamma^{(1)}$ and $\gamma_i^{(1)}$ are the outermost layer surface free energy and the pure component's surface free energy, respectively. Partial molar areas may be evaluated from the change of lattice parameters with alloy composition, thereby accounting for lattice strain effects. Using the data in Table 1-1 we found the maximum deviation of partial molar areas from molar areas to be approximately 5%. Considering the vastly varying molar areas for different

surface faces (see Table 1-5), we decided to neglect differences between partial molar and molar areas in Equation (1-11).

Surface composition calculations for different Pt-Ru alloy surface faces of the hcp and fcc structure at 800°C are plotted in Figure 1-7 together with experimental LEIS data. The two-phase region in the bulk phase diagram is indicated by the hatched area (also see Figure 1-8). Ideally, minimization of the overall surface free energy is achieved by minimizing the number of broken bonds at the surface, implying that equilibrated surfaces should exhibit low-index faces (this was found, *e.g.* for polycrystalline Ag-Au alloys [35]). The lowest number of broken bonds in a fcc lattice occurs for a (111) surface with only 25% of the nearest neighbor bonds being ruptured. Thus, the best fit to the experimental LEIS data in the fcc alloys is achieved by assuming a surface area corresponding to a (111) crystal face. The hcp alloy with a very high bulk concentration of ruthenium (PtRu-6) exhibits a surface platinum concentration corresponding to a fcc bulk structure. This lattice mismatch, we believe, is effecting a very loosely packed surface, approximated by a hcp$(10\bar{1}0)$ surface (see Figure 1-7). The increase in molar area for this structure is characterized by a large fraction of broken surface bonds, *viz* 50%. This effectively increases the difference between the molar surface free energies of platinum and ruthenium, enhancing surface segregation.

The second-layer information we have extracted by means of AES does point towards a deviation of the system from ideality, since the composition of the second surface layer is significantly different from the bulk composition, as shown in Figure 1-10. A small positive enthalpy of mixing would predict this behavior. We have already mentioned the lack of thermodynamic mixing data for the platinum-ruthenium system and so we do not attempt to extend the model in Equation 1-11 to regular solution theory at the present time. To extend the equilibrium model to highly dispersed bimetallic

clusters (see Section 4.1.) a mass balance in addition to the equilibrium equation would be necessary.

5. CONCLUSIONS

$^4He^+$ LEIS indicates that sputter-cleaning of polycrystalline Pt-Ru bulk alloys with 0.5 keV Ar^+ ions at *ca* 60° incidence does not effect any preferential sputtering.

Annealing of these alloys in UHV at 800°C produces a strong surface segregation of platinum. Using first-layer compositions from LEIS data and by employing a calibration method for AES signals based on measurements on the continuously sputtered alloy, we were able to extract second-layer compositions. These compositions indicated that platinum surface enrichment of annealed Pt-Ru alloys follows a smooth decay from the outermost layer to the bulk and does not exhibit any oscillatory behavior.

Segregation for the annealed Pt-Ru alloys is described well by ideal solution thermodynamics with surface free energies and molar areas as input parameters. The best fit to the surface *vs* bulk composition curve for the alloys having the fcc structure (>38 atomic% Pt) was produced by using the molar area for a (111) face. The very strong surface segregation observed for the hcp bulk alloy (9.5 atomic% Pt) is predicted by assuming a relatively open surface face $(10\bar{1}0)$, which appears to be a result of the apparent mismatch of the bulk hcp structure and the fcc structure the surface planes would have if they were bulk planes.

Chapter 2:
CH_3OH Oxidation on Pt-Ru Alloys at 25°C

1. Introduction 37
2. Experimental Procedures 40
   2.1. Electrochemical Measurements 40
   2.2. Sample Transfer Test 43
3. Results 44
   3.1. UHV Characterization 44
   3.2. Electrochemical Measurements 46
      3.2.1. Voltammetry in the Supporting Electrolyte 46
      3.2.2. Voltammetry in the Presence of Methanol 49
      3.2.3. Potentiostatic CH_3OH Oxidation on Pt-Ru Alloys 56
4. Discussion 58
   4.1. Accumulated Surface "Poisons" 60
   4.2. UHV *vs* Electrochemistry on Pt and Ru 61
   4.3. Formulation of a Major Reaction Pathway 62
   4.4. Characteristics of Pt-Ru Alloys 64
   4.5. Statistical Interpretation of Bifunctional Pt-Ru Electrodes 65
5. Conclusions 71

1. INTRODUCTION

The conceptually promising features of a direct methanol fuel cell, which were discussed in the introductory chapter, have stimulated vigorous research efforts on the electrooxidation of methanol in acidic media. Many different electrode materials have been tested for their activity towards the anodic oxidation of methanol, including single crystal surfaces to gain a more fundamental understanding of methanol electrocatalysis on an atomically resolved scale; an excellent overview of the literature may be found in

References 61 and 62. Compared to pure platinum the most active electrocatalysts known so far are alloys of platinum and ruthenium exhibiting lower overpotentials and extended life-time [63-65]. A vast amount of potentiodynamic and potentiostatic performance data of Pt-Ru alloys are reported in the literature, but with the exception of two studies on smooth Pt-Ru bulk alloy electrodes [66, 67], all research has been focused on either electrolytically codeposited Pt-Ru electrodes [*e.g.* 68-70] or on carbon supported Pt-Ru clusters with high specific surface areas [*e.g.* 63-65, 71, 72].

In 1972 Binder *et al* [66] noticed differences in the voltammetry between Pt-Ru Raney catalysts and Pt-Ru bulk alloys of identical bulk composition in H_2SO_4 and suggested that the two preparation methods may effect different surface compositions. Later on, McNicol *et al* [71] observed the strong influence of activation conditions for a carbon-supported bimetallic Pt-Ru catalyst on both their voltammetry in H_2SO_4 and their electrocatalytic activity towards the oxidation of methanol, concluding that heating in either hydrogen or air would produce surfaces enriched in platinum or ruthenium, respectively. Miura *et al* [73] found a strong surface enrichment of platinum on a bimetallic Pt-Ru catalyst supported on either silica or alumina for which the final preparation step consisted of high-temperature reduction in hydrogen. They also found that the catalyst dispersion (ratio of the number of surface atoms over the number of bulk atoms) was a function of its bulk composition as well as of the nature of the precursor molecules and the activation treatment [74]. Since the active surface area of Ru [75] and Pt-Ru alloys [66] cannot be determined unambiguously from electrochemical measurements as is usually done with platinum, varying surface areas for high surface-area fuel cell electrodes of different bulk composition pose a serious difficulty in trying to distinguish changes in true electrocatalytic activity from changes in surface area. Electrochemical measurements on both supported bimetallic clusters and bulk alloys require *in-situ* cleaning of the electrodes in the supporting electrolyte, which in all

previous investigations on Pt-Ru alloys consisted of a potential cycling pretreatment between the hydrogen evolution potential and a positive potential of approximately 1.3 to 1.5 V *vs* the reversible hydrogen electrode (RHE) in order to create surfaces free of adsorbed impurities. Whereas this method is appropriate for Pt electrodes, it has been shown to cause the dissolution of Ru in pure ruthenium electrodes at potentials as low as 0.9 V *vs* RHE [76, 77, 78] as well as the preferential dissolution of Ru in Pt-Ru alloy electrodes [68, 70]. Therefore, although the initial surface composition of the alloy electrodes may be estimated based on their preparation method, the uncontrolled dissolution of Ru during the electrode pretreatment renders it impossible to even approximately quantify its surface composition when its electrocatalytic activity is being measured. Nevertheless, the literature on the electrooxidation of methanol shows remarkable consistency in reporting an optimum alloy composition of 50 atomic% ruthenium, mostly based on the assumption that bulk and surface compositions would be identical; only the data by Éntina *et al* [68] indicate an optimum Ru composition of 25 atomic%. In general, the assessment of the electrocatalytic activity of alloy electrodes has been based either on cyclic voltammetry in the case of electrodeposited alloys or on long-time polarization measurements in the case of supported bimetallic catalysts. Since the former yields activities characteristic of clean catalyst surfaces and the latter type of experiment is more indicative of the long-term activity of a partially deactivated catalyst, it is desirable to attain both kinds of information at the same time in order to gain a more fundamental insight into the mechanism of methanol electrocatalysis.

In Chapter 1 we demonstrated that we were able to simultaneously control the surface composition and the active surface area of Pt-Ru alloys which were used to assess the potentiodynamic and the potentiostatic electrocatalytic activity towards the oxidation of methanol in a potential range envisaged to be of interest for the application in a methanol/air fuel cell ($\leq$ 0.5 V *vs* RHE). These well-characterized alloy surfaces in UHV

were transferred into a meniscus-type electrochemical cell and immersed under potential control, so that no further pretreatment was necessary; in addition, positive potentials were limited to 0.750 V *vs* RHE in order to avoid Ru dissolution. Although there are indications in the literature that oxidized Pt-Ru alloys will be reduced in an electrochemical environment at potentials close to the onset of hydrogen evolution [79], we ascertained that all measurements were carried out on purely metallic, oxygen-free alloy surfaces. In the following we report the potentiodynamic and the potentiostatic activity of sputter-cleaned Pt-Ru alloy electrodes in low and high concentrations of methanol ($5.0 \cdot 10^{-3}$M and 0.50 M CH_3OH in 0.50 M H_2SO_4), discuss the connection between the performance of our model catalysts and supported fuel cell catalysts and present a mechanistic interpretation on the electrooxidation of methanol on Pt-Ru alloys.

2. EXPERIMENTAL PROCEDURES

2.1. Electrochemical Measurements

All electrochemical data shown in this chapter were acquired on sample surfaces which had undergone a final sputtering treatment with 0.5 keV Ar^+ ions; the preparation of the alloy surfaces was outlined in Section 2 of Chapter 1. The sputter-cleaned and UHV characterized specimens were withdrawn from the UHV introduction port (backfilled with argon, Matheson, research grade) into air and immediately covered with a drop of triply pyro-distilled water, as is shown in Figure 2-1. They were then transferred into a standard three-compartment meniscus-type electrochemical cell and contacted with freshly prepared 0.50 M H_2SO_4 (25.0 ml, Baker Analyzed® Ultrex® ultrapure reagent) under potential control at 0.075 V *vs* RHE within less than two minutes. For methanol experiments, methanol (Baker Analyzed®, absolute methanol) was present in the electrolyte during immersion and the electrodes were equilibrated for three minutes at the

immersion potential. A very similar cell and transfer procedure are described in Reference [80]; Figure 2-2 shows the contact of the meniscus drawn between the electrolyte surface and the UHV-characterized sample (transfer time is ≈2 minutes).

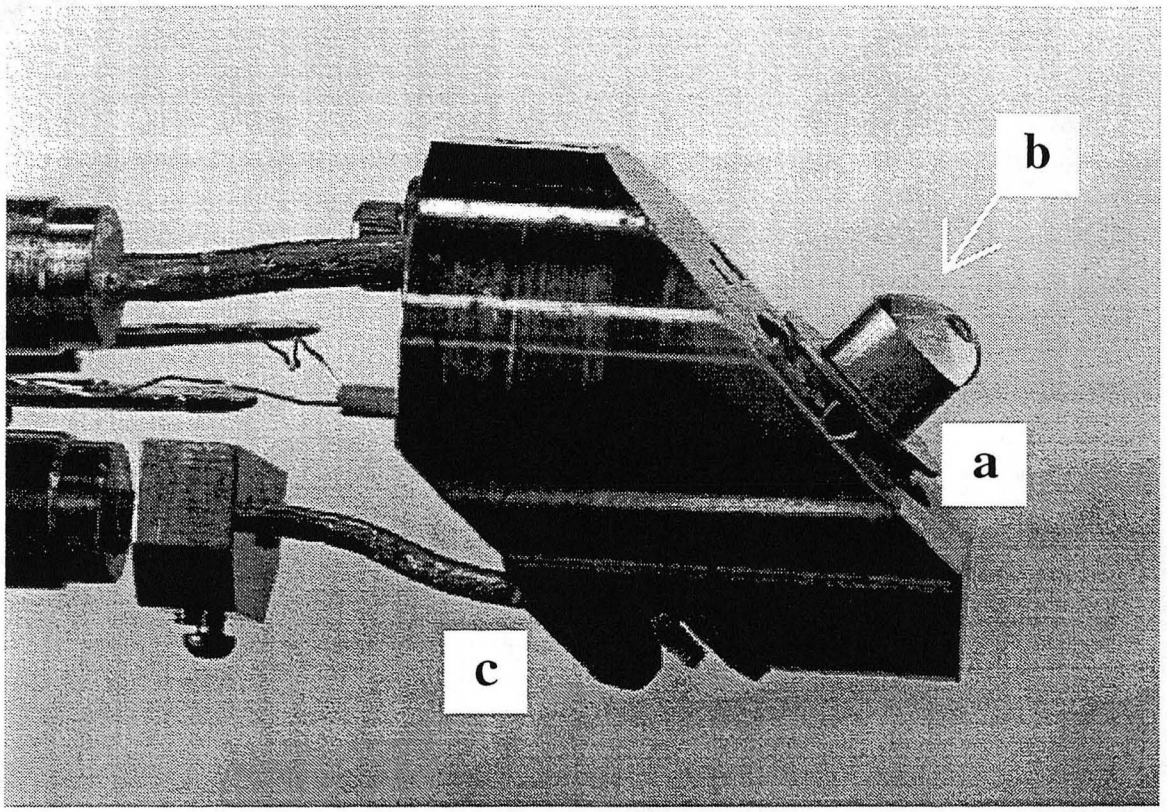

Figure 2-1. UHV sample holder with an alloy sample protected by a drop of water during the transfer from UHV into the electrochemical cell: **(a)** cylindrical alloy sample; **(b)** UHV-characterized cylinder face covered by a water drop; **(c)** heater.

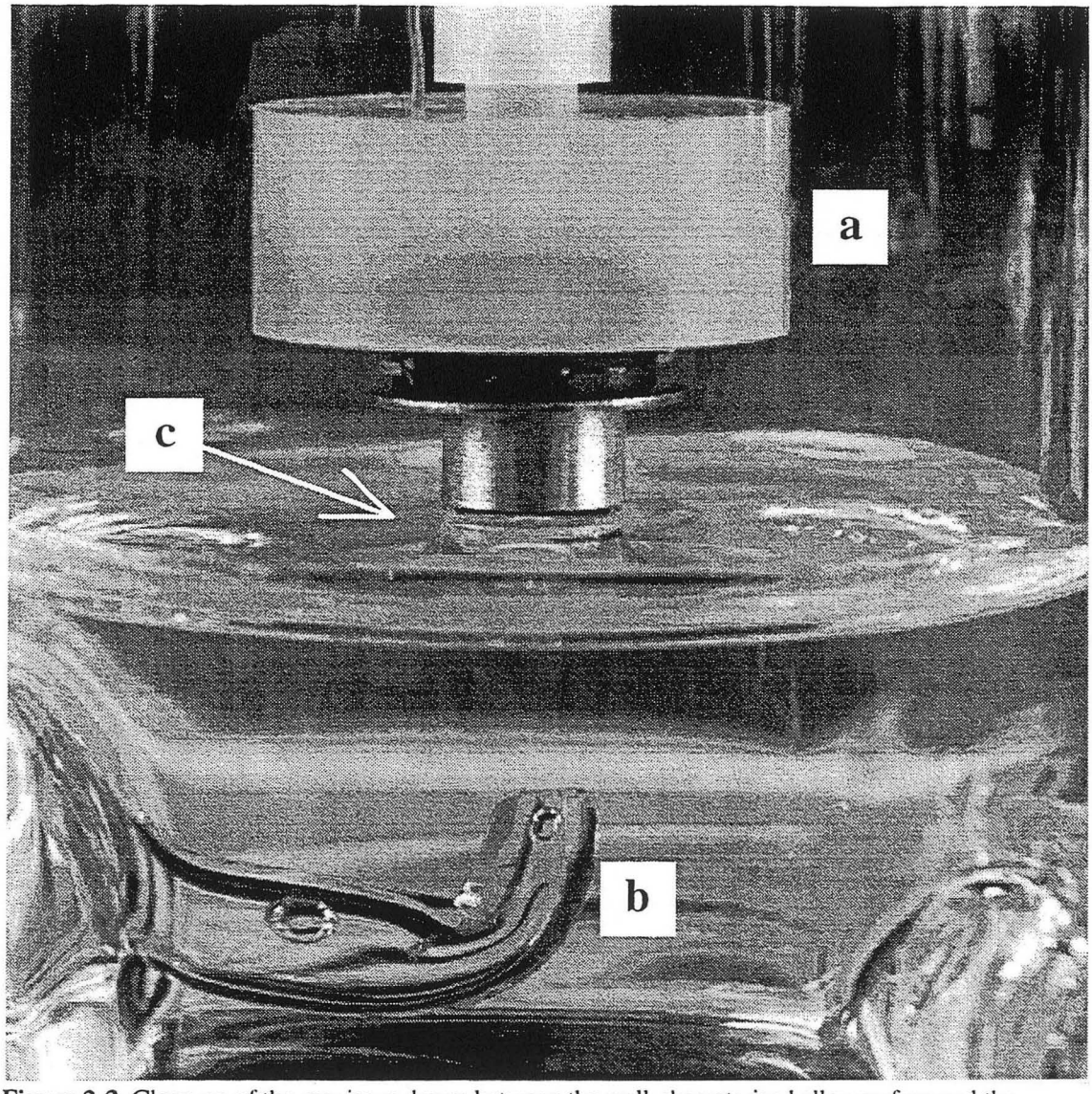

Figure 2-2. Close-up of the meniscus drawn between the well-characterized alloy surface and the electrolyte: (**a**) Kel-F holder; (**b**) Luggin-capillary; (**c**) meniscus.

All electrochemical data on UHV prepared specimens were acquired within the potential range of 0.04 and 0.75 V RHE and their potentiodynamic response in the 0.50 M H_2SO_4 supporting electrolyte remained unchanged after the first cycle, indicating the stability of the alloys under our conditions. In potentiodynamic experiments the initial sweep was going in a negative potential direction and the positive potential limit was 0.7 V RHE; in potentiostatic experiments the potential was stepped from the immersion potential to 0.5 V RHE. A Pd/H reference electrode was used, but all potentials in the

following are referred to the reversible hydrogen electrode in the same solution; the sweep rate in cyclic voltammetry was always 20 mV/s. All measurements were carried out at 25°C.

2.2. Sample Transfer Test

The validity of the transfer procedure from UHV into the electrochemical cell was verified with the platinum sample, since platinum is known to be extremely susceptible to the adsorption of impurities from the environment, resulting in a partial blocking of surface sites by adsorbed organics. The characterization of a clean Pt electrode surface in UHV by AES is depicted in Figure 2-3a, exhibiting the AES signals of Pt and clearly showing the absence of surface active impurities like carbon as well as the absence of oxygen. After the transfer into the electrochemical cell described above, the hydrogen desorption region in the cyclic voltammetry, Figure 2-3b, shows the well-known features of clean polycrystalline platinum [81]. The coulometric charge of hydrogen desorption based on the geometric area is 220 $\mu C/cm^2$, indicating a surface roughness factor of one (210 $\mu C/cm^2$ in Reference 82, 220 $\mu C/cm^2$ in Reference 81). Anodization for one minute at 1.4 V produced a negligible change in the hydrogen desorption area and, therefore, we conclude that our sample transfer from UHV into the electrochemical cell is possible without significant accumulation of adsorbed impurities onto the electrode surface. This also indicates that sputter roughening during the cleaning in UHV does not occur under our experimental conditions so that all current densities in the following are normalized to geometric sample areas, implying a surface roughness factor of one.

3. RESULTS

3.1. UHV Characterization

LEIS measurements presented in Chapter 1 are once more summarized for five

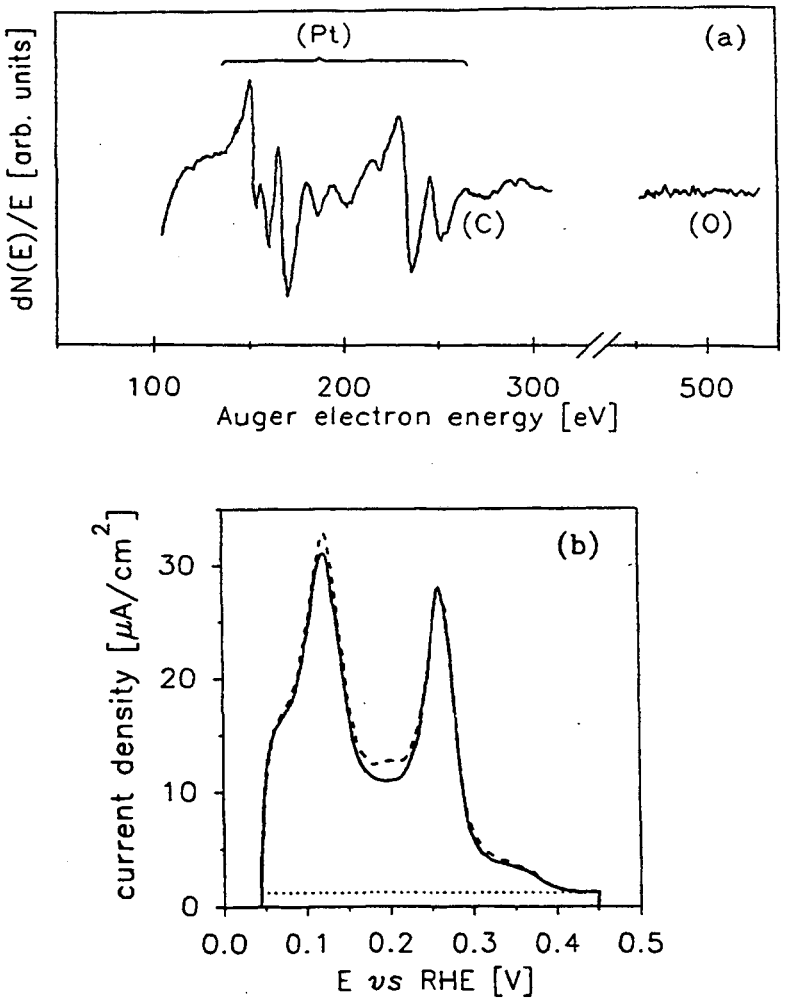

Figure 2-3. **(a)** Auger spectrum of a sputter-cleaned (0.5 keV Ar^+) Pt electrode. **(b)** Hydrogen desorption area of the above electrode in 0.50 M H_2SO_4 at 20 mV/s: (——) second sweep after the transfer with a positive potential limit of +0.750 V; (- - - -) after anodization at +1.4 V for one minute; (· · · · ·) double layer capacity.

sputter-cleaned (0.5 keV Ar^+) Pt-Ru specimens, Figure 2-4a. Within the experimental error of the analysis, surface and bulk compositions of sputter-cleaned alloys are essentially identical, as is expected since the two metals have very similar sputter cross-sections [19].

Annealing of sputtered surfaces in UHV at 800°C effects a strong surface enrichment of platinum as shown in Figure 2-4b, which in Chapter 1 was shown to be due to the lower surface free energy of platinum compared to ruthenium and the solid lines in Figure 2-4b are based on the presented thermodynamic ideal solution model. The miscibility gap of Pt-Ru bulk alloys between 38 and 20 atomic% of ruthenium is

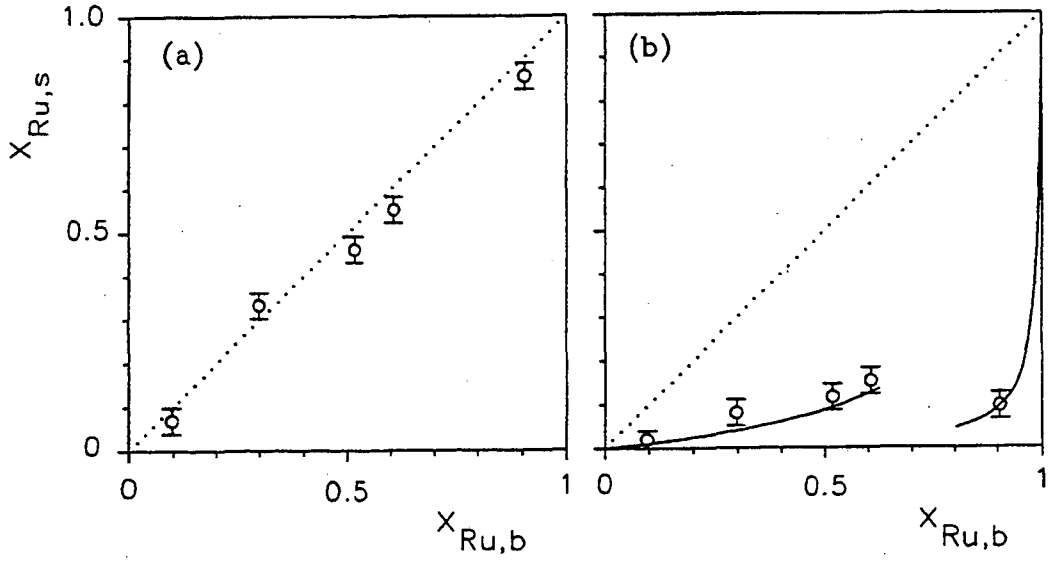

Figure 2-4. Ruthenium surface ($x_{Ru,s}$) vs bulk ($x_{Ru,b}$) composition for Pt-Ru bulk alloys: **(a)** sputtered alloys at 0.5 keV Ar^+; **(b)** annealed alloys at 800°C in UHV, where (——) represents a thermodynamic ideal solution model; (· · · · ·) diagonal.

indicated in the figure. In general, there is very good agreement between our surface enrichment measurements on bulk alloys and platinum surface enrichment measured on bimetallic Pt-Ru clusters supported on either alumina or silica [73], which were prepared by a similar method as is used for Pt-Ru fuel cell electrodes supported on carbon [63]. The final step in the preparation of Pt-Ru clusters is usually a reduction in hydrogen at approximately 400°C over extended periods of time, thereby facilitating the formation of an equilibrium surface similar to annealing in UHV.

3.2. Electrochemical Measurements

3.2.1. Voltammetry in the Supporting Electrolyte

Figure 2-5a gives a comparison of the voltammetry of platinum and ruthenium. Their potentiodynamic response attained a stable steady-state after the first cycle. Anodic and cathodic charges during a full cycle were identical even for the ruthenium electrode, which otherwise is known to exhibit strongly irreversible surface processes if high sweep rates or more positive potentials are applied [76]. For the entire potential range, the voltammetric response of ruthenium compared well with "activated" ruthenium electrodes as reported in References 83 and 78. We suspect that the "activation" of Ru described in the above references merely attests to the *in-situ* "electrochemical annealing" or cleaning of ruthenium during extended potential cycling into the potential region of bulk RuO_2 formation (≈1.1 V). In contrast to the voltammetry of platinum, where the potential range for the desorption of hydrogen ($0 \leq E \leq 0.3$ V) and the formation of surface oxide precursors ($E \geq 0.7$ V) are clearly separated by the double layer region ($0.3 \leq E \leq 0.7$ V), the voltammetric response of ruthenium does not allow a simply potential dependent distinction of these surface processes. The overlap of hydrogen desorption and oxide formation regions on Ru electrodes which seems to be indicated in Figure 2-5a, was investigated *via* "chloride blocking" experiments and electroreflectance experiments by

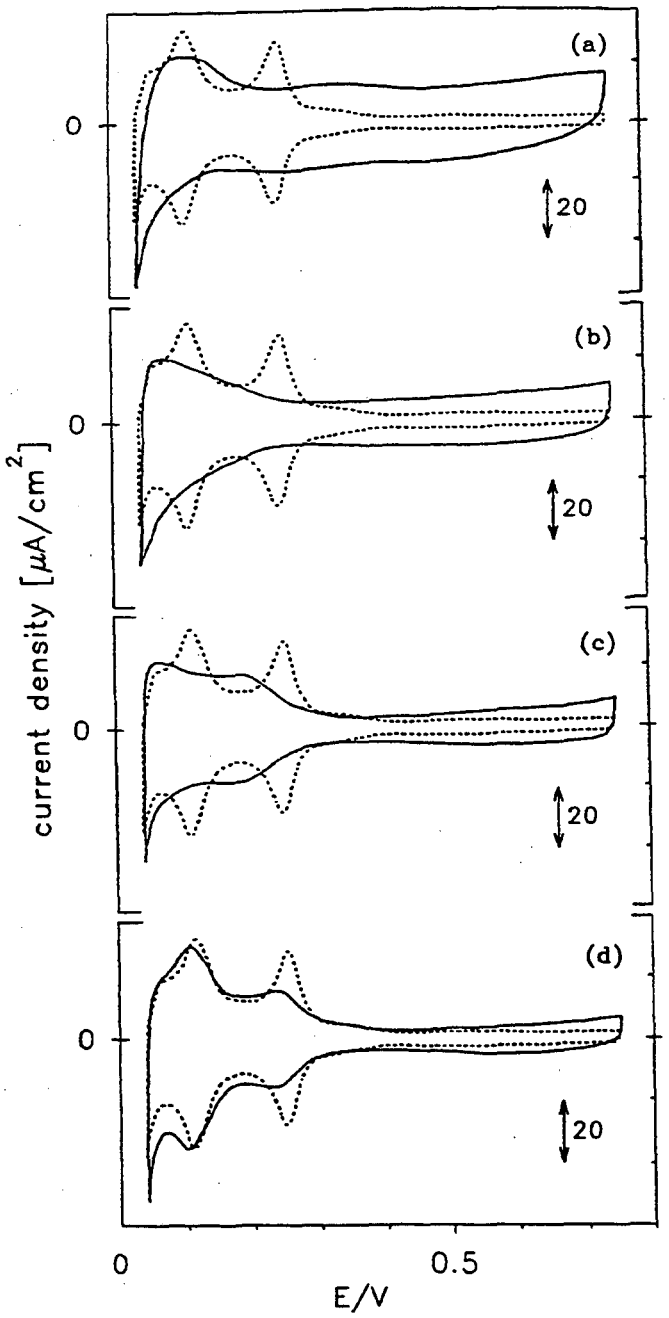

Figure 2-5. Cyclic voltammetry of sputtered Pt, Ru and Pt-Ru alloys in 0.5 M H_2SO_4 at 20 mV/s; (- - - -) Pt potentiodynamic response given for reference. (——) Ru and Pt-Ru potentiodynamic response for: **(a)** pure Ru; **(b)** 46 atomic% Ru surface composition (PtRu-4 bulk alloy, see Table 1-1); **(c)** 33 atomic% Ru surface composition (PtRu-5 bulk alloy, see Table 1-1); **(d)** 7 atomic% Ru surface composition (PtRu-3 bulk alloy, see Table 1-1).

Hadzi-Jordanov *et al* [75] as well as *via* ellipsometric measurements by Ticanelli and coworkers [84]. Both groups concluded that the onset of the adsorption oxygen-like species would occur at potentials as low as 0.2 V, such that it coincides with the desorption of hydrogen. Therefore, they concluded that electrochemical surface areas on ruthenium electrodes could not be assessed by coulometry. For this reason, voltammetric currents on ruthenium electrodes are always quoted as either absolute currents or as current densities based on superficial surface areas. Besides our study we are not aware of any reports in the literature which would give capacitive current densities of ruthenium based on real rather than superficial surface areas.

As we have outlined above, the terms "hydrogen region" referring to the potential range between 0 and 0.3 V, and "double layer region" referring to the potential range between 0.3 and 0.7 V are only meaningful in the context of the cyclic voltammetry of platinum, and bear no specific meaning in the case of ruthenium and Pt-Ru alloys. For the sake of clarity, however, we will in the following discussion apply these terms to indicate the above potential regions in the cyclic voltammetry of both Ru and Pt-Ru alloys.

Figures 2-5b through 2-5d show the effect of reducing the bulk and surface composition of ruthenium in the sputtered Pt-Ru alloys on the cyclic voltammetry; the cyclic voltammetry of Pt was added for comparison. The voltammetry of the alloy with ≈50 atomic% Ru on the surface (PtRu-4) in Figure 2-5b displays no distinct features in the "hydrogen region" but is characterized by large capacitive currents in the "double layer region". As the ruthenium surface concentration is reduced to ≈30 atomic% (PtRu-5, Figure 2-5c) and then to ≈10 atomic% (PtRu-3, Figure 2-5d), the "double layer" currents decrease and the "hydrogen region" begins to resemble the features of pure platinum. The major change in the voltammetric response due to Ru in the Pt surface is the increasing ratio of the "double layer" currents over the currents in the "hydrogen region" as the ruthenium surface concentration is increased, indicating the adsorption of

oxygen-like species at progressively more negative potentials, as was noted also by Ticanelli *et al.* [84]. This plays an important role in the electrooxidation of methanol, which we will address in the following.

3.2.2. Voltammetry in the Presence of Methanol

During the first positive going voltammetric sweep of platinum in 5.0 mM CH_3OH, insert of Figure 2-6a, no change in the hydrogen region is observed, in agreement with methanol adsorption isotherms measured by various authors [85,86], which show that the equilibrium coverage of methanol on a clean, *i.e.* "unpoisoned", platinum surface is negligible below ≈0.1 V. After the almost complete desorption of hydrogen, methanol oxidation currents commence at potentials as low as 0.3 V. Upon returning from 0.75 V in the first negative going sweep a significant fraction of the "hydrogen region" is now blocked, *i.e.*, partially covered by adsorbed organic residues derived from the oxidation of methanol. It has been established *via* radiotracer experiments by Horányi *et al* [87] and *via* infrared measurements by Kunimatsu [88] that methanol dehydrogenation fragments adsorbed at potentials above 0.2 V and above 0.4 V, respectively, cannot be desorbed to any significant extent at lower potentials, thereby effecting the partial blocking of the electrode surface for hydrogen adsorption in the negative going sweep. The 10th sweep in the cyclic voltammetry attests to the strong deactivation of the platinum electrode during the sustained electrooxidation of methanol, commonly referred to as "poisoning" such that no significant oxidation currents persist any more at potentials lower than 0.5 V.

The oxidation currents on platinum in a 0.5 M CH_3OH solution, Figure 2-6b, are very similar to what was observed in a 5.0 mM solution, except that the blocking of the "hydrogen region" by methanol dehydrogenation fragments after the first positive going sweep is increased. This is consistent with the concentration dependence of the methanol

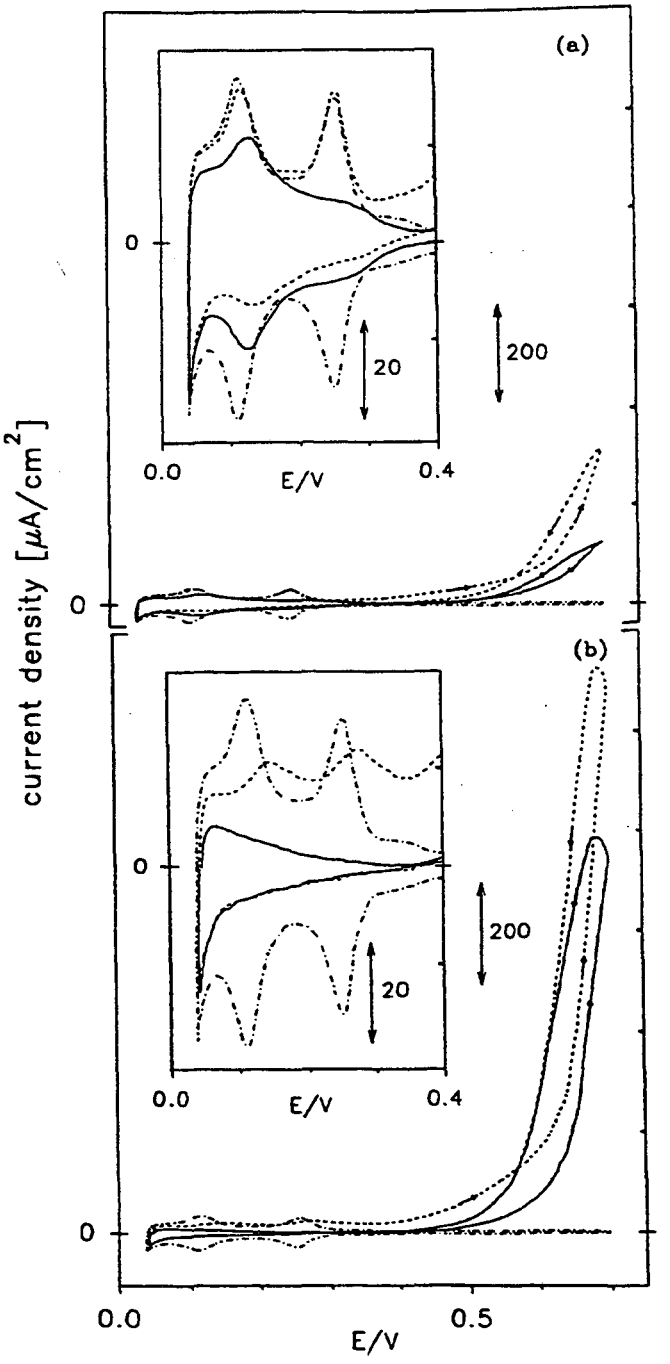

Figure 2-6. Cyclic voltammetry of sputtered Pt in 0.5 M H_2SO_4 at 20 mV/s in **(a)** 5.0 mM CH_3OH and **(b)** 0.5 M CH_3OH: (—·—·—) without CH_3OH; (– – –) first sweep; (——) tenth sweep. Pt was contacted with the methanol solution at 0.075 V. The inserts provide a magnification of the "hydrogen region" by a factor of ≈10.

adsorption isotherm [85,86]. It is important to note, however, that the methanol oxidation currents in the measured potential range increased by not more than a factor of ≈5, although the methanol concentration was increased by a factor of 100. It will be shown in Section 3.2.3 that this very weak dependence of oxidation currents on the concentration of methanol is not observed for the Pt-Ru alloys.

Voltammetry in a 0.5 M CH_3OH solution (Figure 2-7) shows that there is neither methanol adsorption on Ru nor are there any appreciable oxidation currents below 0.75 V. Similarly, radiotracer measurements by Franaszczuk *et al* [89] on Ru electrodeposited on Pt have established that methanol adsorption in electrolyte does not occur on Ru in the potential range of our study.

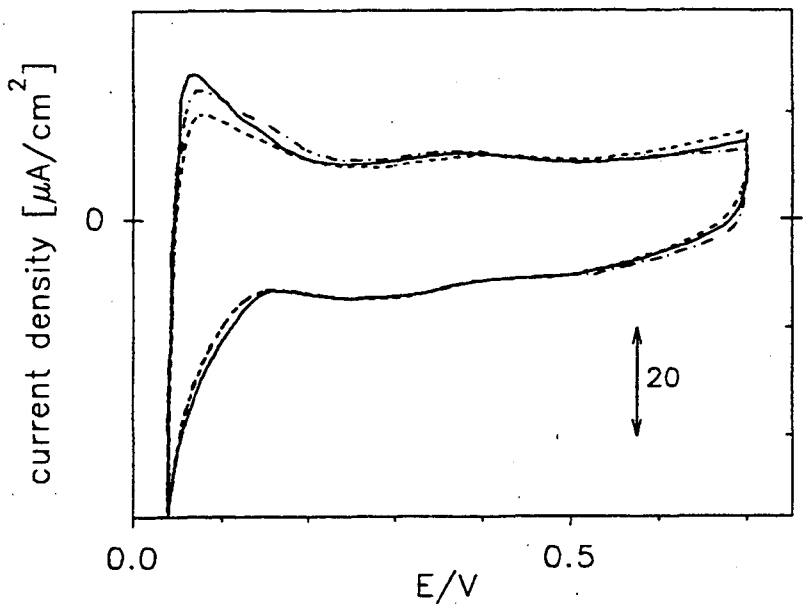

Figure 2-7. Cyclic voltammetry of sputtered Ru in 0.5 M H_2SO_4 at 20 mV/s in 0.5 M CH_3OH: (—·—·—) without CH_3OH; (– – –) first sweep; (——) tenth sweep. Ru was contacted with the methanol solution at 0.075 V.

The electrooxidation of methanol on an alloy with a surface composition of ≈50 atomic% ruthenium (PtRu-4) in 0.5 M CH_3OH is shown in Figure 2-8a. The most striking differences to the observations made on Pt is the small extent of deactivation

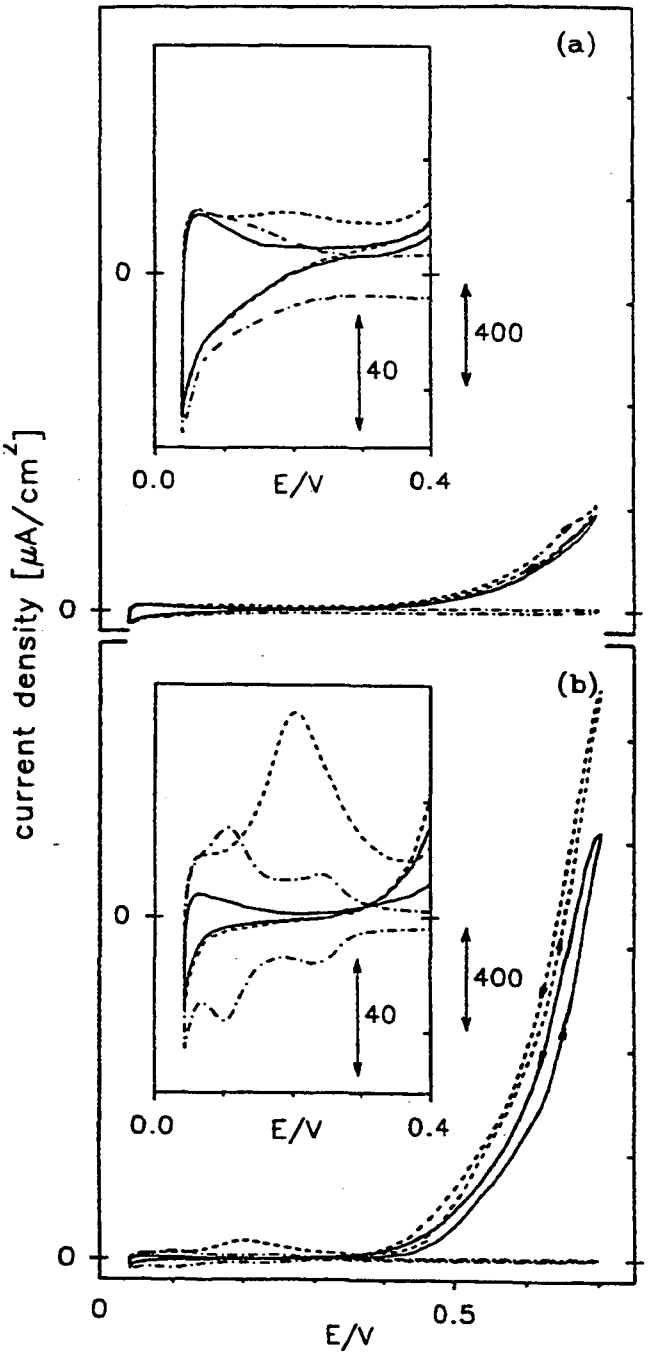

Figure 2-8. Cyclic voltammetry of sputtered Pt-Ru alloys in 0.5 M H_2SO_4 at 20 mV/s in 0.5 M CH_3OH: (–·–·–) without CH_3OH; (– – –) first sweep; (——) tenth sweep. **(a)** 46 atomic% Ru surface composition (PtRu-4 bulk alloy, see Table 1-1); **(b)** 7 atomic% Ru surface composition (PtRu-3 bulk alloy, see Table 1-1). Alloys were contacted with the methanol solution at 0.075 V. The inserts provide a magnification of the "hydrogen region" by a factor of ≈10.

between the first and the 10th cycle in conjunction with the small degree of adsorbed organic residues, evident from the comparison of the "hydrogen region" in the absence and in the presence of methanol. In contrast to the current literature, which suggests the strongest enhancement of methanol oxidation currents (*versus* pure Pt) for a 50 atomic% Pt-Ru alloy [*e.g.* 64, 66 and 90], a comparison of Figures 2-6b and 2-8a seems to indicate higher activities on the platinum electrode. The electrocatalytic activity of a surface with only ≈10 atomic% ruthenium (PtRu-3) recorded in Figure 2-8b, however, exhibits a very strong activity enhancement compared to platinum. During the first positive going sweep, the onset of methanol oxidation concurrent with the desorption of hydrogen appears to occur at ≈0.2 V, in agreement with data reported by Krausa *et al* [91]. This oxidation reaction obviously facilitated by Ru at low potentials is observed only during the first sweep, occurs to a lesser extent on the alloy with a Ru surface composition of ≈30 atomic%, and is only just distinguishable in the insert of Figure 2-8a on the ≈50 atomic% Ru surface; according to the spectroscopic measurements in Reference 91 no production of CO_2 is observed during this process and its origin is not yet understood. The strong attenuation of this reaction with increasing Ru content seems to derive from the reduced adsorption of methanol on Ru-rich surfaces. On pure Pt the oxidation of methanol at such low potentials cannot occur, therefore this feature is not observed in the first sweep.

To facilitate a qualitative comparison of the platinum electrode with Pt-Ru alloy electrodes of different Ru surface concentrations, Figure 2-9a depicts methanol oxidation current densities (*viz.*, the difference between overall and capacitive current densities) for the first positive going sweep in a 5.0 mM CH_3OH solution. Quite obviously, the pure platinum surface and the ≈10 atomic% ruthenium surface yield current densities higher than the Ru-rich alloys in the entire potential range. Because of the negligible methanol adsorption at the immersion potential (References 85 and 86, and Figure 2-6a) in

conjunction with the slow rate of methanol adsorption within the time frame of the first positive going sweep [85, 92], the currents in Figure 2-9a mainly represent the initial rate of methanol dehydrogenation on an "unpoisoned" surface. For Pt these current densities are ≈50 times larger than at the steady-state, as will be shown in Section 3.2.3. The strong decrease of dehydrogenation currents for increasing ruthenium surface concentrations (Figure 2-9a) follows from the lack of methanol adsorption on Ru: the smaller number of Pt surface sites on Pt-Ru alloys effectively reduces the available surface area for the adsorption of methanol. In addition, as we will discuss later, the strong attenuation of methanol dehydrogenation on the Ru-rich alloys is due to the requirement of platinum atom ensembles for methanol adsorption. Therefore, the data in Figure 2-9a characterize the rate of adsorption on "unpoisoned" Pt versus Pt-Ru alloys rather than their intrinsic electrocatalytic activity. This argument is further supported by the behavior of the ≈10 atomic% Ru alloy, which in terms of methanol adsorption should essentially behave like pure Pt, as it does in Figure 2-9a, but which exhibits a much higher electrocatalytic activity than Pt in steady-state experiments at methanol electrooxidation potentials, which we will present in Section 3.2.3.

By means of recording successive voltammetric sweeps, the catalyst surfaces experience an increased coverage with adsorbed organic residues (see *e.g.*, Figures 2-6 and 2-8), resulting in a decreased current density on platinum of approximately one order of magnitude, as is shown in Figure 2-9b. Now the alloy with ≈10 atomic% Ru on the surface exhibits superior activity compared to Pt in the entire potential range, attesting to a smaller extent of electrode deactivation. The alloy with ≈50 atomic% Ru is much less active than platinum, in contrast to what we might expect according to the literature. The extent and rate of deactivation of platinum *versus* Pt-Ru alloys by methanol dehydrogenation fragments is significantly increased in a 0.5 M methanol solution, illustrated by the 10th positive going sweep in Figure 2-9c. We find now that the optimum

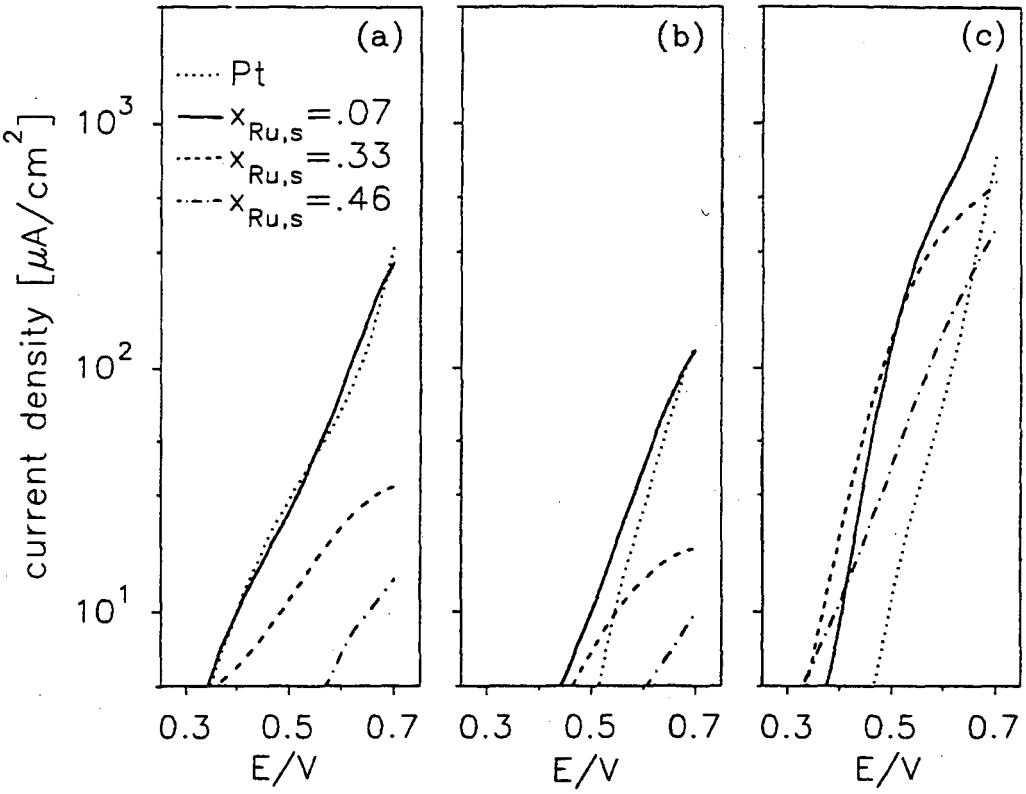

Figure 2-9. Faradaic current densities in the positive going sweeps in the cyclic voltammetry of sputtered Pt and Pt-Ru alloys in 0.5 M H_2SO_4 at 20 mV/s. **(a)** first sweep in 5.0 mM CH_3OH; **(b)** 10th sweep in 5.0 mM CH_3OH; **(c)** 10th sweep in 0.5 M CH_3OH. The alloy surface compositions are shown in the figure legend. Purely capacitive current densities were subtracted.

Ru surface composition for methanol oxidation is a function of the electrode potential: progressively smaller surface concentrations of Ru are required as the electrode potential (*i.e.*, the current density) is increased. More importantly, the negative potential shift of the voltammetric current response as the methanol concentration is increased by a factor of 100 (Figures 2-9b and 2-9c) is relatively small for both Pt and the ≈10 atomic% Ru alloy (≈0.05 V) in contrast to the large negative potential shift of ≈0.3 V for the ≈50 atomic% alloy. This very strong dependency on the methanol concentration shown by Ru-rich alloys points towards the competition between adsorption rates and the rates of oxidative removal of adsorbed organic intermediates on Pt-Ru alloys. An analogous observation for a Pt-Ru and a Pt electrode was made by Éntina *et al* [93].

Since we have observed very different behavior of Pt-Ru alloy electrodes depending on the number of sweeps in the cyclic voltammetry, it is questionable whether any conclusions regarding their long-term activity can be drawn from this type of data. Knowledge of the long-term activity is essential for the successful implementation of the alloy in fuel cell electrodes. One might suspect, that Figures 2-9b and 2-9c should give a fairly good qualitative representation of the long-term activity of different alloy compositions at any given potential and concentration. If this were true, we would infer from Figure 2-9b that the most active surface at 0.5 V in 5.0 mM CH_3OH solution should be the ≈10 atomic% Ru alloy, followed by the ≈30 atomic% alloy, followed by platinum; the ≈50 atomic% alloy should exhibit very little activity. Similar inferences could be drawn from Figure 2-9c for a 0.5 M CH_3OH solution. To test this hypothesis, we conducted potentiostatic measurements at 0.5 V.

3.2.3. Potentiostatic CH_3OH Oxidation on Pt-Ru Alloys

The relative activities of Pt, the ≈10 atomic% and the ≈50 atomic% Ru alloy in 5.0 mM CH_3OH at 0.5 V, shown in Figure 2-10a, are in good agreement with what we would have predicted from their voltammetry in Figure 2-9b. Furthermore, the behavior of the different electrodes at short times illustrated in the insert of Figure 2-10a is reminiscent of the relative activities observed in the first sweep of the cyclic voltammetry, Figure 2-9a. Over longer periods of time, however, the electrocatalytic activity of the ≈50 atomic% alloy increases in relation to platinum, *i.e.*, the deactivation of Pt proceeds at a faster rate than what is observed for the alloys. The insert of Figure 2-10b shows that initially the same relative activities are observed in a 0.5 M CH_3OH solution as were developed at lower concentrations. After several seconds, however, the ≈50 atomic% Ru surface exhibits a higher catalytic activity towards the oxidation of methanol than platinum, but the ≈10 atomic% Ru electrode is still the most active electrocatalyst.

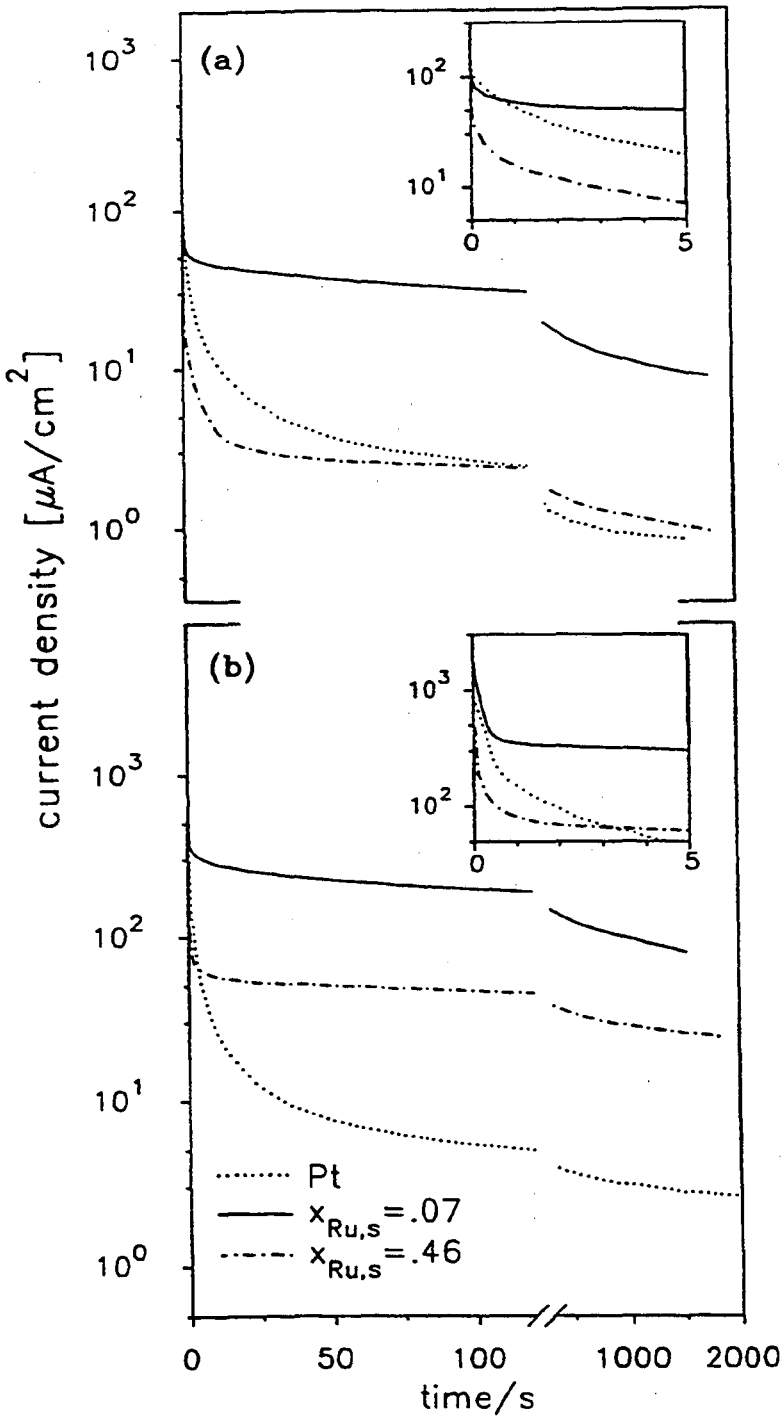

Figure 2-10. Potentiostatic methanol oxidation current densities on Pt and Pt-Ru alloys at 0.5 V in 0.5 M H_2SO_4: **(a)** in 5.0 mM CH_3OH; **(b)** in 0.5 M CH_3OH. The alloy surface compositions are shown in the figure legend.

The concentration dependencies of the different catalyst surfaces as well as the catalytic superiority of the alloy catalysts over pure platinum at 0.5 V are summarized in Table 2-1. The most striking difference between the three samples lies in the concentration dependence of the currents: although the CH_3OH concentration is changed by a factor of 100, methanol oxidation currents on pure Pt increase by only a factor of 3, whereas the current densities on the ≈50 atomic% Ru alloy increase by a factor of 25. This strong effect of surface composition on the concentration dependence of the oxidation current has important implications for the reaction pathway and changes in the rate determining step due to Ru in the surface. In summary: the most significant catalytic enhancement over platinum at 0.5 V is observed for the ≈10 atomic% Ru concentration alloy, namely a factor of 12 in 5.0 mM CH_3OH and a factor of 30 in 0.5 M CH_3OH.

Table 2-1. Methanol oxidation current ratios at 0.5 V from Figure 2-10 (averaged between 10 and 30 minutes). CH_3OH concentrations and alloy surface compositions in atomic% Ru are indicated below (for bulk compositions see Table 1-1).

	Pt	7% Ru (PtRu-3)	46% Ru (PtRu-4)
$i_{0.5\,M} / i_{5.0\,mM}$	3	8	24
$\left(i_{alloy} / i_{Pt}\right)_{5.0\,mM}$	--	12	≈1
$\left(i_{alloy} / i_{Pt}\right)_{0.5\,M}$	--	30	9

4. DISCUSSION

In our study we were able for the first time to carefully control both the surface composition of Pt-Ru alloys as well as their true surface area, rather than knowing only bulk composition and the superficial geometric area. Before discussing the mechanism of the electrooxidation of methanol on Pt-Ru alloys based on the presented data, we would

like to emphasize the most pertinent observation stated in Section 3, *viz*, that the most active surface for the electrooxidation of methanol (ranging from 0.005 to 0.5 M) at 25°C and 0.5 V in 0.5 M H_2SO_4 is a Pt-Ru alloy with a Ru surface concentration of ≈10 atomic%. This is in apparent contrast to the current literature, which consistently reports a ≈50 atomic% Pt-Ru alloy to be the most active surface towards the electrooxidation of methanol [*e.g.*, 64, 66 and 90]. This comparison does not, however, take adequate account of the significant difference between bulk and surface composition in the Pt-Ru system. As we have shown by LEIS experiments, annealed Pt-Ru alloys exhibit a very strong surface enrichment of Pt and a similar effect is expected to occur during the preparation of supported Pt-Ru electrodes. Furthermore, the usual "pretreatment" of high surface area electrodes involves potential cycling to relatively positive potentials, effecting preferential dissolution of Ru and, possibly, "electrochemical annealing" of the electrode surface. This implies that electrodes of a nominal 50 atomic% Ru bulk composition will exhibit very much lower concentrations of Ru on the surface, as low as ≈15 atomic%. Therefore, it is likely that the actual Ru surface concentrations employed in many previous literature studies were very similar to our ≈10 atomic% Ru surface.

In addition to the surprisingly high activity of an alloy with a Ru surface composition of only ≈10 atomic%, we have found indications that the activity of Pt-Ru alloy electrodes toward the electrooxidation of methanol is a balance of the primarily concentration dependent rate of the dissociative chemisorption of methanol and the potential dependent oxidation rate of "poisons" accumulated on the surface during sustained methanol oxidation.

4.1. Accumulated Surface "Poisons"

Numerous investigations on the nature of these surface "poisons" on a platinum electrode, derived from the electrooxidation of methanol have been conducted over the past twenty years. Two principally different *in-situ* methods were employed: infrared spectroscopy and differential electrochemical mass spectroscopy (DEMS), both of which yielded very different conclusions, giving rise to much controversy. In summary, linearly bonded CO ($*C{\equiv}O^{|}$, where the asterisk symbolizes the substrate/adsorbate bond) is the primary surface "poison" detected by different infrared spectroscopies, *viz.*, electrochemically modulated infrared spectroscopy (EMIRS, *e.g.*, [94]), single potential alteration infrared spectroscopy (SPAIRS, e.g., [95]), and polarization modulated infrared reflection-adsorption spectroscopy (PM-IRRAS, *e.g.*, [88, 96]); bridge bonded CO ($\ddagger C{=}\underline{\bar{O}}$) is generally detected as a minor species at short times. In contrast, the major "poisoning" surface species detected *via* DEMS experiments in combination with radiotracer experiments are formyl (CHO, *e.g.*, [97]) and methyl ($\ddagger COH$, *e.g.*, [98]) species. At present it is believed that the discrepancy between the various *in-situ* techniques derives from different experimental conditions, and it has been concluded that linearly bonded CO is the major long-term "poison", whereas formyl and methyl species are formed primarily on "unpoisoned" electrodes, *i.e.*, at short times in combination with low methanol concentrations [99]. In addition to the above *in-situ* studies on the interaction of Pt with methanol, the current scientific literature provides numerous investigations on the decomposition of methanol on both Pt and Ru in UHV, which we will examine in the following to complement our understanding of their different electrocatalytic activity for the oxidation of methanol in electrolyte.

4.2. UHV *vs* Electrochemistry on Pt and Ru

A comparison of the cyclic voltammetry of Ru (Figure 2-7) with Pt (Figure 2-6) in the presence of methanol shows that there is no significant interaction of Ru with methanol. This observation is very surprising in view of the experimental results on the adsorption and decomposition of methanol in UHV on both Pt and Ru single crystal surfaces. Methanol adsorbs molecularly on Pt(111) [100] and Pt(110) [101, 102] at temperatures below ≈170 K and decomposes into molecularly adsorbed H and CO above ≈170 K on the clean single crystal surfaces. In the presence of preadsorbed oxygen, adsorbed methoxy is formed at ≈140 K, but it decomposes into adsorbed CO and H at ≈170K. On Ru(001) [103, 104] molecularly adsorbed methanol decomposes into methoxy surface species on both clean and oxygen precovered surfaces at temperature as low as 85 K. Again, above ≈230 K adsorbed methoxy decomposes into adsorbed H and CO. Therefore, for both Pt and Ru we would expect adsorbed CO and H to be the stable methanol decomposition products at room temperature, which explains why *in-situ* electrochemical measurements have failed so far to detect any significant amounts of methoxy surface species. The driving force for the low temperature decomposition of methanol and methoxy surface species into adsorbed CO and H is the very large heat of adsorption of both species on Ru and Pt surfaces, *e.g.*, ≈30 kcal/mole for CO and ≈17.8 kcal/mole for H adsorbed on Pt [100]; the respective values for Ru surfaces are within approximately ≈20% of the above values [105]. If the metal surfaces are precovered with strongly adsorbed atoms or molecules, the favorable lowering of the overall free energy upon the decomposition of methanol by the high adsorption energies of H and CO will be reduced by the desorption energy of preadsorbed surface species. This effect may render the decomposition reaction thermodynamically unfavorable and, indeed, no methanol adsorption is observed in UHV on Ru(001) with a full monolayer coverage of oxygen [103]. Since Pt and Ru behave very similarly in UHV, why do they

display vastly different methanol adsorption properties in the electrochemical environment? The adsorption of methanol on Pt commences above ≈0.1 V [85, 86], where the surface is only partially covered by hydrogen, and it seems that the methanol adsorption isotherm follows very closely the desorption of hydrogen on Pt, leaving bare Pt sites. The maximum in the methanol adsorption isotherm is observed in the double layer potential region, where a maximum of bare Pt sites is exposed. In this context it is interesting to note that potentiodynamic current peaks during the oxidation of methanol on Pt single crystals occur at the onset potential for the adsorption of oxygen-like species [106], where the number of bare Pt sites decreases. On Ru, however, the desorption of adsorbed hydrogen is concomitant with the adsorption of oxygen-like surface species, as we have already mentioned (Figure 2-5a), and there does not exist a "double layer region" where a large number of bare Ru surface sites are exposed. Therefore, the driving force for methanol decomposition on this surface, *viz*, the high adsorption energy of H and especially CO, is negated by the desorption energy of oxygen-like species and/or adsorbed hydrogen which cover the Ru surface in the entire potential range. These considerations appear to rationalize the observed behavior of a Ru electrode with methanol. We should mention that it was demonstrated by Hoffmann *et al* [107], that the adsorption energy of CO on Ru(001) in UHV is inversely proportional to the surface coverage with oxygen, decreasing from 38 kcal/mole to ≤11 kcal/mole for a fully oxygen precovered surface.

4.3. Formulation of a Major Reaction Pathway

Based on the above examination of both the *in-situ* and the UHV literature on the interaction of methanol with Pt and Ru, we will now attempt to establish a major reaction pathway for the electrooxidation of methanol on Pt-Ru alloys, relevant to our experimental conditions. Considering that our experiments were focused on the long-term activity of Pt and Pt-Ru electrodes, linearly bonded CO is likely to be the predominant

electrode "poison" during the electrooxidation of methanol. Therefore, we will present in the following an approximate reaction mechanism for methanol oxidation, which will ignore details, but which will capture the essence of the overall process. The first step involves the adsorption of methanol from the bulk of the solution onto the electrode surface and its successive dehydrogenation to form linearly bonded CO:

$$CH_3OH_{sol} \xrightarrow{k_1} CH_3OH_{ads} \xrightarrow{k_2} {}^{*}C{\equiv}O^{l} + 4H^{+} + 4e^{-} \qquad (2\text{-}1)$$

where $^{*}C{\equiv}O^{l}$ represents methanol dehydrogenation fragments bonded to either Pt or Ru on the electrode surface. The adsorption and initial dehydrogenation of methanol yielding $^{*}C{\equiv}O^{l}$, however, does only proceed through Pt sites as we have outlined in Section 4.2. In experiments on a millisecond time scale (≈0.1 s) Franaszczuk *et al* [102] have shown *via* radiotracer experiments that the rate determining step in the electrooxidation of methanol is the initial scission of a methyl hydrogen, *i.e.*, the initial dehydrogenation of methanol. On the time scale of several seconds, however, the oxidation currents decrease by almost two orders of magnitude, indicating a change in the rate determining step due to the accumulation of methanol dehydrogenation fragments on the surface (see Figures 2-6 and 2-8). For these conditions, the simplified mechanism, Equation 2-1, should well represent the dehydrogenation step of methanol. The successive oxidative removal of methanol dehydrogenation products ($^{*}C{\equiv}O^{l}$ in Equation 2-1) is generally thought to proceed through the interaction of CO with coadsorbed oxygen-like species from aqueous electrolyte. The potential dependent discharge of water on Pt and Ru, respectively, to form oxygen-like surface species (symbolized by OH) will be approximated by the following two equations:

$$H_2O + Pt \rightarrow PtOH + H^{+} + e^{-} \qquad (2\text{-}2)$$

$$H_2O + Ru \rightarrow RuOH + H^{+} + e^{-} \qquad (2\text{-}3)$$

Based on cyclic voltammetry and ellipsometry, the adsorption of oxygen-like species on Pt (Equation 2-2) will not occur to any appreciable extent below ≈0.7 V, while it occurs on Ru at potentials as low as ≈0.2 V (Equation 2-3) [84]. Finally, given that the electrode potential is sufficiently positive to coadsorb these oxygen-like species the electrooxidation of the electrode "poison" to CO_2 will be expressed as:

$$*C{\equiv}O^{l} + *OH \xrightarrow{k_3} CO_2 + H^+ + e^- \qquad (2\text{-}4)$$

In the following we will examine our experimental data on the electrooxidation of methanol on Pt-Ru alloys and show that the proposed major reaction pathway (Equations 2-1 through 2-4) is consistent with their experimentally observed behavior.

4.4. Characteristics of Pt-Ru Alloys

As we have already discussed, methanol oxidation currents during the first voltammetric sweep in 5.0 mM CH_3OH (Figure 2-9a) derive mainly from the initial dehydrogenation of methanol on the electrode and finally lead to the build-up of linearly bonded CO according to Equation 2-1. The lower dehydrogenation currents on Ru-rich alloys are understood in terms of the lack of methanol interaction with Ru and the smaller number of Pt sites available for methanol adsorption on the alloys. The exponential decrease in these initial currents as the Ru surface concentration is increased can only be rationalized by assuming that more than one Pt site is necessary for the methanol dehydrogenation reaction. The requirement of multiple sites to facilitate the adsorption of methanol on Pt has been proposed before [61] and it is conceivable that the dehydrogenation reaction, Equation 2-1, would require at least two, possibly even more sites (four were postulated in [61]). By sustaining the electrooxidation of methanol over an extended period of time, the initially high current densities drop by almost two orders of magnitude and the accumulation of linearly bonded CO is clearly visible in the inserts

of Figures 2-6 and 2-8. The rate determining step on pure Pt at steady-state is the oxidative removal of CO *via* the reaction with adsorbed oxygen-like species (Equation 2-4) a hypothesis supported by the negligible increase in oxidation currents following the 100-fold increase in methanol concentration (Figures 2-9a and 2-9bb, Figure 2-10 and Table 2-1). In contrast, the alloy with a Ru surface concentration of ≈50 atomic% significantly reduces the deactivation of Pt by reducing the coverage with linearly bonded CO (insert of Figure 2-8a). Its poor activity in 5.0 mM CH_3OH is due to the reduced rate of methanol adsorption on the Ru-rich surface, Equation 2-1, limiting the overall reaction rate. In 0.5 M CH_3OH, however, methanol adsorption rates are much higher [85, 92] and methanol oxidation currents (at 0.5 V) are 25 times those in 5.0 mM solution. The property of Ru to supply oxygen-like species at relatively low potentials (≤ 0.5 V) to aid the oxidation of adsorbed CO, Equations 2-3 and 2-4, coupled with high methanol adsorption rates produces an electrocatalytic activity for the ≈50 atomic% alloy that surpasses Pt by a factor of 9 (Figure 2-10b). Therefore, it is clear that the mechanism of methanol oxidation on Pt-Ru alloys is characterized by a balance of reduced methanol adsorption rates due to the presence of Ru, Equation 2-1, and the ability of Ru to provide oxygen-like species at lower potentials to remove adsorbed CO. Our results indicate that this balance is optimized for a ≈10 atomic% Ru surface when the oxidation of methanol (0.005 to 0.5 M) is carried out at 25°C and 0.5 V, as shown in Figure 2-10.

4.5. Statistical Interpretation of Bifunctional Pt-Ru Electrodes

In attempting to quantify our mechanistic interpretations outlined above, it is best to envisage a schematic representation of sputtered Pt-Ru alloy surfaces with 10 and 50 atomic% Ru, shown in Figure 2-11a. A random distribution of Pt and Ru surface atoms is expected for sputtered Pt-Ru alloys, since both the bulk phase diagram and estimated enthalpies of mixing indicate a nearly ideal solution behavior of the Pt-Ru bulk system

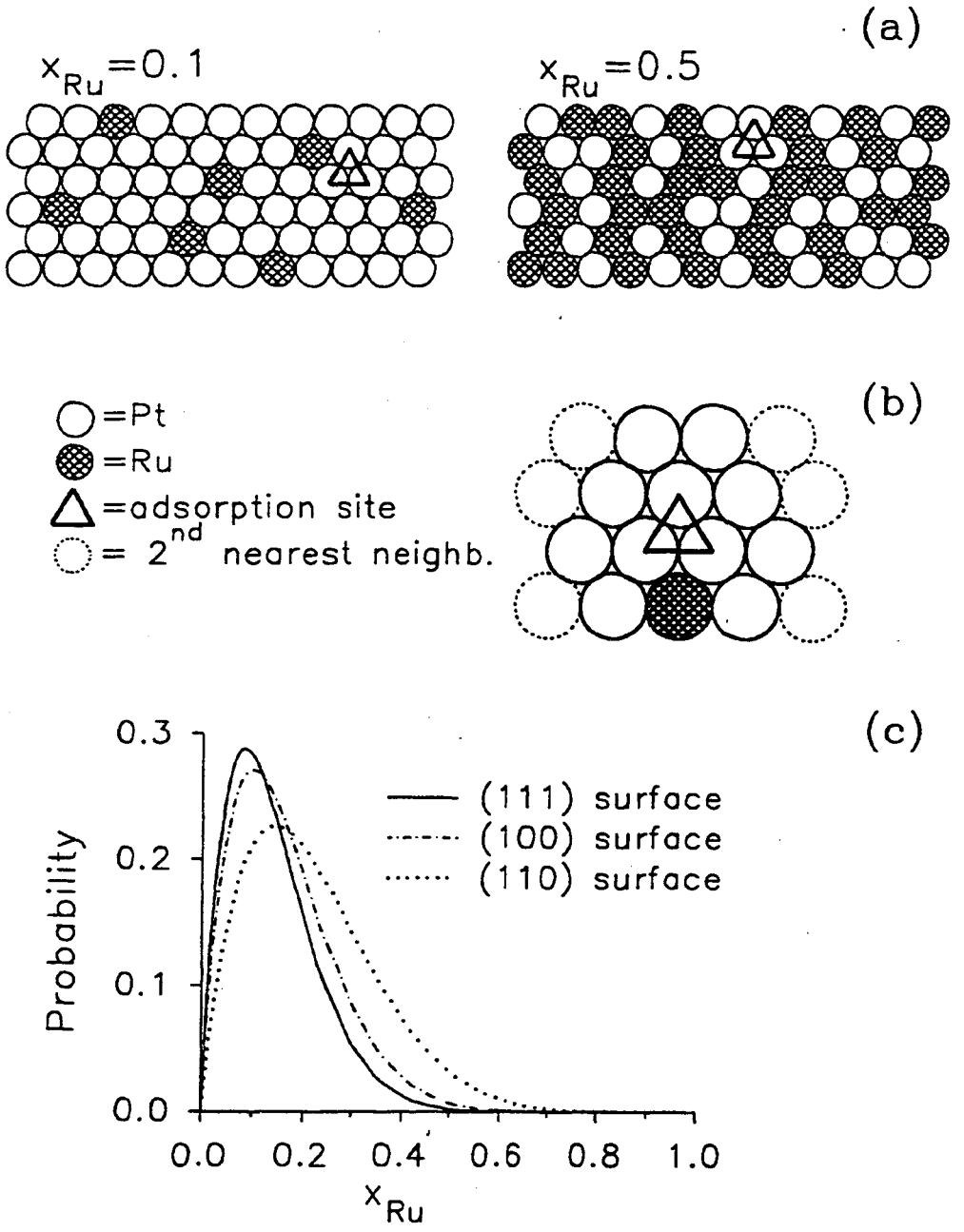

Figure 2-11. **(a)** Schematic representation of sputtered Pt-Ru alloy surfaces with 10 and 50 atomic% Ru. **(b)** Geometric arrangement of atoms around a three-fold methanol adsorption site for a hexagonal surface face (face centered cubic (111) face). **(c)** Probability distribution for the occurance of a three-fold Pt-site surrounded by exactly one Ru atom for different low-index crystal face geometries as a function of the Ru surface composition in atomic%.

with no tendency for ordering or clustering as was shown in Chapter 1. In bimetallic catalysis it is common to differentiate between three possible catalytic effects: blocking of surface sites to prevent the formation of strongly bound "poisons", bifunctional catalysis, and electronic interactions of the catalyst's components [61]. Figure 2-11a clearly conveys that the high activity of the ≈10 atomic% Ru surface, showing a very open structure, cannot derive from blocking effects. The possibility of electronic interactions of Pt and Ru, modifying the adsorption strength of adsorbed CO was suggested by Iwasita *et al* [67]. Considering that surface diffusivities [108] and CO adsorption energies [105] found in UHV measurements are rather similar for both Pt and Ru, we presently tend to rule out a significant electronic interaction effect. Therefore, we have derived a mechanism of enhancement by Ru using a statistical interpretation of the bifunctional action of the alloy surface. It should be noted that our statistical model developed in the following is not based on a rigorous treatment of rate expressions since we only acquired methanol electrooxidation data for two concentrations (different, however, by two orders of magnitude). Rather it represents a phenomenological approach in attempting to understand the high activity of the alloy with a Ru surface composition of only ≈7 atomic%.

In the following we assume that the adsorption of methanol requires an ensemble of three adjacent Pt atoms; a similar analysis carried out assuming ensembles of two or four Pt atoms does not, however, yield significantly different results. Figure 2-11a clearly shows that the number of three-fold Pt sites available for methanol adsorption is larger on the 10 atomic% than on the 50 atomic% Ru surface, and on the former most of the Pt ensembles are adjacent to a Ru atom allowing the supply of oxygen-like species. In the bifunctional mechanism, the optimum alloy surface composition would both maximize the adsorption of methanol through a large number of Pt adsorption sites (Equation 2-1) as well as allow the oxidative removal of CO *via* "hydroxide shuttling" by Ru at low

potentials (Equation 2-3 in conjunction with Equation 2-4). Therefore, we sought to establish a statistical probability distribution which maximizes the number of three-fold Pt ensembles adjacent to exactly one Ru atom, with the assumption that these are the most active sites for methanol oxidation on the alloy surfaces. In Figure 2-11b this configuration is shown for a hexagonal surface face (fcc(111)), where the indicated three-fold methanol adsorption site is surrounded by nine adjacent atoms: one Ru atom and eight Pt atoms. The probability of forming a three-fold Pt ensemble on a random Pt-Ru alloy surface is given by:

$$P_{\Delta-Pt} = x_{Pt}^{3} \tag{2-5}$$

where x_{Pt} is the atomic fraction of Pt on the alloy surface. The probability that this three-fold site is adjacent to exactly one Ru atom, out of a total of nine neighboring atoms can be found through a binomial distribution function:

$$P_{1/9\,Ru} = 9\,x_{Ru}\,x_{Pt}^{8} \tag{2-6}$$

The combined probability, namely the one of forming three-fold Pt ensembles which are surrounded by only one Ru atom is given by the product of Equations 2-5 and 2-6:

$$P_{tot} = 9\,x_{Ru}\,x_{Pt}^{11} = 9\,x_{Ru}\left(1-x_{Ru}\right)^{11} \tag{2-7}$$

This overall probability distribution, P_{tot}, is plotted in Figure 2-11c, exhibiting a maximum at an alloy surface composition of 8 atomic% Ru. The analogous analysis for different low-index faces results in a maximum probability of three-fold Pt sites being adjacent to exactly one Ru atom at 10 and 14 atomic% Ru for the (100) and the (110) face, respectively.

The observed maximum activity of the ≈10 atomic% Ru surface composition alloy, shown in Figure 2-10, follows therefore quite precisely (averaging the three crystals faces) from the above hypothesis of the bifunctional character of Pt-Ru alloys in the oxidation of methanol. The predicted enhanced activity of the alloy with a Ru surface composition of ≈7 atomic% over the ≈46 atomic% alloy for the different low-index faces as inferred from Figure 2-11c is: 60 for (111), 18 for (100) and 4 for (110). Based on methanol electrooxidation studies on Pt single-crystals Lamy *et al* [109] showed that methanol oxidation on a polycrystalline Pt electrode is mainly reflected by the behavior of a Pt(110) surface with small contributions of the (100) and (111) faces. It therefore seems that predictions based on our statistical model are in rather good agreement with our measurements in 5.0 mM CH_3OH, where oxidation currents on the alloy with a Ru surface concentration of ≈7 atomic% compared to the ≈46 atomic% alloy are larger by a factor of 12 (see Figure 2-10a and Table 2-1). The smaller enhancement, a factor of 3, in 0.5 M CH_3OH (see Figure 2-10b and Table 2-1) derives from the significantly faster methanol adsorption kinetics at this two orders of magnitude larger concentration [85, 86], thereby relaxing the requirement of the maximizing the number of Pt atoms in the ensemble depicted in Figure 2-11b. Nevertheless, phenomenologically, our statistical model does capture the basic phenomena which govern the activity of Pt-Ru alloy electrodes. Since both methanol equilibrium coverages and adsorption kinetics increase only up to a methanol concentration of ≈0.5 M [85, 86], we would not expect any significant changes in the relative activities of Pt-Ru alloy electrodes, even at higher methanol concentrations of 1 M [65, 71], 2 M [64] and 2.5 M [63].

An implicit assumption in our model is the mobility of CO on the alloy surface, so that CO formed on a Pt site may diffuse to a Pt site adjacent to a Ru site at a rate sufficiently large so as not to impose kinetic resistances. Although CO is well known as a strong adsorbate, its lateral mobility on both Pt and Ru was shown to be very high, in the

order of 10^{-9} cm^2/s at room temperature [108]. Based on the Einstein-Smoluchowski relation, the frequency factor evaluated for mean square displacements of ≈10 Å to allow the diffusion of CO bonded to Pt to the nearest Ru site would translate into current densities of 10^2 to 10^3 A/cm^2. Most likely, the surface diffusivity on an immersed electrode surface will be significantly smaller, but overall current densities are approximately three orders of magnitude smaller than "surface diffusion-limited rates" and therefore we would not expect that migration effects assert any significant resistance to the low observed methanol oxidation rates at room temperature. Applying the principles of our mechanistic arguments as outlined above, one would expect an optimum Ru surface concentration of 50 atomic% for reactants requiring only one adsorption site, *e.g.*, carbon monoxide. This indeed was be confirmed by CO stripping experiments on Pt-Ru alloys described in Chapter 3.

The premise of the above statistical model is the maximization of both the rate of methanol adsorption on Pt ensembles (Equation 2-1) which is first order in the concentration of methanol, and the oxidative removal of CO via "hydroxide shuttling" by Ru (Equations 2-3 and 2-4) which is more or less independent of the methanol concentration, *i.e.*, of zero order. On Ru-rich alloy surfaces the overall electrooxidation rate of methanol at steady-state is mainly limited by the reduced rate of adsorption of methanol (Equation 2-1), so that the apparent reaction order with respect to methanol is close to one (Table 2-1). In contrast, for a pure Pt electrode the apparent reaction order with respect to methanol is found to be close to zero (Table 2-1), since here the rate determining step is the oxidative removal of CO (Equation 2-2).

In conclusion, the mechanistic model discussed here is able to predict the activity of Pt-Ru alloys towards the electrooxidation of methanol under our experimental conditions, supporting the hypothesis that Pt-Ru alloy electrodes act as bifunctional catalysts.

5. CONCLUSIONS

In this study we presented for the first time the catalytic activity for methanol electrooxidation of sputter-cleaned polycrystalline Pt-Ru bulk alloys, which were well-characterized in terms of both surface composition and real surface area. LEIS confirmed that bulk and surface compositions were essentially identical for the sputtered alloys as would be expected from the similar differential sputter cross-sections of Pt and Ru.

It was shown that the sputter-cleaned alloy with a surface of ≈10 atomic% Ru exhibited the highest catalytic activity at the steady-state towards the electrooxidation of methanol (0.005 to 0.5 M) at 25°C and 0.5 V. Its catalytic enhancement over platinum was a factor of 12 in 5.0 mM CH_3OH solution and a factor of 30 in 0.5 M CH_3OH. Alloy surfaces with ≈50 atomic% Ru yielded rates which were close to first order with respect to the methanol concentration in solution, whereas pure Pt and the ≈10 atomic% Ru surface showed a relatively weak dependency on the methanol concentration in the electrolyte. This was explained by the limiting rate of methanol adsorption on Ru-rich surfaces, whereas the oxidative removal of methanol dehydrogenation fragments is the rate determining step on pure Pt electrodes.

We conclude that the high catalytic activity of Pt-Ru alloys for the electrooxidation of methanol is described very well by the bifunctional action of the alloy surface, where the adsorption of methanol occurs on Pt ensembles and the further electrooxidation of methanol dehydrogenation fragments is catalyzed by oxygen-like species adsorbed on adjacent Ru atoms. A statistical model based on the bifunctional mechanism of Pt-Ru alloy surfaces was presented, and found to predict quite accurately the optimum alloy surface composition of ≈10 atomic% for the electrooxidation of methanol under our conditions.

Chapter 3:
CO Oxidation on Pt-Ru Alloys at 25°C

1. Introduction 72
2. Experimental Procedures 75
   2.1. Electrochemical Measurements 75
   2.2. Sample Transfer Test from CO- to Stripping-Cell 77
3. Results 79
   3.1. CO Stripping Voltammetry on Pt and Ru 79
   3.2. CO Stripping Voltammetry on Pt-Ru Alloys 82
   3.3. Potentiostatic Oxidation of Adsorbed CO 87
      3.3.1. Potentiostatic Oxidation of CO on Ru and $Pt_{0.54}Ru_{0.46}$ 87
      3.3.2. Potentiostatic Oxidation of CO on Pt and Ru 90
   3.4. CO Oxidation on Sputtered *vs* Annealed Pt-Ru Electrodes 93
4. Discussion 94
   4.1. CO Electooxidation on Pt-Ru Alloys 95
   4.2. Gas Phase Oxidation of CO on Pt and Ru 98
   4.3. Origin of the Synergistic Behavior of Pt-Ru in CO Electrooxidation 100
   4.4. Comparison of Methanol and CO Oxidation on Pt-Ru Alloys 101
5. Conclusions 102

1. INTRODUCTION

In the previous chapter we demonstrated evidence for the bifunctional character of Pt-Ru alloy electrodes, where adsorption and initial dehydrogenation of methanol into surface-bound CO-like species on Pt sites is followed by its oxidation *via* oxygen-containing species adsorbed on Ru sites at low electrode potentials. The optimum Ru surface composition under our experimental conditions was found to be only ≈10 atomic%. This optimum composition was attributed to the requirement of multiple Pt

atom ensembles for the adsorption of methanol, which does not adsorb on Ru surface sites. Carbon monoxide, in contrast to methanol, adsorbs readily on both Pt and Ru surface sites and measuring its electrooxidation rate on well-characterized Pt-Ru alloy electrodes as a function of Ru surface composition will serve as a test-case for their bifunctional character in methanol electrooxidation proposed in Chapter 2.

The electrooxidation of carbon monoxide on Pt-Ru alloy electrodes was last studied in the late sixties and the early seventies in the context of the electrooxidation of hydrogen derived from steam-reformed hydrocarbons. It was shown that these alloys alleviate the substantial deactivation experienced by platinum electrodes in the presence of small concentrations of CO in the hydrogen feed stream, which are typically contained in hydrogen from steam-reformed hydrocarbons [110-112]. Reports on the optimum Ru composition of carbon supported bimetallic clusters of Pt-Ru alloys differed widely, ranging from essentially pure Ru to 30 atomic% Ru, clearly requiring further investigation on more carefully characterized alloy surfaces. Quite contrary to the scarce information available on the oxidation of CO on Pt-Ru alloy electrodes, the current research efforts on the interaction of CO with polycrystalline platinum [*e.g.*, 113-115] and platinum single crystals [*e.g.*, 116-119] furnishes us with a fairly comprehensive insight into its fundamental mechanism. This interest in the electrooxidation of carbon monoxide on platinum electrodes derives from both an attempt to elucidate the fundamental processes involved in the electrooxidation of the simplest organic molecule and the knowledge that adsorbed CO species occur as intermediates or catalyst "poisons" in the electrooxidation of larger organic molecules which are potential fuel cell reactants [120]. The decomposition of one- and two-carbon molecules during their electrooxidation on a Pt electrode into CO-like adsorbates has been established quite firmly by different spectroscopic techniques [*e.g.*, 121-123] and similar observations have been made on a Pt-Ru alloy electrode during the electrooxidation of methanol in an FTIR study by Iwasita

et al [67]. To our knowledge there have been only two studies on the electrooxidation of CO on a pure ruthenium electrode, primarily investigating the vibrational modes of CO adsorbed on Ru *via* EMIRS (electromodulated infrared spectroscopy) [124], and *via* SERS (surface-enhanced Raman spectroscopy) [125].

In the following we will present measurements on the electrocatalytic activity of well-characterized Pt-Ru alloy electrodes towards the electrooxidation of CO in sulfuric acid electrolyte. All electrode surfaces were well-defined in terms of surface area, their chemical state (purely metallic, monophasic), and in terms of their surface composition as was outlined in Chapter 1; we will also comment on their stability in the electrolyte under applied positive potentials. In order to avoid mass transfer resistances, electrocatalytic activities were measured for adsorbed monolayers of CO in both stripping voltammetry and potential-step experiments. Thus we could accurately determine the optimum alloy composition for the electrooxidation of CO. Aided by a careful examination of the UHV literature on the interaction of CO and oxygen with single-crystal surfaces of both Pt and Ru we were able to put forth an explanation for the observed synergistic nature of these bifunctional Pt-Ru alloy catalysts in the electrooxidation of CO. Considering that CO is one of the major reaction intermediates in the electrooxidation of CH_3OH we will discuss the implications of this study on the proposed reaction scheme of methanol electrooxidation on Pt-Ru alloy electrodes (Chapter 2). Finally, we will address certain differences between sputtered and annealed surfaces, a pertinent issue in the preparation of high surface area fuel cell electrodes.

2. EXPERIMENTAL PROCEDURES

2.1. Electrochemical Measurements

The UHV characterized specimens were withdrawn from the UHV introduction port (backfilled with argon, Matheson 5N5 purity) into air and covered immediately with a drop of triply pyro-distilled water, as was described in Section 2 of Chapter 2. They were then transferred into one of two standard three-compartment meniscus-type electrochemical cells, both containing freshly prepared, oxygen-free (purged and blanketed with argon, Alphagaz, 5N5 purity) 0.50 M H_2SO_4 (Baker Analyzed®, Ultrex® ultrapure reagent) and immersed under potential control at 0.075 V *vs* RHE (reversible hydrogen electrode). Reference potentials were measured *versus* a Pd/H electrode in the same electrolyte, but all potentials in the following will be referred to the RHE scale.

Both cells were located in an "atmos-bag" (Aldrich), which was sealed off from the atmosphere after having been flushed with standard grade argon at a sufficiently high rate to replace all residual air which had entered during the sample transfer, so that both electrochemical cells were surrounded by an argon atmosphere. The glove-bag assembly with both electrochemical cells is shown above in Figure 3-1. Subsequently, a cyclic voltammogram was recorded in this first cell (further referred to as the "stripping-cell") to verify the cleanliness of the transfer, yielding a stable cyclic voltammogram from the second cycle on with a maximum positive potential limit of 0.75 V (RHE). The 0.5 M H_2SO_4 electrolyte in the second cell was saturated with CO (Matheson, 4N purity) and will be referred to as the "CO-cell".

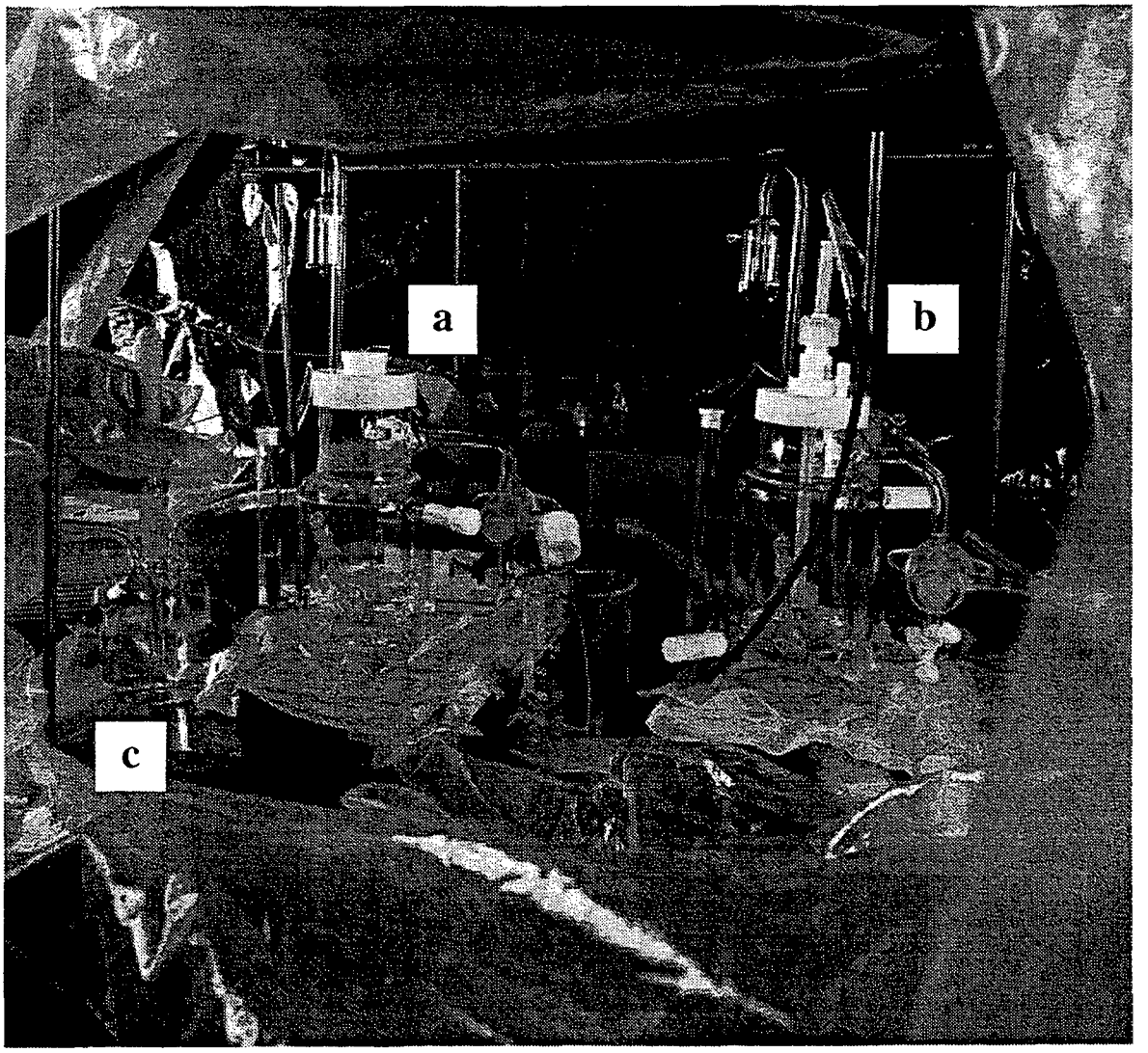

Figure 3-1. Glove bag with two meniscus-type electrochemical cells for CO electrooxidation experiments: **(a)** "CO-cell"; **(b)** "stripping cell" with sample; **(c)** bubbler with oxygen-free water.

CO was adsorbed by withdrawing the electrode at 0.075 V and by immersing it under potential control in the CO-cell. Adsorption from the electrolyte saturated with CO was carried out for three minutes, whereupon the electrode was emersed at the adsorption potential, rinsed with deoxygenated, triply pyro-distilled water under argon atmosphere and immersed under potential control at 0.075 V in the stripping-cell. In subsequent voltammetric experiments the initial sweep was in the negative direction and was started after the electrode had been immersed in the pure electrolyte for three minutes to establish a reproducible meniscus; voltammograms were recorded with a X/Y-recorder. Potential-step experiments were similarly conducted after the adsorption of CO as described above and data were acquired with a PAR 273 potentiostat and an IBM-compatible computer, interfaced with a GPIB card. A stripping voltammogram was recorded immediately after each potential-step experiment in order to monitor the completeness of the CO oxidation and to prepare a clean surface for successive experiments.

2.2. Sample Transfer Test from CO- to Stripping-Cell

Although CO is known to be very strongly adsorbed on platinum, spurious amounts of oxygen are known to partially oxidize or displace adsorbed CO. Therefore, we conducted a transfer test of a platinum sample with adsorbed CO from the CO-cell to the stripping-cell in order to verify that a full monolayer of CO could be preserved under our experimental conditions. For this purpose we chose to use a flame-annealed Pt(111) single crystal (0.57 cm^2 surface area) [80], since its CO stripping voltammetry is very well defined and documented extensively in the literature. Figure 3-2 shows the CO stripping voltammetry of Pt(111) in the stripping-cell (no CO in solution) at 50 mV/s; CO had been adsorbed at 0.075 V as described above. Both the coulombic charge under the stripping peak ($\approx$400 $\mu C/cm^2$) and the peak position as well as peak shape were consistent with the literature [126, 127]. The complete suppression of the pseudocapacitive currents in the

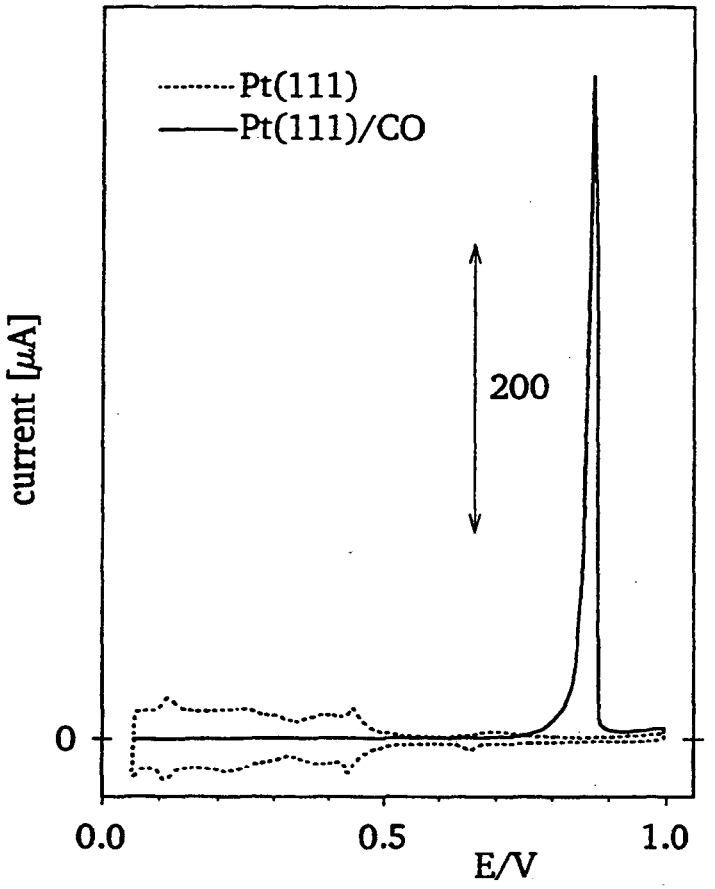

Figure 3-2. CO stripping voltammetry of a Pt(111) single crystal in 0.5 M H_2SO_4 at 50 mV/s. (——) stripping of a monolayer of CO in the first positive-going sweep; (- - - -) first negative-going sweep after the stripping of CO, followed by a positive-going sweep. CO was adsorbed under potential control at 25 mV from CO saturated electrolyte, and the stripping voltammogram was recorded upon immersion of the electrode at 25 mV in CO-free electrolyte.

potential region below ≈0.7 V is a clear sign that a full monolayer of CO was adsorbed onto the surface. The successive negative-going sweep and the second cycle traced accurately the base voltammogram of clean Pt(111) in sulfuric acid electrolyte, attesting to a proper transfer of adsorbed CO from the CO-cell to the stripping-cell, without any carry-over of dissolved CO.

3. RESULTS

3.1. CO Stripping Voltammetry on Pt and Ru

Figure 3-3a shows the CO stripping voltammogram obtained on sputter-cleaned polycrystalline platinum at a CO adsorption potential of 0.075 V. The onset of CO oxidation as well as the stripping peak potential agree favorably with literature data in 0.5 M H_2SO_4 [113, 118]. The coulombic charge under the CO stripping peak (corrected for double layer charging and oxide formation) corresponds to a coverage of ≈90%, equivalent to an essentially saturated monolayer of CO [118]. Additional evidence for a saturation coverage of the electrode surface with adsorbed CO is the complete blocking of the pseudocapacitive currents in the potential region below ≈0.4 V. The shoulder at ≈0.5 V in the CO stripping peak has been correlated with the oxidation of bridge-bonded CO [113] and the multiplicity in the main current peaks is speculated to derive from different low-index crystal faces on a polycrystalline electrode [118, 120]. In general, the oxidation of an adsorbed monolayer of CO on Pt is understood to proceed along the perimeters of CO islands on the electrode surface, initiating from nucleation sites which facilitate the electrochemical adsorption of oxygen-containing species necessary for the formation of CO_2 [115, 128].

The voltammetry in the pure supporting electrolyte and the CO stripping voltammetry for a CO adsorption potential of 0.075 V of sputter-cleaned Ru is shown in Figure 3-3b. A balance of cathodic and anodic charges in the cyclic voltammogram in the supporting electrolyte attests to the absence of dissolved oxygen, and more importantly, to the fact that no irreversible Ru oxide is formed during the positive-going sweep. The onset of the CO oxidation current commences at ≈0.25 V, a significantly more negative potential than for CO on Pt (Figure 3-3a). Similarly, the CO stripping peak on Ru is

shifted ≈0.15 V negative compared to Pt such that the apparent electrocatalytic activity of a Ru electrode is far superior to Pt. It was discussed thoroughly in Chapter 2 that the adsorption of oxygen-containing species onto a Ru electrode commences at potentials as low as 0.2 V [75, 84], approximately 0.5 V more negative than on Pt. Thus, oxygen-containing surface species are supplied to a Ru electrode at low potentials, thereby facilitating the onset of the oxidation of CO to CO_2 at a potential significantly more negative than on Pt. The intrinsic reaction rate constant for the reaction of surface-bound species of CO and oxygen, however, seems to be lower as indicated by the greater width of the CO stripping peak on Ru at 20 mV/s (as well as at 5 mV/s).

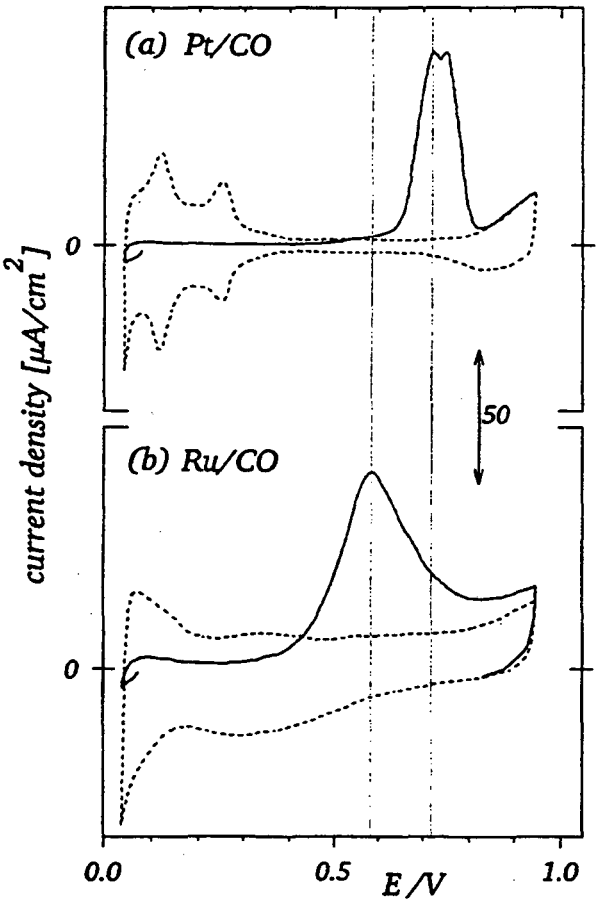

Figure 3-3. CO stripping voltammetry of sputter-cleaned electrodes in 0.5 M H_2SO_4 on: (**a**) Pt, and (**b**) Ru. Vertical lines indicate the CO stripping peak potentials. (——) stripping of a monolayer of CO in the first positive-going sweep; (- - - -) first negative-going sweep after the stripping of CO, followed by a positive-going sweep. 20 mV/s; adsorption and immersion at 25 mV.

As was discussed by Weaver *et al* [127] the evaluation of the coulombic charge of CO oxidation for metals with significant adsorption of oxygen-containing species in the potential range where the stripping of CO takes place cannot be assessed accurately because of the overlap of CO electrooxidation currents and pseudocapacitive currents deriving from the adsorption of oxygen-containing species on bare metal surface sites exposed upon the electrooxidation of adsorbed CO. An approximate evaluation of the coulombic charge for the oxidation of CO on Ru may be attained by the difference between the coulombic charges passed during CO oxidation and in the base voltammogram for the potential region ≥0.2 V (approximate end of the hydrogen desorption region on Ru). The resulting CO oxidation charge as referred from Figure 3-3b corresponds to ≈550 $\mu C/cm^2$, which would indicate a CO coverage of more than 100% on Ru. In view of the very approximate nature of the above estimation we believe that more or less a full monolayer of CO is adsorbed on Ru under our experimental conditions, which is also supported by the almost complete suppression of pseudocapacitve currents in the CO stripping voltammetry at potentials before the onset of CO oxidation. The high activity of a Ru electrode towards the electrooxidation of CO shown above is at variance with the much lower activity of Ru electrodeposited on gold in a previous SERS study [125]. Upon inspection of the cyclic voltammetry of the Ru electrode in Reference 125 it does become clear, however, that the electrode was strongly oxidized rather than purely metallic as it was in this study. A similar observation is true for the CO stripping voltammetry in Reference 124, where either oxygen was present in the solution or irreversibly formed oxide covered the electrode surface, effecting an excess of cathodic charge in the base voltammogram of Ru.

3.2. CO Stripping Voltammetry on Pt-Ru Alloys

After having observed a substantial enhancement of the electrooxidation reaction of adsorbed CO on a Ru electrode in comparison to CO on Pt, we investigated the electrocatalytic activity of various sputter-cleaned Pt-Ru bulk alloys as a function of their Ru surface concentration. Figure 3-4 summarizes our results for the stripping voltammetry of essentially saturated monolayers of CO on Pt-Ru alloy surfaces in 0.5 M H_2SO_4 for a CO adsorption potential of 0.075 V. To afford a more condensed representation, only the anodic currents in the voltammetry of the respective alloys after the stripping of CO are plotted (for complete voltammograms see Chapter 2); the CO stripping voltammetry on pure Ru is added for comparison. The Ru surface concentration in atomic fractions for the different bulk alloys is given in the figure and the bulk concentrations may be obtained from Tables 1-3 and 1-4.

It is clear from Figure 3-4 that even small amounts of Ru on the alloy surface, *e.g.* ≈7 atomic%, effect a substantial enhancement over pure Pt in their electrocatalytic activity towards the oxidation of adsorbed CO (top voltammogram in Figure 3-4), indicated by the peak shift of the CO stripping peak to more negative potentials, by roughly 0.18 V. Increasing the surface concentration of Ru on Pt-Ru alloys further improves their electrocatalytic activity and the alloy with ≈46 atomic% yields a CO stripping peak 0.25 V more negative than pure Pt. The common feature of the CO stripping voltammetry on both pure Ru and Pt-Ru alloys, in contrast to what was observed for pure Pt, is the onset of CO oxidation at the same potential on electrode surfaces containing Ru as is indicated by the cross-over of CO oxidation currents and pseudocapacitive currents in the absence of adsorbed CO. This clearly points towards the nucleation of oxygen-containing species on the small fraction of freed Ru sites, which then catalyze the CO electrooxidation reaction. The tremendous activity enhancement

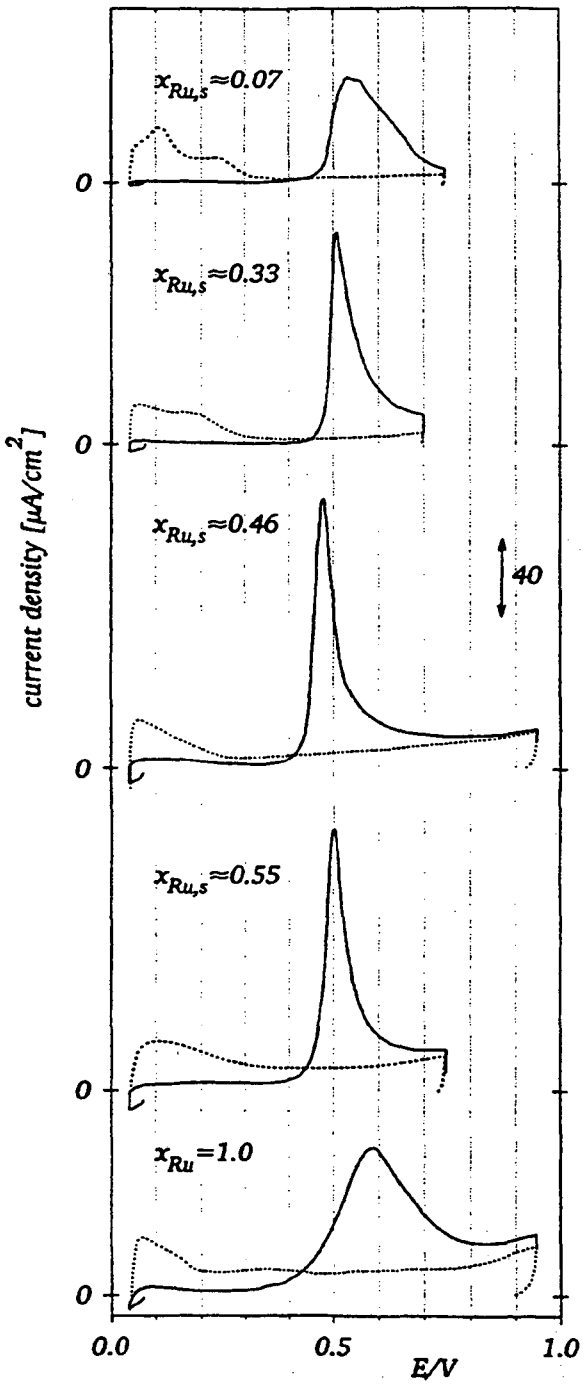

Figure 3-4. CO stripping voltammetry of sputter-cleaned Pt-Ru alloy electrodes and of pure Ru. Ru surface compositions ($x_{Ru,s}$) are indicated in the figure in atomic fractions; the corresponding bulk compositions are listed in Tables 1-3 and 1-4. (——) stripping of a monolayer of CO in the first positive-going sweep; (- - - -) second positive-going sweep. 20 mV/s; 0.5 M H_2SO_4; adsorption and immersion at 25 mV.

based on stripping peak positions as a function of Ru surface composition is accompanied by a striking decrease in the corresponding peak widths, implying that the electrocatalytic activity of Pt-Ru alloys cannot be expressed by a mere linear combination of the individual elements' properties. Even if one hypothesizes that the early onset of CO oxidation on Ru would create nucleation sites for the adsorption of oxygen-containing species in the vicinity of Pt sites, thereby facilitating the oxidation of CO bound to Pt in a narrow peak similar to the peak widths found for pure Pt , it remains unclear why the oxidation of CO bound to Ru atoms on the alloy surface would proceed at an apparently faster rate than is observed on pure Ru. A possible explanation for this synergistic behavior of Pt-Ru alloys may be an intrinsically higher rate constant for the oxidation of surface-bound CO with surface-bound oxygen-containing species on the alloy electrode compared to pure Ru, an idea which we will pursue further in Section 4. On the other hand, the broad CO stripping peak on the alloy with a Ru surface concentration of ≈7 atomic% may be understood by the limited contact area of Pt and Ru atoms on a Ru-poor surface, reflecting the increased diffusional path length for the surface migration of CO bound to Pt atoms in order to reach oxygen-containing species adsorbed on Ru atoms.

Figure 3-5 gives a comprehensive overview of CO stripping peak potentials *versus* Ru surface concentrations for the measurements at 20 mV/s shown in Figure 3-4 and for both lower and higher sweep rates. At all sweep rates, the Pt-Ru alloy with a surface composition of ≈46 atomic% Ru yields the lowest oxidation peak potentials combined with the narrowest stripping peaks.

Before proceeding to a more careful investigation of the intrinsic CO oxidation rate constants on pure Pt and Ru electrodes we would like to point out a key issue in measuring electrocatalytic activities on well-characterized Pt-Ru alloys, *viz*, with regard to their stability under applied positive potentials. To capture the entire CO oxidation wave on the electrode found to be the most active in this study (≈46 atomic% Ru), we had

extended the positive potential limit to 0.95 V. Under these conditions, the CO stripping peak could be reproduced in all details over approximately 10 cycles in a series of experiments, indicating that the electrode surface remained essentially unchanged. However, when examining the stability at positive electrode potentials of the Pt-Ru alloy with a Ru surface composition of ≈7 atomic% , we observed significant preferential dissolution of Ru when the positive potential limit was extended from 0.75 V (Figure 3-6a) to 0.95 V (Figure 3-6b). Both an increase in the charge of adsorbed hydrogen (at ≈0.1V) and decreased (pseudo)capacitive currents in the potential region between ≈0.4 to ≈0.7 V clearly indicate the loss of Ru from the surface. This is illustrated even more dramatically by a comparison of the CO stripping voltammetry: whereas the characteristics of CO electrooxidation shown in Figure 3-6a remained unchanged over approximately 10 cycles at a positive potential limit of 0.75 V, its extension to 0.95 V effected irreversible positive-going shifts in the CO stripping wave, which more and more resembled the characteristics of pure Pt. These observations are indeed consistent

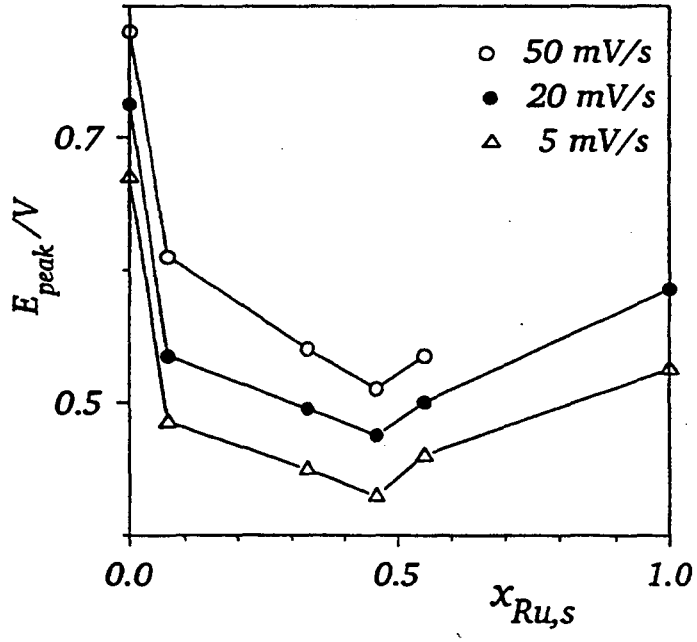

Figure 3-5. CO stripping peak potentials *vs* Ru surface composition ($x_{Ru,s}$) of sputter-cleaned electrodes at various sweep rates (bulk compositions are listed in Tables 1-3 and 1-4). 20 mV/s; 0.5 M H_2SO_4; adsorption and immersion at 25 mV.

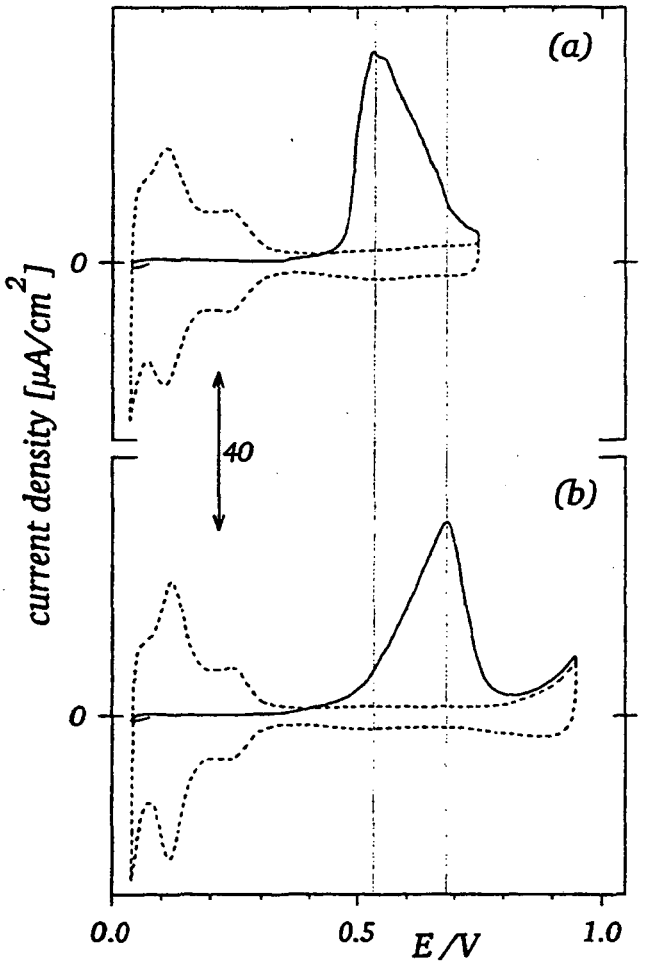

Figure 3-6. Influence of the positive potential limit on the CO stripping voltammetry of a sputter-cleaned Pt-Ru alloy electrode with a surface composition of 7 atomic% Ru. Positive potential limit: **(a)** 750 mV, and **(b)** 950 mV. (——) stripping of a monolayer of CO in the first positive-going sweep; (- - - -) first negative-going sweep after the stripping of CO, followed by a positive-going sweep. Electrodes were subjected to ≈10 cycles between 25 mV and the respective positive potential limit prior to the CO stripping experiment. 20 mV/s; 0.5 M H_2SO_4; adsorption and immersion at 25 mV.

with the onset of Ru dissolution from pure Ru at 0.9 V [76] and it is not surprising that it is more apparent for an alloy with an already low surface concentration of Ru. Since it is a common technique in electrochemical experimentation to subject electrodes to positive potentials prior to measurements in order to establish clean electrode surfaces, we would like to emphasize here that this is not without complications in the case of Pt-Ru alloy electrodes.

3.3. Potentiostatic Oxidation of Adsorbed CO

The electrooxidation rates of adsorbed CO on Pt-Ru alloy electrodes were measured at constant potential to further investigate the phenomena observed in the CO stripping voltammetry. In particular, we will seek to address the above hypothesis of nucleation of oxygen-containing species on Ru surface atoms, and the synergism displayed by Pt-Ru alloy electrodes in the CO stripping voltammetry. The diffusion-limited current density of CO in a saturated solution (≈1 mM) is only on the order of $0.5\ t^{-1/2}\ mA/cm^2$ (based on the Cottrell equation), so that after ≈1 s current densities larger than ≈50 $\mu A/cm^2$ would reflect both kinetic and mass-transfer resistances. Current densities measured at ≥ 0.5 V are significantly larger than 50 $\mu A/cm^2$ and, therefore, in order to avoid the contribution of mass-transfer resistances potential-step experiments were carried out in CO-free electrolyte on electrodes with adsorbed monolayers of CO, analogous to the CO stripping voltammetry. For each experiment the electrode potential was stepped from the CO adsorption potential of 0.075 V to the specified oxidation potential, at which the adsorbed monolayer of CO was oxidized for 10 seconds. Subsequently, the electrode potential was reset to 0.075 V and a CO stripping voltammogram was recorded in order to assess whether the oxidation of CO was complete. After several cycles between 0.075 V and 0.9 V the above potential-step experiment was repeated in the absence of adsorbed CO to record the currents due to the pseudocapacitance of the electrodes.

3.3.1. Potentiostatic Oxidation of CO on Ru and $Pt_{0.54}Ru_{0.46}$

Figure 3-7 shows the potentiostatic CO oxidation currents on Ru and the most active Pt-Ru alloy (Ru surface composition of ≈46 atomic%) at electrode potentials of 0.5, 0.6 and 0.7 V *versus* the logarithm of time. The dashed lines represent the difference between the currents measured on electrodes with preadsorbed CO and the currents in the absence of CO. From the discussion in Section 3.2 it is clear that this correction is only a

first order approximation in extracting the real oxidation currents, but it will be fairly accurate in view of the generally shorter time-constants of pseudocapacitance charging in contrast to electrooxidation.

The background-corrected oxidation current on Ru at 0.5 V in Figure 3-7a, approximately 0.1 V negative of its CO stripping peak potential in Figure 3-4, shows that the oxidation current of CO on pure Ru is slowly decaying with time, and only ≈50% of the total CO oxidation charge is passed in the first 10 seconds (note that coulombic charges in a plot of current *vs* the logarithm of time do not scale linearly with the area in the plot). This was confirmed by subsequent CO stripping voltammetry as described above, where the charge under the CO stripping peak was ≈50% of what was observed for a saturated surface layer of CO. In contrast, as expected from the results in Figure 3-4, the oxidation of CO on the alloy electrode at the same potential (Figure 3-7a) is fully completed after 10 seconds. In analogy to the alloy electrode's very narrow CO stripping wave (see Section 3.2), the shorter time necessary for the complete oxidation of a CO monolayer at constant potential on this electrode attests to its strong synergism in the CO electrooxidation reaction. In addition, the propensity of bare Ru atoms to provide nucleation sites for the adsorption of oxygen-containing species is indicated by the accordance of the onset of the rather symmetric oxidation current on the alloy with the onset of CO oxidation on pure Ru as shown in Figure 3-7. It quite clearly reveals the strong impact of the intermittent exposure of bare Ru sites on the overall electrooxidation rate, underscoring the importance of nucleation sites onto which one of the two reactants in the overall oxidation of CO to CO_2 can be formed, namely oxygen-containing surface species. The induction-time to the inflection point in the oxidation currents of the alloy with a Ru surface concentration of ≈46 atomic% at all of the measured potentials in Figure 3-7 coincides with the respective induction-time to the onset of oxidation on pure Ru. It very clearly provides evidence for the bifunctional character of Pt-Ru alloys in the

electrooxidation of CO: nucleation of oxygen-containing species on Ru surface atoms, which then interact at low electrode potentials with CO adsorbed on neighboring surface atoms. The fact that the entire monolayer of CO, originally adsorbed with equal facility on both Pt and Ru atoms, is oxidized at a much higher rate than is observed on pure Ru again leads to the hypothesis that the intrinsic oxidation rate constant may be larger on Pt-Ru alloys than on a pure Ru electrode.

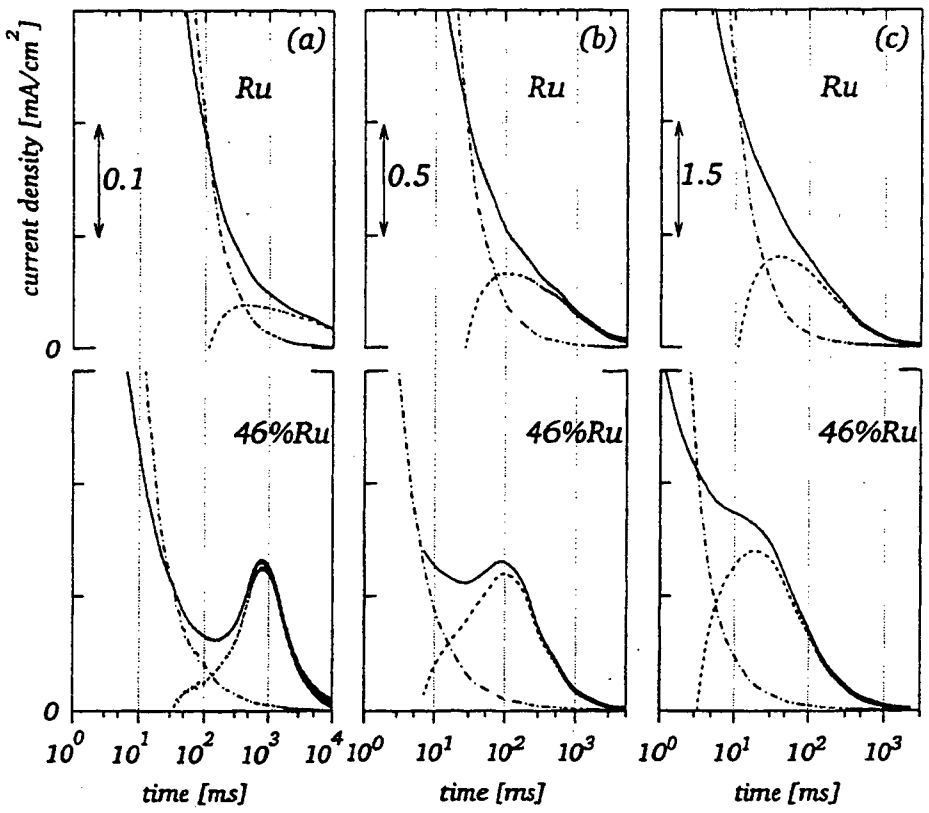

Figure 3-7. Electrooxidation at constant potential of an adsorbed monolayer of CO on sputter-cleaned Ru and the most active Pt-Ru alloy with a Ru surface composition of 46 atomic%: **(a)** 500 mV, **(b)** 600 mV, and **(c)** 700 mV. (——) oxidation currents in the presence of preadsorbed CO; (—·—·—) background currents for CO-free surfaces; (- - - -) difference between oxidation and background currents. 20 mV/s; 0.5 M H_2SO_4; adsorption and immersion at 25 mV.

3.3.2. Potentiostatic Oxidation of CO on Pt and Ru

In the experiment described below we sought to determine whether there is a difference in the intrinsic bi-molecular rate constants, k_{Ru} and k_{Pt} ,for the electrooxidation reaction of adsorbed CO on the pure metals to elucidate the possible reasons for the strong synergism displayed by Pt-Ru alloy electrodes:

$$Ru-CO + Ru-OH_{ads} \xrightarrow{k_{Ru}} CO_2 + H^+ + e^- \quad (3\text{-}1)$$

$$Pt-CO + Pt-OH_{ads} \xrightarrow{k_{Pt}} CO_2 + H^+ + e^- \quad (3\text{-}2)$$

where OH_{ads} is used to symbolize oxygen-containing surface species, the molecular identity of which is unknown. For the ease of discussion without, however, affecting the general course of the argument, CO is assumed to be adsorbed linearly (on-top site); *in-situ* FTIR measurements currently in progress [129] do indicate linearly-bonded CO as the predominant surface species under similar experimental conditions. Based on Equations 3-11 and 3-2, assuming simple Langmuir-Hinshelwood kinetics, CO oxidation rates on Ru and Pt, respectively, may be formulated as:

$$r_{Ru} = k_{Ru}\,\theta_{CO}\,\theta_{OH_{ads}} \quad (3\text{-}3)$$

$$r_{Pt} = k_{Pt}\,\theta_{CO}\,\theta_{OH_{ads}} \quad (3\text{-}4)$$

Consequently, to attain a comparative measure of the potential-dependent rate constants k_{Ru} and k_{Pt}, reaction rates, *i.e.* electrooxidation currents, must be measured at the same electrode potential and at the same CO coverage (θ_{CO}) of the electrode. More importantly, however, the equilibrium coverage of the surface with oxygen-containing species ($\theta_{OH_{ads}}$) must be similar. If these conditions are satisfied, the ratio of measured CO electrooxidation currents on pure Ru and pure Pt yield an approximate measure for the ratio of the respective rate constants, k_{Ru} and k_{Pt}:

$$r_{relative} = \frac{r_{Ru}}{r_{Pt}} = \frac{k_{Ru}}{k_{Pt}} \tag{3-5}$$

Since, in contrast to the situation on Ru, the adsorption of oxygen-containing species on a Pt electrode in acid electrolytes does not occur to any significant extent below 0.9 V, relative electrooxidation rate constants can only be extracted at potentials above 0.9 V, where the difference between the equilibrium coverage of adsorbed oxygen-containing species on Ru and Pt is relatively small. Guided by the above considerations, we conducted potential-step experiments on a Ru and a Pt electrode with preadsorbed CO. Figure 3-8a gives a comparison of the electrooxidation currents (corrected by the subtraction of background currents) of adsorbed CO on both metals at 0.8 V: after 1 second the CO layer is fully oxidized on Ru, whereas the oxidation on Pt requires ≈3 seconds for completion. A very similar shape in the potentiostatic oxidation of adsorbed CO on a polycrystalline Pt electrode was observed by Santos *et al* [130] at an electrode potential of 0.62 V; in analogy to References 118 and 120, the multiplicity of current peaks at various oxidation times was rationalized by the different activities of the low-index crystal faces present on a polycrystalline sample. Indeed, the potential-step experiments on Pt(100) by Love and Lipkowski [117] produced a single current peak, in close relation of the single feature observed in CO stripping voltammetry. At 0.8 V the equilibrium coverage of platinum with oxygen-containing surface species is very small compared to Ru and the apparently slower kinetics of CO electrooxidation on Pt *versus* Ru may derive from this low concentration of one of the reactants in the bimolecular reaction (Equation 3-2), namely the minute coverage with OH_{ads} on the Pt electrode at this potential. Consequently, a very different situation emerges as the potential is stepped to 0.9 V (Figure 3-8b) and higher (Figure 3-8c). At 0.9 V, the oxidation kinetics of Pt and Ru are very similar and the reaction is completed after the same reaction time on both surfaces. At 1.0 V the equilibrium coverage of Pt with oxygen-containing species is

≈50% of a monolayer, comparable to the coverage on Ru at this potential, so that the measured electrooxidation currents on Pt and Ru should directly reflect the relative magnitudes of the bi-molecular rate constants k_{Pt} and k_{Ru}, according to Equation 3-5. Figure 3-8c shows quite clearly that k_{Pt} is significantly greater than k_{Ru}. Thus, the principal reason for the hindered electrooxidation of CO to CO_2 on Pt at low potentials is the absence of OH_{ads}, as suggested in earlier works. The implications of this intrinsic difference in the rate constants k_{Pt} and k_{Ru} will be discussed in Section 4.

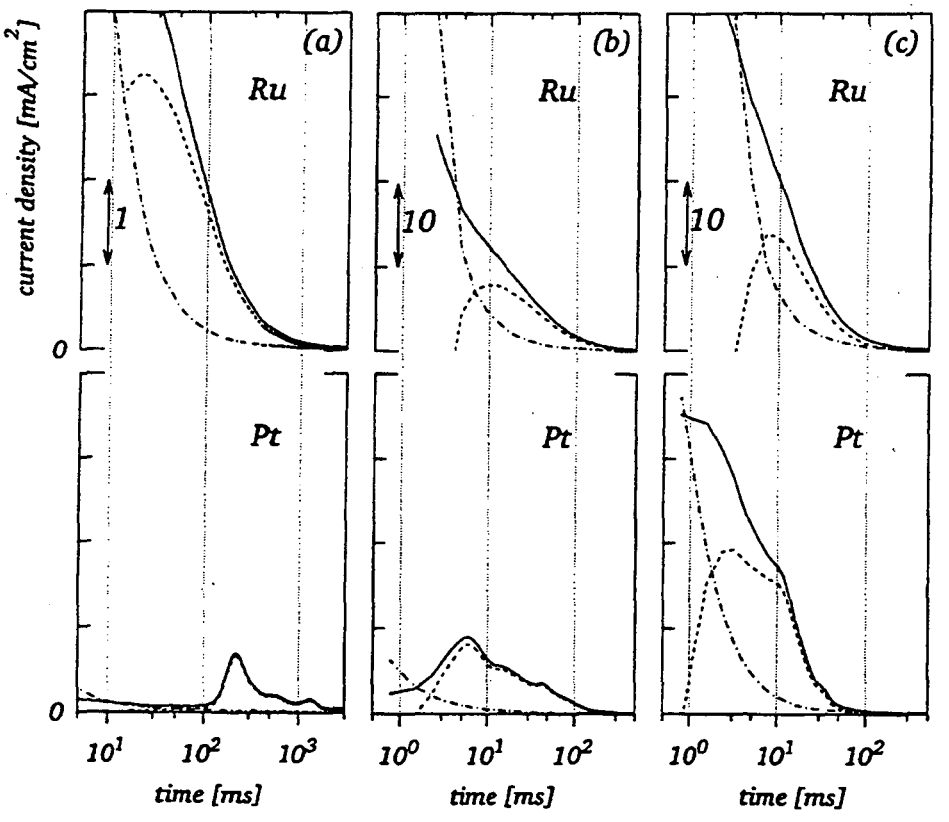

Figure 3-8. Electrooxidation at constant potential of an adsorbed monolayer of CO on sputter-cleaned Ru and Pt electrodes: **(a)** 800 mV, **(b)** 900 mV, and **(c)** 1000 mV. (——) oxidation currents in the presence of preadsorbed CO; (—·—·—) background currents for CO-free surfaces; (- - - -) difference between oxidation and background currents. 20 mV/s; 0.5 M H_2SO_4; adsorption and immersion at 25 mV.

3.4. CO Oxidation on Sputtered *vs* Annealed Pt-Ru Electrodes

Even if CO surface migration takes place to a significant extent as was discussed in Chapter 2, the distribution of the elements constituting the alloy should assert a strong influence on the CO electrooxidation rate. All experiments described above were conducted on sputter-cleaned electrodes, a preparation process which exposes at the surface the bulk arrangement of Pt and Ru atoms in the alloy. Pt and Ru form an essentially ideal solution in the bulk, without any intermetallic compound formation and with a quite small miscibility gap (see Figure 1-6), so that the arrangement of the alloy components in the bulk is expected to be well approximated by a random distribution of atoms. Therefore, sputtered Pt-Ru alloy surfaces will also be characterized by a more or less random arrangement of Pt and Ru surface atoms. Annealed alloys, however, allow the equilibration of the respective surface concentration, and in the absence of intermetallic compound formation there is a tendency for cluster formation at the surface [131].

As was shown in Figure 2-4, the sputtered surface of the Ru-poor alloy, PtRu-3, has a Ru surface composition of ≈7 atomic%, very similar to the annealed Pt-enriched surface of the 30 atomic% Ru bulk alloy (PtRu-5) with a Ru surface composition of ≈8 atomic%. The electrocatalytic activity, however, of these two nominally identical surfaces is quite different as shown in Figure 3-9. Here, at a sweep rate of 20 mV/s the stripping voltammetry of the annealed alloy closely resembles a linear combination of the CO stripping voltammetry of pure Pt and pure Ru. This may be understood by viewing the inserts in Figure 3-9, which sketch the expected surface arrangement for the two differently prepared surfaces: the annealed alloy, where Ru is expected to cluster into islands [131], is conceptually close to Ru "nano-electrodes" embedded in a large Pt electrode, and the expected behavior would be a linear superposition of the oxidation

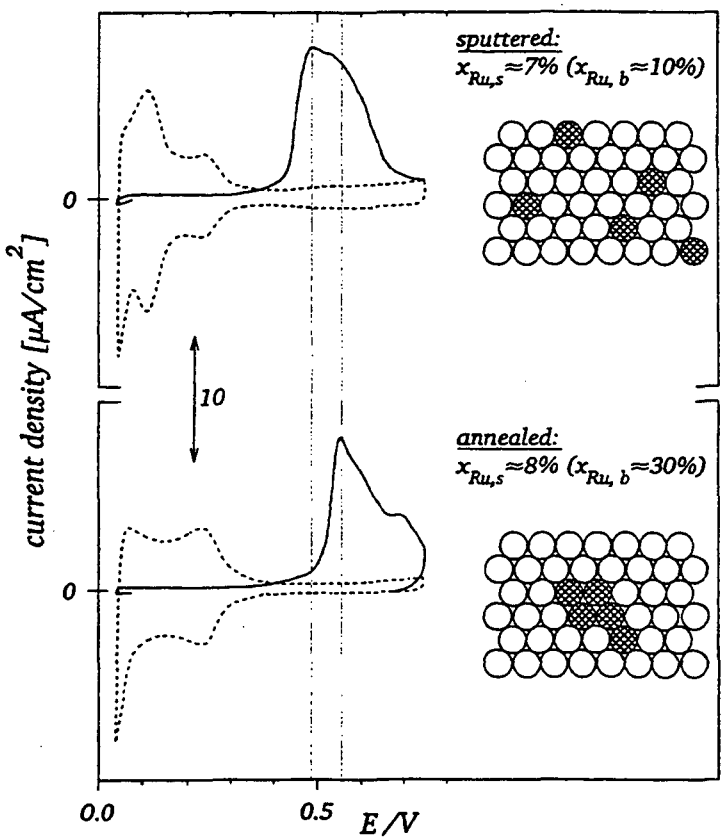

Figure 3-9. CO stripping voltammetry of sputtered and annealed Pt-Ru alloy surfaces with essentially identical Ru surface compositions as indicated in the figure (see Table 1-3 and 1-4 or Figure 2-4). (——) stripping of a monolayer of CO in the first positive-going sweep; (- - - -) first negative-going sweep after the stripping of CO, followed by a positive-going sweep. 20 mV/s; 0.5 M H_2SO_4; adsorption and immersion at 25 mV.

behavior of both Pt and Ru; and the atomically dispersed structure, where Pt-Ru pairs are maximized and any synergism due to Pt-Ru pairs is also maximized.

4. DISCUSSION

The strikingly synergistic character of Pt-Ru alloys in CO electrooxidation observed in both CO stripping voltammetry and potential-step experiments will be discussed in terms of the propensity of Ru atoms to provide nucleation sites for the

adsorption of oxygen-containing species, and in respect to the observed differences in the intrinsic rate constants of CO electrooxidation on Pt *versus* Ru surface atoms. The origin of the latter will be discussed after a careful examination of the abundant gas-phase literature on CO oxidation on Pt and Ru surfaces in UHV. Lastly, we will address the implications of this study on the mechanistic study of the electrooxidation of methanol on Pt-Ru alloy electrodes in Chapter 2.

4.1. CO Electooxidation on Pt-Ru Alloys

Above we presented measurements on the electrocatalytic activity of Pt-Ru alloys towards the oxidation of adsorbed CO in sulfuric acid electrolyte. CO adsorption at 0.075 V was found to be equally facile on all investigated electrode surfaces, resulting in essentially saturated monolayer coverages. The onset of CO oxidation in stripping voltammetry experiments on a pure Ru electrode could be observed at a potential as low as 0.25 V, although the voltammetric current peak was far more positive, by ≈0.3 V, in contrast to the behavior of a Pt electrode, which has a smaller potential separation between the onset of the oxidation and the oxidation current peak (Figure 3-3). CO stripping voltammetry at sweep rates ranging from 5 to 50 mV/s indicated the highest activity for an alloy with a Ru surface composition of ≈46 atomic%, with a negative shift in the potential of the peak current by 0.25 V compared to Pt and by ≈0.1 V in comparison to a Ru electrode (Figures 3-3 and 3-5). In contrast to pure Ru, the CO stripping voltammetry of the ≈46 atomic% alloy electrode was characterized by a relatively sharp current peak similar to CO oxidation on Pt but shifted negatively in potential. The most important conclusion to be drawn from the above experiments is the fact that the CO stripping voltammetry of Pt-Ru alloy electrodes cannot be constructed by a mere linear superposition of the pure elements' response, pointing towards the synergistic character displayed by Pt-Ru in CO electrooxidation.

Potentiostatic oxidation of adsorbed CO on the most active Pt-Ru alloy (≈46 atomic% Ru) at low potentials (Figure 3-7) revealed that the development of current maxima *versus* time was closely related to the "induction time" necessary to develop discernible oxidation currents on a pure Ru electrode at the same electrode potential, at potentials sufficiently low to exclude any oxidation of CO on Pt surface atoms within the time frame of the experiment. Following oxidation of the CO adsorbed on Ru sites, the resulting bare Ru surface atoms appear to provide nucleation sites for the adsorption of oxygen-containing species , which then can initiate the further electrooxidation of CO adsorbed either on a Pt or a Ru site nearby:

$$Ru + H_2O \longleftrightarrow (OH)_{ads} + H^+ + e^- \tag{3-6}$$

$$(CO)_{ads} + (OH)_{ads} \xrightarrow{rds} CO_2 + H^+ + e^- \tag{3-7}$$

The results can be explained qualitatively in terms of surface Reactions 6 and 7 with the assumption that Reaction 3-7 is rate-determining (rds) and Reaction 3-6 is in quasi-equilibrium. These reactions neglect details of the CO adsorption geometry. On Pt electrodes a small fraction of adsorbed CO will be present in a bridge configuration [*e.g.* 120, 132] whereas linearly-bonded CO is indicated to be the only species on a Ru electrode [124, 129]; nevertheless, the binding geometry of adsorbed CO is not a crucial issue in the following arguments. The importance of nucleation sites in the electrooxidation of adsorbed CO on a Pt(100) electrode was shown *via* "seeding" experiments by Love *et al* [117], who "seeded" a Pt(100) surface with oxygen-containing species by stepping the electrode potential to 1.1 V for 2 milliseconds, followed by potentiostatic oxidation at ≈0.8 V. "Seeded" electrodes showed an approximately four-fold increase in the oxidation kinetics, demonstrating the importance of nucleation sites on the overall electrode reaction of CO to CO_2. In our case, the number of nucleation sites

for the adsorption of oxygen-containing species at low electrode potentials will then be roughly proportional to the atomic fraction of Ru in the alloy, effecting a successively more negative CO stripping peak potential as the Ru surface concentration is increased. Above a Ru surface concentration of ≈50 atomic%, however, the voltammetric peak current begins to shift towards the more positive potential value observed on a pure Ru electrode, indicating the increasing impact of the seemingly slower electrooxidation rate of CO adsorbed on Ru rather than on Pt surface atoms, as it was similarly evident from the relatively wide voltammetric peak on pure Ru in contrast to Pt. Incidentally, the same conclusion is reached by examining the potentiostatic oxidation currents of adsorbed CO on Ru and PtRu-4 (≈46 atomic% Ru) at 0.5 V (Figure 3-6a), where only ≈50% of the saturated monolayer of CO is oxidized on pure Ru when the oxidation is already complete on the alloy electrode.

We conducted potential-stepping experiments comparing CO electrooxidation on Pt and Ru in the potential range of 0.8 to 1.0 V to further investigate this obvious synergistic property of Pt-Ru alloy electrodes. Relatively high potentials were chosen to assure comparable equilibrium coverages of oxygen-containing species on both electrodes, such that measured oxidation currents on Pt and Ru would directly reflect the ratio of the bi-molecular rate constants (see Equation 3-5), as already discussed in Section 3.3.2. Indeed, it was found that the rate constant for the electrooxidation of CO adsorbed on a pure Pt surface was larger than for CO adsorbed on a pure Ru surface at a potential where the equilibrium coverage of the surfaces of the two metals by OH_{ads} is comparable (Figure 3-8c). The increasingly longer induction times on the pure Pt electrode at 0.9 and 0.8 V (Figures 3-8b and a) may be understood by the decreasing probability of nucleating oxygen-containing species on Pt at these lower potentials. The possible origin for the observed difference in the rate constants between a Pt and a Ru site is discussed below in the context of the gas-phase catalysis literature.

4.2. Gas Phase Oxidation of CO on Pt and Ru

A direct comparison of catalytic mechanisms derived from data on a metal surface in UHV *versus* the aqueous electrochemical environment is not always straightforward: the most obvious draw-back is the absence of potential control in the UHV environment, but there is the additional essential difference in this case that the source of oxygen in the two media is very different, *i.e.* H_2O versus O_2 . Nevertheless, the basic commonalities and differences of Pt and Ru surfaces observed under the well-defined conditions of UHV might be utilized to develop a clearer understanding of their electrochemical properties.

A striking similarity exists between the facile adsorption of CO on both Pt and Ru electrodes from CO saturated acid electrolyte, and the rapid adsorption of CO on both Pt(111) and Ru(001) in UHV to saturation coverages of 0.64 [133] and 0.68 [134] on Pt and Ru, respectively. In addition, CO adsorption energies on the various crystal planes of Pt and Ru are identical to within ±15%, in the order of 120 kJ/mole for small CO coverages [135], indicating very little difference in the nature of CO bound to either surface, and a similarly high CO surface mobility on Pt(111) and Ru(001) [108]. However, there are major differences between Pt and Ru single-crystal surfaces in UHV in the energetics of oxygen adsorption, and the surface reactivity of adsorbed oxygen and adsorbed CO. UHV techniques, in contrast to electrochemical experiments, allow one to create surfaces of the pure metals with initially different and independently variable surface coverages of CO and oxygen at low temperatures where no reaction can occur. Upon increasing the surface temperature the reaction-rate limited formation of CO_2 can be monitored *via* temperature programmed desorption (TPD). Despite of the equal ease of coadsorption of oxygen and CO on Pt(111) and Ru(001), references in the literature indicate that Pt(111) is a far superior catalyst in the oxidation of CO to CO_2 [135, 136]. Indeed, it was shown by TPD of coadsorbed oxygen and CO that the formation of CO_2 on Pt(111) occurs in the temperature range between 250 and 390 K [137], whereas no CO_2

formation was observed on Ru(001) even up to 550 K, by which point all of the previously adsorbed CO was desorbed molecularly [138]. In a review paper on CO oxidation on platinum-metal surfaces in 1979, Engel and Ertl [135] proposed that the unique inactivity of Ru towards the oxidation of CO in contrast to its facile oxidation on all the other platinum-metal surfaces would be due to the exceptionally strong oxygen adsorption on Ru. Indeed, oxygen adsorption energies on Pt(111) are in the order of ≈230 kJ/mole [139, 140], whereas desorption energies on Ru(001) are ≈330 kJ/mole [141] (adsorption and desorption energies are very close for unactivated adsorption, which is believed to occur on both of the above surfaces); on both surfaces oxygen was found to adsorb in three-fold hollow sites [142, 143].

Clearly, the two major observations in our study on the electrochemical oxidation of CO on Pt-Ru alloys are consistent with properties inferred from gas-phase data, *viz*, the observed equally strong adsorption of CO on both Pt and Ru and the inference from potentiostatic experiments on the intrinsically larger rate constant for the electrooxidation of CO to CO_2 on Pt in comparison to Ru electrodes. In addition, a induction-period like that we observed in the CO electrooxidation reaction on Pt (Figure 3-8a) was also reported in an UHV study of CO oxidation on Pt(111) where the reaction was found to proceeds *via* Langmuir-Hinshelwood kinetics [139]. The oxygen-containing species in the electrochemical environment most likely are in the form of adsorbed hydroxyls, OH_{ads}, whereas the adsorbed state of oxygen in UHV is just O_{ads}. But the relative adsorption strengths of OH on Pt and Ru electrodes in electrolyte appears to reflect the behavior of adsorbed oxygen in gas-phase experiments. OH in UHV does adsorb on a Pt(111) surface with the oxygen atom towards the metal surface [144], so that the relative bonding of OH and atomic oxygen to different metals might be expected to be similar.

4.3. Origin of the Synergistic Behavior of Pt-Ru in CO Electrooxidation

The faster CO electrooxidation kinetics on a pure Pt electrode *versus* pure Ru at high potentials, evidenced by potential-step experiments on the pure metals (Figure 3-8), may either derive from a different binding state of CO or a different binding state of OH_{ads} on the two electrode surfaces. In light of the gas-phase literature on Pt(111) and Ru(001) cited above , there is little reason to believe that CO would interact significantly differently on either electrode surface. It is more likely that the difference in electrooxidation kinetics derives from variations in the adsorption strength of the oxygen-containing surface species, formulated as Pt-OH and Ru-OH in Equations 3-1 and 3-2, especially since it is well known that Ru forms irreversible oxides at potentials where on Pt reversibly adsorbed oxygen-containing species just begin to develop (as discussed in Chapter 2). Unfortunately nothing is known about the adsorption sites of oxygen-containing species on electrodes in aqueous electrolytes, but they will probably be very similar to what is observed in the gas-phase adsorption of atomic oxygen, *viz.* highly-coordinated sites. Under this premise, it is reasonable to assume that oxygen-containing species on the alloy surface (namely OH_{ads} in Equations 3-6 and 3-7) would display a modified adsorption strength depending on the nature of atoms constituting the surface ensemble for its adsorption, thereby producing a larger rate constant for Reaction 3-7 on the alloy surface than the rate constants for the corresponding reactions on the pure metal surfaces (Reactions 3-1 and 3-2). The reported maximum activity of the alloy with a Ru surface composition of ≈46 atomic% then seems to reflect a balance between maximizing OH_{ads} nucleation sites at low potentials, which are approximately proportional to x_{Ru} , and reducing the adsorption strength of OH_{ads} by limiting the number of Ru-Ru neighbors, which scale by approximately x_{Ru}^2. An optimum "mixing" of Pt and Ru surface atoms in an ideal solution alloy would occur at a Ru surface composition of 50%, for which the number of Pt/Ru pairs is maximized, thereby avoiding the suggested stronger adsorption

of OH_{ads} on multiple Ru sites while maintaining a high surface concentration of Ru atoms to provide nucleation sites. Consequently, significantly lower CO oxidation rates would be expected on annealed alloy surfaces, where Ru island formation is highly probable. This indeed, was indicated in Section 3.4, where the CO stripping voltammetry on an annealed alloy with a Ru surface concentration of ≈8 atomic% could be interpreted as a Ru "nano-electrode" embedded in a Pt electrode.

4.4. Comparison of Methanol and CO Oxidation on Pt-Ru Alloys

Besides its implications for the electrooxidation of steam-reformed hydrogen, our major interest in the electrooxidation of CO on Pt-Ru alloy electrodes originated from our study on their electrocatalytic activity in the electrooxidation of methanol, surpassing pure Pt electrodes by a factor of up to ≈30 on alloys with a Ru surface concentration of ≈10 atomic% (Chapter 2). We had found that methanol did not adsorb on pure Ru and that methanol oxidation currents on Pt-Ru alloys were determined by a balance of the methanol adsorption rate followed by its initial dehydrogenation, and the oxidative removal of methanol dehydrogenation fragments aided by the nucleation of oxygen-containing species on Ru surface sites. The observed maximum activity for the electrode with a Ru surface composition of ≈10 atomic% was predicted by a statistical model under the assumption that the most active surface atom ensemble would consist of three-fold Pt ensembles to allow the adsorption of methanol, adjacent to one Ru surface atom to provide a nucleation site for the complete electrooxidation of methanol. Quite clearly, the situation here with preadsorbed CO is very different in two aspects: rate-limiting factors due to reactant adsorption are excluded for preadsorbed reactant, and CO adsorption seems equally facile on both Pt and Ru sites in contrast to CH_3OH adsorption. Nevertheless, the previous assumption as to the promotion of the nucleation of oxygen-containing species by Ru surface atoms was corroborated by our present experiments on CO electrooxidation on Pt-Ru alloy electrodes. The absence of an adsorption limitation in

this study, however, resulted in a higher optimum Ru surface concentration (≈50 atomic%) for the maximum activity in contrast to the optimum Ru surface concentration of ≈10 atomic% in the adsorption-limited methanol electrooxidation reaction. As will be seen shortly, the electrooxidation of formic acid is strikingly similar to the electrooxidation of CO, probably due in large part to the fact that adsorption of the respective reactant occurs on both Pt and Ru surface atoms.

5. CONCLUSIONS

Based on CO stripping voltammetry and on the potentiostatic oxidation of an adsorbed monolayer of CO on sputter-cleaned Pt-Ru alloy electrodes in sulfuric acid electrolyte we found that an alloy with a Ru surface composition of ≈50 atomic% exhibited the highest activity, with an approximate reduction of the oxidation overpotential of 0.25 V compared to pure Pt, and 0.1 V compared to Ru. Furthermore, the optimum alloy electrode displayed strikingly synergistic properties which could not be rationalized by a mere linear superposition of the properties of the pure metals. The bifunctional character of Pt-Ru alloys emerged quite clearly from the above study: the ability of Ru surface atoms to provide nucleation sites for oxygen-containing species at low electrode potentials, and the oxidation of CO migrating to these sites from either Pt or Ru sites nearby. In addition it was found that the intrinsic activity of Pt in the bi-molecular oxidation reaction of CO to CO_2 was larger than that observed for Ru, which we suggest is due to the lower adsorption strength of oxygen-containing species on Pt-Ru pair sites *versus* pure Ru. The observed maximum activity at a Ru surface composition of ≈50 atomic% corresponds to a surface with a maximum number of Pt-Ru pairs.

The strong synergistic effect of sputter-cleaned Pt-Ru alloy electrodes towards the electrooxidation of CO was not observed for an annealed alloy electrode with a

comparable Ru surface composition. The electrocatalytic behavior of the annealed electrode was merely a linear superpostion of the properties of the pure elements. This was rationalized by the thermodynamic preference for cluster formation on annealed surfaces, which would essentially create Ru "nano-electrodes" embedded in a Pt electrode.

Chapter 4:
HCOOH Oxidation on Pt-Ru Alloys at 25°C

1. Introduction 104
2. Experimental Procedures 105
3. Results 105
   3.1. Potentiodynamic Experiments 105
      3.1.1. Pure Pt 105
      3.1.2. Pure Ru 108
      3.1.3. Pt-Ru Alloy Electrodes 110
   3.2. Potentiostatic Experiments 112
      3.2.1. Pure Pt and Ru 112
      3.2.2. Pt-Ru Alloy Electrodes 113
4. Discussion 116
   4.1. Pure Pt and Ru Electrodes 116
   4.2. Pt-Ru Alloys 119
5. Conclusions 122

1. INTRODUCTION

Formic acid is known to be a by-product in the electrooxidation of methanol on Pt electrodes in acidic electrolytes [145-147], therefore it is of interest to investigate the activity of Pt-Ru alloy electrodes for electrooxidation of formic acid. In contrast to methanol and CO electrooxidation on Pt, where a reaction intermediate is poisoning the electrode reaction, the poisoning of Pt electrodes in the electrooxidation of HCOOH is believed to be a side-reaction [128, 109], *viz* one branch of the so-called dual path reaction mechanism [*e.g.* 148, 149]. In light of the models we have proposed for CO and CH_3OH oxidation on Pt-Ru alloys, we were interested to see if we could explain the

activity of the same alloys for HCOOH oxidation within the same mechanistic framework.

2. EXPERIMENTAL PROCEDURES

All electrochemical measurements reported in this chapter were conducted on mildly sputtered surfaces (0.5 keV Ar^+) which were transferred from UHV into a standard three-compartment electrochemical meniscus-type cell as outlined in Chapter 2. Surface and bulk composition of sputter-cleaned electrodes were essentially identical as verified by LEIS (see Chapter 1), and Ru compositions will be given in terms of surface compositions throughout this study. Electrochemical measurements were taken at 25°C in 0.5 M H_2SO_4 (Baker Analyzed, Ultrex) prepared with triply pyro-distilled water. Electrooxidation current densities were recorded in cyclic voltammetry and in potentiostatic experiments in 0.5 molar solutions of formic acid (EM Science, GR Grade) and methanol (Baker Analyzed); argon (Alphagaz, 5N5) was used to deoxygenate the electrolyte. In CO stripping experiments (Matheson, 4N) two electrochemical cells were used, where the electrolyte in one of the cells was saturated with CO (for details see Chapter 3). Potentials were measured *versus* a Pd/H electrode, but all potentials in the following are referred to the reversible hydrogen electrode in the same solution (RHE).

3. RESULTS

3.1. Potentiodynamic Experiments

3.1.1. Pure Pt

Figure 4-1a shows the cyclic voltammetry of a sputter-cleaned Pt electrode transferred from UHV into 0.5 M HCOOH in 0.5 M H_2SO_4 supporting electrolyte. All

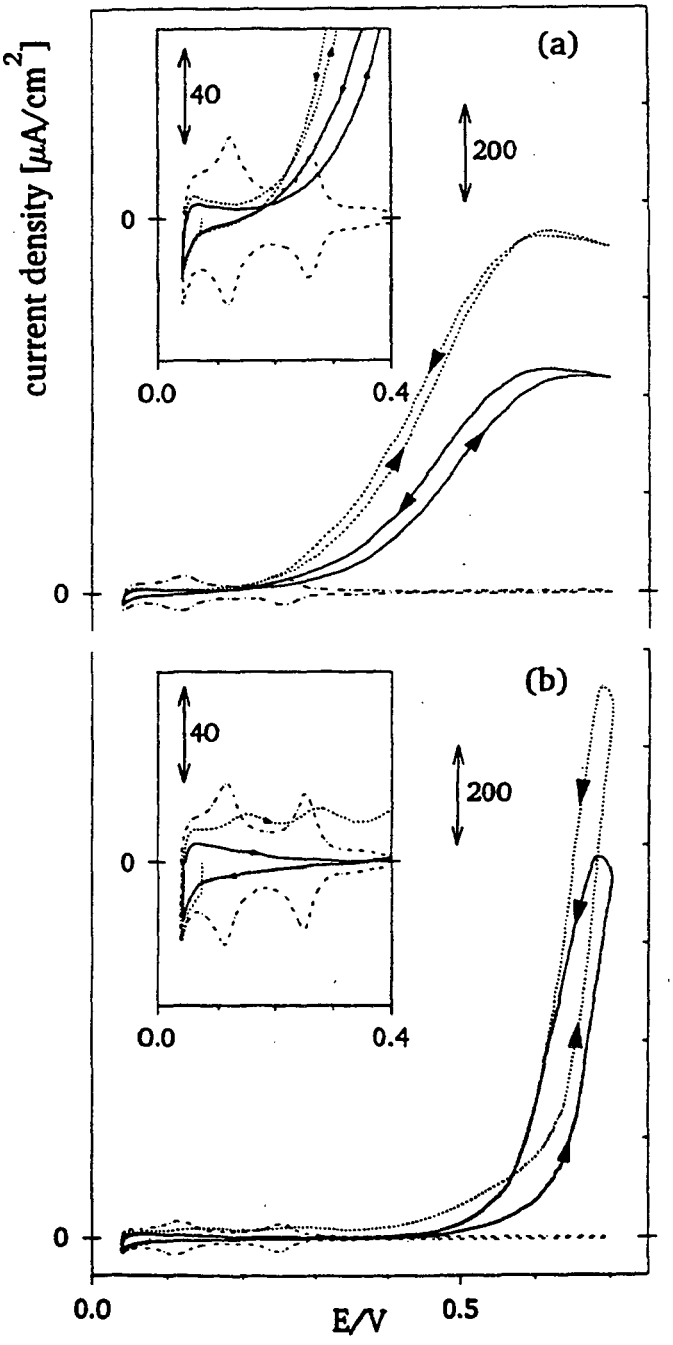

Figure 4-1. Cyclic voltammetry of sputter-cleaned Pt in 0.5 M H_2SO_4 supporting electrolyte and: **(a)** 0.5 M HCOOH; **(b)** 0.5 M CH_3OH. (-·-·-·-·) base voltammetry in 0.5 M H_2SO_4; (- - - -) first sweep after immersion at 0.075 V for 3 minutes; (——) 10th sweep. The inserts are a magnification of the potential region between 0 and 0.4 V. 20 mV/s.

cyclic voltammograms in the following originated from a potential of 0.075 V sweeping negatively after immersion of the electrode for 3 minutes; sweep rates were 20 mV/s. In accordance with formic acid adsorption isotherms in the literature [85 ,150, 151] already the first sweep indicates a large coverage of the electrode with adsorbed organic residues (commonly referred to as "poisons"), conveyed clearly in the insert of Figure 4-1a. In the first positive-going sweep significant HCOOH oxidation occurred at ≈0.3 V and upon sweep reversal at 0.7 V very little hysteresis in the oxidation currents was observed. Significantly larger currents during negative- *versus* positive-going sweeps on Pt only develop if the positive potential limit exceeds ≈0.8 V [149], *i.e.* beyond a potential which marks the onset of the adsorption of oxygen-containing species on Pt (see Chapter 2 Section 3.2). In contrast to the adsorption behavior of formic acid, the adsorption of methanol on Pt at 0.075 V is very small [85, 152], as indicated by the essentially unperturbed hydrogen coverage of a Pt electrode during the first sweep in 0.5 M CH_3OH, shown in the insert of Figure 4-1b. Furthermore, while the first sweep in the voltammetry of Pt in formic acid was not very different at low potentials from the 10th sweep (insert Figure 4-1a), the deactivation of Pt in 0.5 M CH_3OH from the first to the 10th sweep was dramatically larger (insert Figure 4-1b), since in the case of methanol the first sweep was recorded on an unblocked, *i.e.* unpoisoned electrode in contrast to what was observed for fomic acid oxidation. The initial methanol dehydrogenation currents at low potentials during the first sweep disappeared in successive sweeps presumably due to the lack of oxygen-containing species on the electrode surface necessary for the complete oxidation of methanol dehydrogenation fragments to CO_2. On the contrary, the oxidation of HCOOH to CO_2 apparently does not require any additional oxygen source and can thus proceed at much lower potentials concomitant, however, with the simultaneous formation of adsorbed organic residues *via* the dehydration of HCOOH in a parallel reaction path [149].

3.1.2. Pure Ru

Whereas the voltammetry of Pt in the presence of formic acid is well documented in the literature, we are not aware of any published voltammetry of Ru in formic acid solutions, shown in Figure 4-2a. Analogous to Pt, Ru was significantly poisoned at the beginning of the first sweep. The turnover number (number of oxidized reactant molecules per surface site) during the first positive-going potential sweep was less than one, very much in contrast to the turnover number on Pt (Figure 4-1a), which approached 25 in the same potential interval. In addition, the poisoning of a Ru electrode by formic acid was quite different from the essentially inert character of Ru in contact with methanol solutions (Figure 4-2b), at least in the investigated potential range of up to 0.7 V.

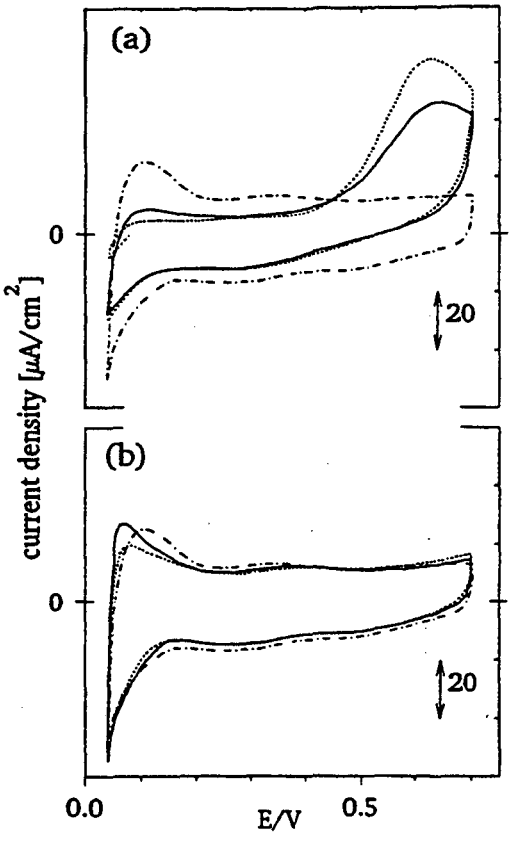

Figure 4-2. Cyclic voltammetry of sputter-cleaned Ru in 0.5 M H_2SO_4 supporting electrolyte and: **(a)** 0.5 M HCOOH; **(b)** 0.5 M CH_3OH. (·-·-·-·-·) base voltammetry in 0.5 M H_2SO_4; (- - - -) first sweep after immersion at 0.075 V for 3 minutes; (——) 10th sweep. 20 mV/s.

Figure 4-3 compares the first sweep in the cyclic voltammetry of Ru in 0.5 M HCOOH with the stripping voltammetry of an adsorbed monolayer of CO. Both the onset of the oxidation and the peak current potential were strikingly similar, suggesting that the reaction of formic acid with Ru proceeds through the oxidation of adsorbed CO, whereas the voltammetry of Pt in 0.5 M HCOOH (Figure 4-1a) did not resemble its CO stripping voltammetry (see *e.g.* Figure 3-3). The slight positive shift in the peak current potential of HCOOH *versus* CO electrooxidation on Ru may be understood by the concomitant readsorption of formic acid from the bulk electrolyte (in the CO experiments there was no CO in solution).

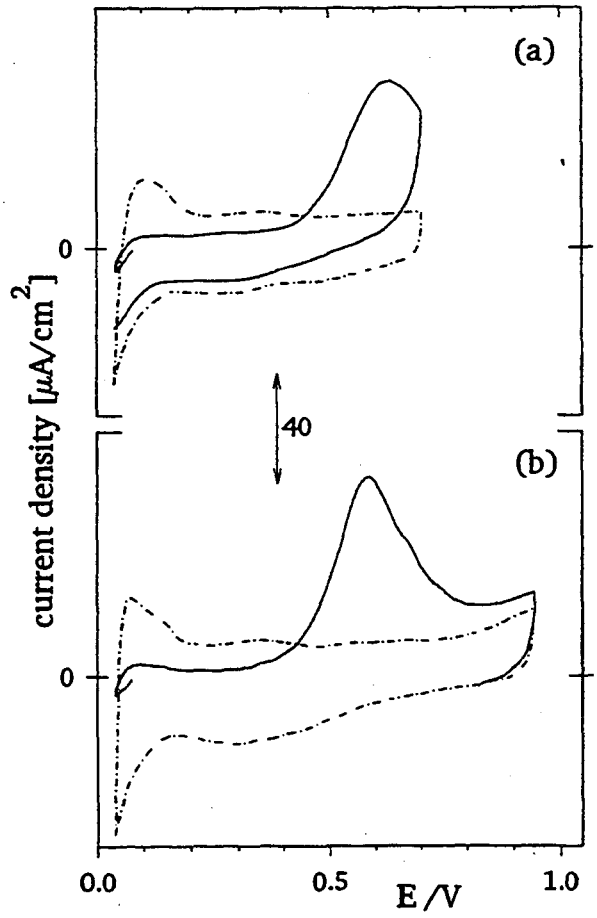

Figure 4-3. (a) Cyclic voltammetry of sputter-cleaned Ru in 0.5 M H_2SO_4 and 0.5 M HCOOH: (-·-·-·-) base voltammetry ; (——) first sweep after immersion at 0.075 V for 3 minutes. (b) CO stripping voltammetry of Ru in 0.5 M H_2SO_4 after CO adsorption at 0.075 V: (-·-·-·-) base voltammetry; (——) first sweep. 20 mV/s.

3.1.3. Pt-Ru Alloy Electrodes

In the following we will examine the voltammetry of the alloy with a Ru surface concentration of ≈7 atomic%, found to be the most active catalyst in the electrooxidation of methanol at room temperature (see Chapter 2).The cyclic voltammogram of this alloy electrode in 0.5 M HCOOH is shown in Figure 4-4a. Quite different from HCOOH oxidation on pure Pt (Figure 4-1a), the ≈7 atomic% Ru surface exhibited a strong hysteresis between positive- and negative-going sweeps, which on Pt only develops if the positive potential limit exceeds approximately 0.8 V, as discussed above. Quite clearly, the oxidative removal of strongly adsorbed organic intermediates from the alloy surface can proceed at lower electrode potentials than on pure Pt, thereby facilitating larger oxidation currents during the negative-going sweep. This restitution of the alloy electrode surface due to the positive potential excursion is apparent also in the increased currents from the first to the 10th sweep in the potential region between 0 and 0.2 V (insert of Figure 4-4a), contrary to the behavior of a pure Pt electrode (insert of Figure 4-1a). The opposite effect, *viz* the larger oxidation currents on Pt versus the alloy electrode during the positive-going sweep is apparently connected with the strong poisoning of Ru sites in the region of low electrode potentials, as will be discussed in Section 4. Similarly it is evident that HCOOH electrooxidation currents during the negative-going sweep on pure Pt *versus* the alloy electrode are lower because of the lesser extent of surface poisoning on the alloy electrode after having been exposed to more positive potentials. This difference in the electrooxidation currents between positive- and negative-going sweeps at low potentials increased consistently with the Ru suface composition, *i.e.* from ≈7 atomic% to 33 atomic% to 46 atomic%, and was very small for pure Pt.

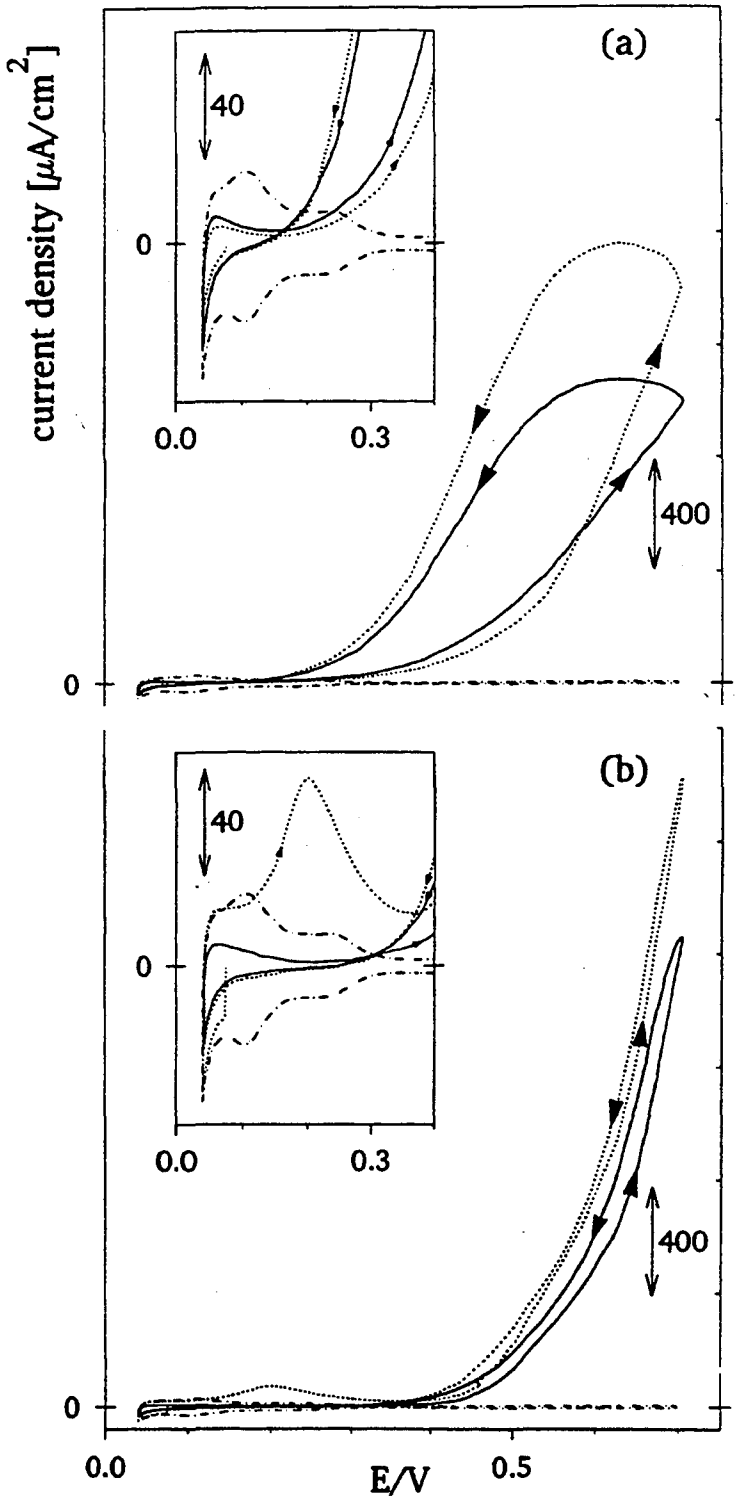

Figure 4-4. Cyclic voltammetry of sputter-cleaned Pt-Ru with a Ru surface concentration of ≈7 atomic% in 0.5 M H_2SO_4 supporting electrolyte and: **(a)** 0.5 M HCOOH; **(b)** 0.5 M CH_3OH. (·-·-·-·-·) base voltammetry in 0.5 M H_2SO_4; (- - - -) first sweep after immersion at 0.075 V for 3 minutes; (——) 10th sweep. The inserts are a magnification of the potential region between 0 and 0.4 V. 20 mV/s.

The absence of hysteresis in the cyclic voltammetry of the alloy with a Ru surface composition of ≈7 atomic% in 0.5 M CH_3OH (Figure 4-4b) most likely derives from the slower adsorption of methanol compared to formic acid [87]. In addition, the adsorption and initial dehydrogenation of methanol was shown in Chapter 2 to be limited to surface ensembles of Pt atoms, whereas Figure 4-2a revealed that the adsorption of formic acid may also occur on Ru surface atoms and probably on ensembles of Pt and Ru, which in turn will allow comparably larger rates of HCOOH adsorption on equally poisoned surfaces leading to the observed pronounced hysteresis in contrast to methanol oxidation. In this context, it should be noted that the turnover numbers during the first positive-going sweep in 0.5 M HCOOH and 0.5 M CH_3OH were ≈18 and 7, respectively.

3.2. Potentiostatic Experiments

3.2.1. Pure Pt and Ru

Potentiostatic oxidation currents for 0.5 M HCOOH in 0.5 M H_2SO_4 were measured at 0.4 V, resulting in maximum current densities of less than ≈1% of the estimated diffusion-limited current densities. Experiments were conducted in two different ways: direct contact of the electrode at 0.4 V with 0.5 M HCOOH (further referred to as "direct stepping"), and stepping of the electrode potential to 0.4 V after immersion of the electrode at 0.075 V in 0.5 M HCOOH for 3 minutes (further referred to as "indirect stepping"). Direct stepping data were not reliable at short times (≈30 s) because of the turbulence created by the establishment of the meniscus, whereas data for the potential step from 0.075 to 0.4 V were acquired with a time resolution of 3 ms. As may be expected considering the substantial coverage of a Pt electrode with adsorbed organic residues after adsorption at 0.075 V (Figure 4-1a), direct immersion at 0.4 V yielded higher current densities than the indirect stepping method (Figure 4-5a), for which at zero time the electrode surface was already partially deactivated by adsorbed organic residues. The current densities at 0.4 V on Pt measured by these two methods

differed by a factor of ≈2, in contrast to a factor of ≈10 for current densities measured on Ru (Figure 4-5b), attesting to its stronger poisoning at low potentials. In general, current densities on Ru were found to be approximately one order of magnitude lower than on Pt.

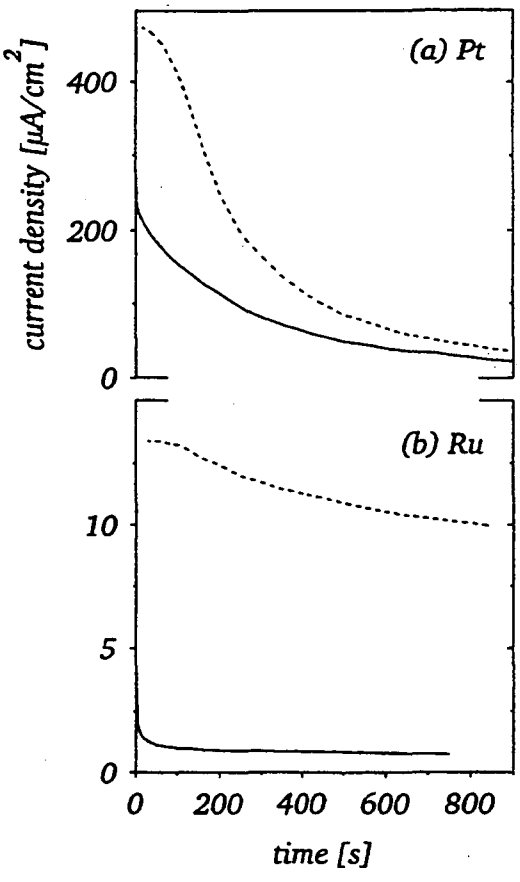

Figure 4-5. Potentiostatic oxidation of 0.5 M HCOOH in 0.5 M H_2SO_4 on sputter-cleaned **(a)** Pt and **(b)** Ru: (——) emersion at 0.4 V; (——) immersion at 0.075 V for 3 minutes, then stepping to 0.4 V.

3.2.2. Pt-Ru Alloy Electrodes

Figure 4-6 shows the potentiostatic current densities at 0.4 V in 0.5 M HCOOH on sputter-cleaned Pt-Ru alloys (Ru surface concentrations are indicated in the figure) as measured by the indirect stepping method. After the decay of pseudocapacitive currents, electrooxidation currents were fairly low, somewhere between the currents observed on the pure metals (see Figure 4-5). After a short induction time, τ_{ind} , (time to reach the

minimum in the observed current density, see insert Figure 4-6) which was inversely proportional to the Ru surface concentration of the respective alloy electrode, formic acid oxidation currents increased by almost one order of magnitude. Current densities on the most active electrode (≈46 atomic% Ru surface concentration) were ≈5 times larger after 15 minutes than on a pure Pt electrode.

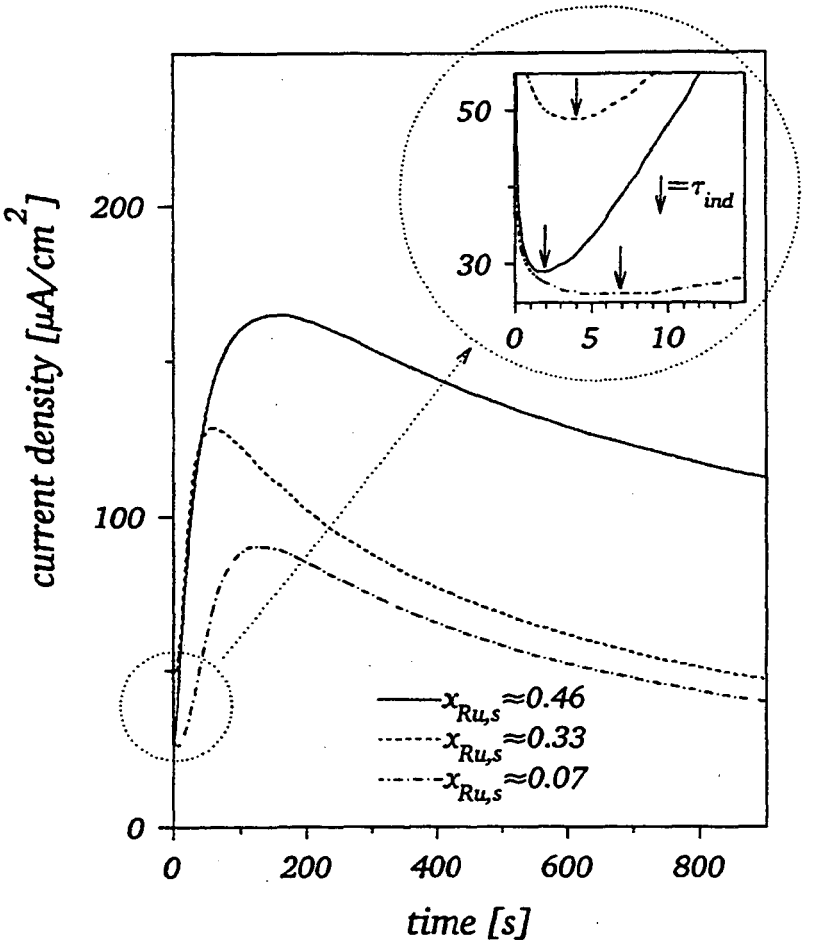

Figure 4-6. Potentiostatic oxidation of 0.5 M HCOOH in 0.5 M H_2SO_4 on sputter-cleaned Pt-Ru alloys at 0.4 V after immersion at 0.075 V for 3 minutes. Ru surface compositions are indicated in the figure. The insert shows the first 15 seconds on a magnified scale; induction times, τ_{ind} , are marked by an arrow.

Approximately the same induction time of ≈2 s was observed in the electrooxidation of an adsorbed monolayer of CO on the alloy with a Ru surface concentration of ≈46 atomic% at the same potential, Figure 4-7. It was correlated with the initial slow electrooxidative removal of CO adsorbed on Ru surface atoms, thereby

creating bare Ru atoms providing nucleation sites for the adsorption of oxygen-containing species at relatively low potentials, which then would aid the complete oxidative removal of CO (see Chapter 3). The cyclic voltammetry of both pure Ru and Pt in 0.5 M HCOOH (Figures 4-1a and -2a) attested to the equally strong interaction of formic acid at low potentials with the two metals, similar to the equally facile adsorption of CO on Ru and Pt. As a consequence, the electrooxidative removal of formic adsorption fragments during potential-step experiments shows the same characteristic induction time. The longer time necessary to reach the maximum in the current density on formic acid *versus* CO oxidation is most likeley due to the simultaneous adsorption of HCOOH from the bulk. In addition, a larger atomic fraction of Ru surface atoms should result in a shorter induction time necessary to create a sufficient number of nucleation sites for oxygen-containing species, in agreement with Figure 4-6.

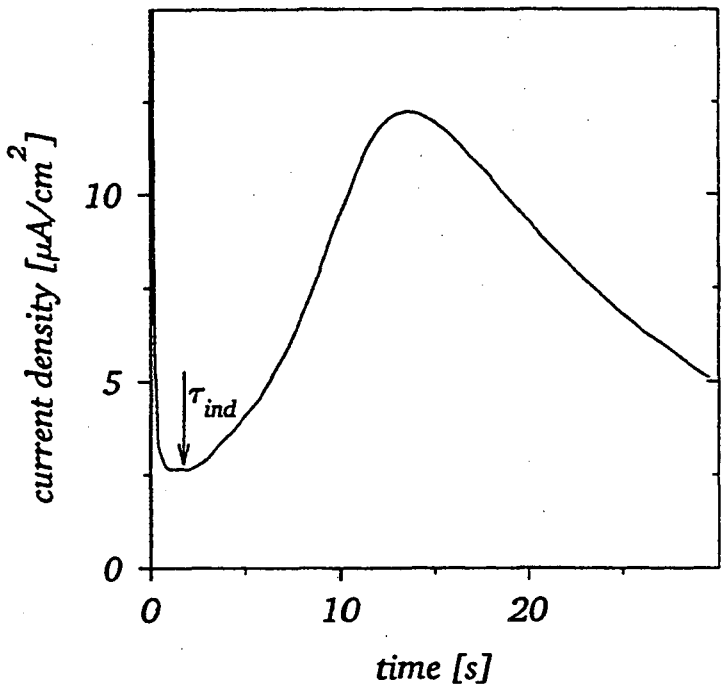

Figure 4-7. Potentiostatic oxidation of adsorbed CO on sputter-cleaned Pt-Ru with a Ru surface composition of ≈46 atomic%. The electrode was immersed at 0.075 V for 3 minutes in 0.5 M H_2SO_4 prior to stepping to 0.4 V.

4. DISCUSSION

4.1. Pure Pt and Ru Electrodes

Formic acid, methanol and CO electrooxidation on Pt have been studied extensively in the past [*e.g.* 109, 149] and the observed deactivation (poisoning) of electrode surfaces in the course of the electrooxidation reaction was found to be predominantly due to linearly-bonded CO [128, 121, 151]. Although other minor surface species have been proposed in the literature, we will in our discussion refer to surface poisons in terms of linearly-bonded CO only, without, however, compromising the conceptual course of the arguments presented. High HCOOH electrooxidation currents on Pt are observed at potentials well below 0.5 V (Figure 4-1a) and are generally thought to derive from the fact that no additional source of oxygen is necessary for its complete oxidation to CO_2, corroborated by isotope-labeling experiments [153]. The concomitant deactivation of Pt by adsorbed CO, however, led to the now widely accepted hypothesis of a "dual path" reaction mechanism [*e.g.* 149]:

$$\mathrm{HCOOH} \begin{array}{l} \xrightarrow{\text{dehydrogenation}} \mathrm{CO_2 + 2H^+ + 2e^-} \\ \xrightarrow{\text{dehydration}} \mathrm{M-CO + H_2O} \end{array} \qquad (4\text{-}1)$$

namely the direct dehydrogenation of HCOOH yielding fairly high current densities and its simultaneous dehydration resulting in adsorbed CO (M symbolizing the substrate atom), thermodynamically stabilized by its large energy of adsorption on Pt (≈120 kJ/mole, [100]). The precursor state of HCOOH oxidation, omitted in Reaction 4-1, is probably adsorbed formate as indicated by UHV data [154]. Although it is commonly reported that HCOOH interacts with adsorbed H at low potentials forming strongly adsorbed intermediates [149, 153], it seems that the poisoning of the electrode at

low potentials is merely due to the formation of CO while its oxidative removal (see Reaction 4-3 below) is not catalyzed at potentials ≤0.5 V, thereby leading to the accumulation of CO during the voltammetric sweep through the "hydrogen-region" (0≤ E ≤0.35 V). In contrast, potentiodynamic CH_3OH oxidation on Pt after the first sweep does not commence below ≈0.5 V (Figure 4-1b) and CO_2 forms only by oxidation of adsorbed CO, *i.e.* CO is a reaction intermediate formed by the initial dehydrogenation of methanol:

$$CH_3OH \xrightarrow{\text{dehydrogenation}} M-CO + 4H^+ + 4e^- \tag{4-2}$$

$$M-CO + (OH)_{ads} \xrightarrow{k_{CO}} CO_2 + H^+ + e^- \tag{4-3}$$

This is supported by the similar onset potential of CO (see Chapter 3) and CH_3OH electrooxidation on Pt, as well as their similar voltammetry on Pt single-crystals [155]. The potential-dependent adsorption of oxygen-containing species, OH_{ads}, is necessary for Reaction 4-3 to proceed:

$$H_2O \xrightarrow{k_{OH}} (OH)_{ads} + H^+ + e^- \tag{4-4}$$

In contrast to Pt, Ru is completely inactive in a methanol solution up to potentials of 0.7 V (Figure 4-2b), suggesting that the initial dehydrogenation of CH_3OH (Reaction 4-2) does not occur on Ru. In HCOOH, however, the Ru surface is fully covered with organic adsorbates even at the onset of the first voltammetric sweep (Figure 4-2a), but oxidation currents do not commence before ≈0.4 V and are small up to the positive potential limit of 0.7 V with a total turnover number of less than one. No oxidation was observed during the negative-going sweep, in which the strongly adsorbed oxygen-containing species prevent the further adsorption of HCOOH; similar observations were made on a Rh electrode [148]. A comparison of the voltammetric stripping of adsorbed CO with the first positive-going sweep in 0.5 M HCOOH reveals an

astounding similarity in both the onset of the oxidation and the oxidation current density (Figure 4-3). This, together with the fact that Ru was shown to be inactive in the dehydrogenation of CH_3OH, strongly indicates that the interaction of Ru with HCOOH proceeds *via* the dehydration pathway only (see Reaction 4-1), forming adsorbed CO which again is stabilized by its large energy of adsorption (≈120 kJ/mole, [100]). The facile dehydrogenation reaction of HCOOH on Pt *versus* the major dehydration reaction on Ru is consistent with gas-phase studies, which show that HCOOH adsorption on Pt(111) leads only to the formation of CO_2 at -13°C [156], whereas CO and CO_2 are formed at equal rates on Ru(001) above 55°C [157].

The poisoning of Pt in contact with the electrolyte at 0.075 V is apparent in potential-step experiments (Figure 4-5a). Initial current densities on a Pt electrode immersed at 0.4 V ("direct stepping") are on the order of 400 $\mu A/cm^2$, resulting in a turnover number of ≈160 during the first 200 s mainly *via* HCOOH dehydrogenation since CO oxidation is insignificant at 0.4 V (Reaction 4-3), but its finite formation-rate *via* HCOOH dehydration slowly poisons the Pt surface. The electrode deactivation by CO leads to a more than ten-fold decrease in the current density after 15 minutes. Current densities on a Pt electrode immersed for 3 minutes at 0.075 V prior to stepping to 0.4 V ("indirect stepping") are initially lower by a factor of ≈2 if compared to direct stepping, because of the poisoning of the electrode during immersion at low potentials, but after 15 minutes the differences between direct and indirect stepping current densities decrease, seemingly reaching a common "steady-state". Current densities in the direct stepping experiment on Ru (Figure 4-5b) are smaller by an order of magnitude compared to Pt with, however, small deactivation of the electrode over 15 minutes on account of the higher activity of Ru towards the oxidative removal of the HCOOH dehydration product, CO (Reaction 4-3), which is catalyzed by the nucleation of OH_{ads} (Reaction 4-4) at lower potentials (see Chapter 3). In an indirect stepping experiment the Ru surface is strongly

poisoned by CO as suggested in Figure 4-3 and current densities on this surface are only on the order of 1 $\mu A/cm^2$ with a turnover number of only ≈2 after 15 minutes. In striking contrast to Pt, no common "steady-state" for direct and indirect stepping experiments is approached during this time, indicating that the surface removal of CO adsorbed during immersion in HCOOH at 0.075 V in indirect stepping is prevented by the slow surface oxidation of CO (Reaction 4-4) while competing with the concomitant adsorption and dehydration of HCOOH. The "inactive" state of Ru is therefore represented by a surface predominantly covered with CO and its "active" state is characterized by a surface predominantly covered with OH_{ads} . The same observations were made in the electrooxidation of CO on pure Ru at 0.4 V, where immersion of the clean electrode in CO saturated electrolyte (0.5 M H_2SO_4) resulted in ≈10 times larger current densities (≈10 $\mu A/cm^2$) than the oxidation of preadsorbed CO (≈1 $\mu A/cm^2$). Similarly active and inactive surface states were reported for HCOOH oxidation on Pt(100), effecting sustained current oscillations [158].

4.2. Pt-Ru Alloys

A Pt-Ru alloy with a Ru surface concentration of ≈10 atomic% was found to be the most active surface for CH_3OH electrooxidation at 25°C, maximizing the number of Pt ensembles necessary for CH_3OH adsorption while providing OH nucleation on adjacent Ru atoms (Chapter 2), whereas the optimum Ru surface in CO oxidation was ≈50 atomic% with a strong synergistic effect, which was attributed to a reduced adsorption strength of OH_{ads} on Pt-Ru pairs (Chapter 3). In investigating the activity of Pt-Ru alloys towards the electrooxidation of HCOOH we will first discuss the cyclic voltammetry of an alloy with a Ru surface concentration of ≈7 atomic% in 0.5 M HCOOH (Figure 4-4a). A comparison with pure Pt (Figure 4-1a) reveals the property of Ru atoms to allow the adsorption of OH_{ads} at relatively low potentials according to Reaction 4-4, thereby facilitating the removal of adsorbed organic residues. The lack of

hysteresis on the same alloy in 0.5 M CH_3OH (Figure 4-4b) is probably due to the different reaction mechanism of CH_3OH oxidation (Reaction 4-2 and 4-3), where CO is a reaction intermediate.

Indirect stepping experiments in 0.5 M HCOOH yielded initially low current densities (inactive state), but after a short induction time, inversely proportional to the Ru surface concentration, current densities increased by an order of magnitude (active state). As was discussed above, the electrodes are strongly poisoned with CO during the immersion at 0.075 V, and the induction time reflects the time necessary to create bare Ru sites for the Ru-catalyzed nucleation of OH_{ads} for the removal of CO through Reaction 4-3. Very strong support that CO is the poisoning species in this reaction is given by Figure 4-7, which shows the oxidation of preadsorbed CO at 0.4 V on the alloy with a Ru surface concentration of ≈46 atomic%: the observed induction time in the electrooxidation of both adsorbed CO and HCOOH after adsorption at 0.075 V is ≈2 s. The transition, however, from the inactive to the active state in Figure 4-6, *i.e.* the transition from a predominantly CO covered electrode surface to a surface with comparable coverages with OH_{ads} and CO, was not observed on a pure Ru electrode (Figure 4-5b). This synergism of Pt-Ru alloy electrodes is quite analogous to what was observed in the electrooxidation of CO, where it was attributed to the reduced adsorption strength of OH_{ads} (Reaction 4-4) on Pt-Ru pairs *versus* Ru, thereby increasing k_{CO} in Reaction 4-3. The optimum Ru surface concentration for HCOOH electrooxidation is ≈46 atomic% (Figure 4-6), analogous to the optimum concentration for CO electrooxidation. This optimum surface composition is expected from the reaction mechanism, since the adsorption of both reactants is not limited to Pt sites and since Pt-Ru pairs are the active sites for reaction 3 and the number of these sites is maximized at ≈50 atomic%.

An optimum Ru surface concentration of ≈50 atomic% for HCOOH electrooxidation was also observed in direct stepping experiments (Figure 4-8a) with a five-fold improvement over pure Pt. The initially higher current densities in direct *versus* indirect stepping experiments approached the current densities of the active state in indirect stepping experiments (Figure 4-6), as was observed for pure Pt (Figure 4-5a).

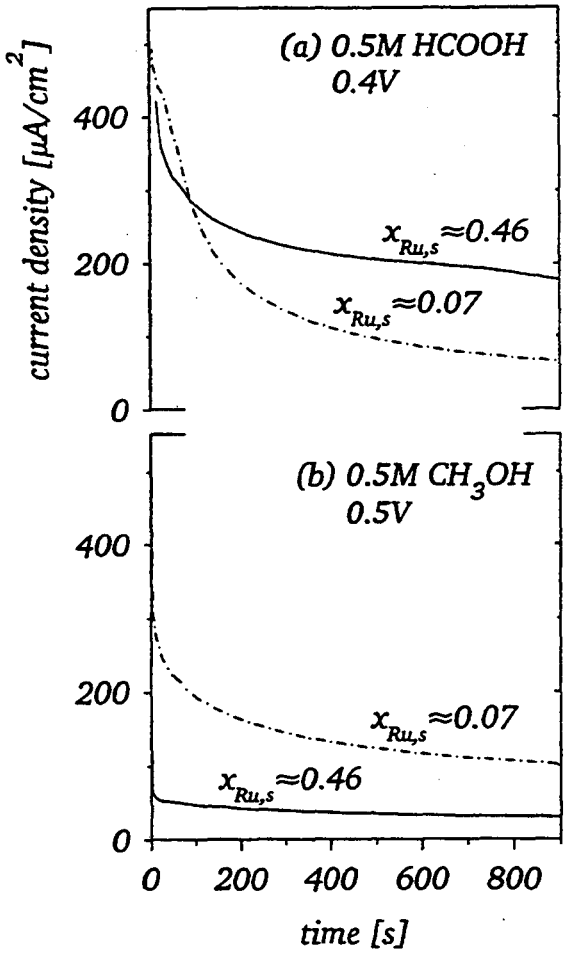

Figure 4-8. Potentiostatic oxidation of: (**a**) 0.5 M HCOOH at 0.4 V, and (**b**) 0.5 M CH_3OH at 0.5 V on sputter-cleaned Pt-Ru alloys. For HCOOH oxidation the electrode was immersed at 0.4 V; for CH_3OH oxidation the electrode was stepped to 0.5 V after emersion at 0.075 V for 3 minutes.

In contrast to HCOOH electrooxidation on Pt-Ru alloys, indirect stepping experiments in 0.5 M CH_3OH to 0.5 V showed no sign of an induction period (Figure 4-8b), because of the insignificant dissociative chemisorption of CH_3OH at 0.075 V (Figures 4-1b and 4-4b). The high activity observed for the alloy with a Ru surface concentration of

only ≈7 atomic% was shown to be due to the requirement of Pt ensembles to facilitate the dissociative adsorption of CH_3OH (Reaction 4-2) with an adjacent Ru atom to nucleate oxygen-containing species necessary for the oxidative removal of methanol dehydrogenation fragments (Reaction 4-3) . This most active Pt-Ru alloy increased the electrooxidation of methanol (0.5 M) at 0.5 V by a factor of ≈30. The larger enhancement of Pt-Ru alloys in the electrooxidation of CH_3OH *versus* HCOOH probably derives from the inert character of Ru towards CH_3OH, such that all Ru sites are available for the adsorption of OH (Reaction 4-4) in CH_3OH solution, in contrast to the competition between H_2O (leading to OH formation) and HCOOH (leading to CO formation) for Ru sites in formic acid solution. This competition leads to the existence of an active and an inactive state in HCOOH oxidation on pure Ru (Figure 4-5b).

5. CONCLUSIONS

In agreeement with the literature, the electrooxidation of HCOOH on a pure Pt electrode was found to proceed *via* the "dual path" mechanism, namely HCOOH dehydrogenation (to form CO_2) and dehydration (to form adsorbed CO). In the electrooxidation of CH_3OH on pure Pt , however, adsorbed CO is a reaction intermediate, consistent with the similarity observed between CO and CH_3OH oxidation, in contrast to the unique behavior in HCOOH oxidation.

The electrooxiation of HCOOH on pure Ru was observed to proceed mainly *via* HCOOH dehydration leading to adsorbed CO, whereas Ru was shown to be inert in CH_3OH solution, further supporting the inactivity of Ru towards the dehydrogenation reaction. Accordingly, both CO and HCOOH electrooxidation on pure Ru and on Pt-Ru alloy electrodes were very similar.

The bifunctional character of Pt-Ru alloys in CH_3OH electrooxidation derives from the property of Ru to nucleate oxygen-containing species, which aid the oxidation of CH_3OH dehydrogenation fragments on adjacent three-fold Pt ensembles. A statistical model predicted that the number of active ensembles is maximized on a surface with ≈10 atomic% Ru and the highest activity for CH_3OH oxidation on the alloy with a Ru surface composition of ≈7 atomic% was in good agreement with these predictions. For both CO and HCOOH, adsorption is not rate-limiting since it is equally facile on both Pt and Ru sites and the optimum Ru surface composition was found to be ≈50 atomic%. This surface maximizes the number of Pt-Ru pair sites which nucleate a more active form of oxygen-containing species than Ru-Ru pair sites or Ru clusters, leading to the observed synergism of Pt-Ru alloy electrodes in CO electrooxidation. The smaller catalytic enhancement of Pt-Ru alloys over pure Pt in HCOOH (factor ≈5) compared to CH_3OH (factor ≈30) electrooxidation was attributed to the competition between H_2O (leading to OH formation) and HCOOH (leading to CO formation) for Ru sites in formic acid solution.

Chapter 5:
CH_3OH Oxidation at Elevated Temperatures

1. Introduction 124
2. Experimental Procedures 126
3. Results 128
   3.1. CH_3OH Electrooxidation at 25°C 128
   3.2. CH_3OH Electrooxidation at Elevated Temperatures 130
      3.2.1. Voltammetry at Elevated Temperatures 130
      3.2.2. Potentiostatic CH_3OH Oxidation at Elevated Temperatures 136
      3.2.3. Activation Energies of Pt-Ru Alloys 138
4. Discussion 141
   4.1. Formulation of the Reaction Pathway on Pt-Ru Alloy Surfaces 142
   4.2. Interpretation of Activity Data 144
      4.2.1. CH_3OH Electrooxidation at 25°C 144
      4.2.1. CH_3OH Electrooxidation at 60°C 146
   4.3. Interpretation of Activation Energies 147
   4.4. Comparison With Fuel Cell Electrodes and Performance Projections 150
5. Conclusions 151

1. INTRODUCTION

All methanol performance data at elevated temperature, that are available in the literature were acquired on high surface area catalysts, *viz* Raney-type electrodes [66], electrochemically codeposited alloys [68], solid polymer electrodes (SPE) [159, 160], and bimetallic alloy clusters supported on carbon [64, 65, 161 ,162]; most commonly, the supporting electrolyte was H_2SO_4 (0.5 to 5 M) with methanol concentrations ranging from 1 to 2.5 M at temperatures up to 80°C. As was discussed extensively in Chapter 2, alloy surface compositions for identical bulk compositions depends on both their

preparation method [66, 71, 163] and the applied "activation" pretreatment in the electrolyte; in addition, a distinction of changes in the true electrocatalytic activity with alloy composition from mere changes in surface area is difficult with high-surface area alloy catalysts. Therefore, it is not surprising that on differently prepared Pt-Ru alloy electrodes at 60 to 75°C under otherwise identical reaction conditions the optimum Ru concentration (bulk) for methanol electrooxidation at 0.4 V was quoted as 30 [66], 40 [68], and 50 atomic% [64].

At the risk of being repetitive, it seems helpful at this point to briefly summarize the conclusions drawn in the previous chapters. It was found that the optimum Ru surface composition at room temperature and 0.5 V *vs* the reversible hydrogen electrode in the same solution (RHE) was ≈10 atomic%, especially at low methanol concentrations (5 mM), while pure Ru was completely inactive. This was explained by the bifunctional mechanism of Pt-Ru alloys, namely the adsorption and initial dehydrogenation of methanol on Pt surface atom ensembles followed by the oxidative removal of methanol dehydrogenation fragments *via* oxygen-containing species on adjacent Ru atoms (Chapter 2). The subsequent study of the electrooxidation of CO on the same Pt-Ru alloy surfaces, where adsorption is equally facile on both Pt and Ru atoms, confirmed the proposed nucleation of oxygen-containing species on Ru atoms. The alloy with a Ru surface composition of ≈50 atomic% was the most active and displayed a strong synergistic effect, suggesting a modified adsorption strength of oxygen-containing species on Pt-Ru pair sites in contrast to Ru-Ru pair sites (Chapter 3). The same optimum Ru surface composition of ≈50 atomic% was observed for the electrooxidation of formic acid, which was found to adsorb on both pure Pt and pure Ru sites, thereby eliminating the requirement of Pt surface atom ensembles for the adsorption/dehydrogenation step (Chapter 4). Consequently, there is a striking similarity between CO and HCOOH

electrooxidation on Pt-Ru alloy electrodes, in contrast to methanol electrooxidation at room temperature.

According to the above, the nature of the interaction of small organic molecules with Ru is the dominant factor in forming the most active surface for their oxidation on a Pt-Ru alloy electrode. In the case of methanol at room temperature, there is a complete lack of interaction of Ru with methanol in solution. If this inert character of Ru were to change at elevated temperatures, our present understanding of the fundamental mechanism of the methanol electrooxidation reaction on Pt-Ru alloy electrodes would lead us to predict an increase in the optimum Ru surface concentration with increasing temperatures. Clearly, a measurement of the electrocatalytic activities of Pt-Ru alloy electrodes with different Ru surface concentrations at elevated temperature is both of fundamental and practical interest, since any conceivable direct methanol fuel cell would need to operate above ambient temperatures. Therefore, we will present in the following voltammetric and potentiostatic measurements on the electrooxidation of methanol on pure Pt, pure Ru and Pt-Ru alloy electrodes at temperatures up to 80°C, and discuss the relevance of these data in the context of the fundamental electrode reactions as well as in respect to activity measurements reported in the literature.

2. EXPERIMENTAL PROCEDURES

All electrochemical measurements reported in this study were conducted on mildly sputtered surfaces (0.5 keV Ar^+) which were transferred from UHV into a standard three-compartment electrochemical menisus-type cell equipped with a water jacket. A circulating constant temperature bath (Fisher Isotemp Circulator) maintained the temperature of the 0.5 M H_2SO_4 supporting electrolyte (25 ml, Baker Analyzed Ultrex, prepared from triply pyro-distilled water) within ±0.5°C. The surface and bulk

compositions of sputter-cleaned electrodes were essentially identical as verified by LEIS (Chapter 1), and Ru compositions will be given in terms of surface compositions throughout this report. Again, no measurable sputter-roughening was observed, consequently all current densities in the following are reported in terms of geometric area, implying a roughness factor of one.

Before immersion of the UHV-characterized circular face of the cylindrically cut samples (see Figure 2-2), the sample perimeter was wrapped with Teflon tape (DuPont) to avoid the undesired wetting of the uncharacterized perimeter area caused by condensation due to the initial temperature gradient between the alloy and the thermostated electrolyte . In order to avoid background currents originating from dissolved oxygen, the electrolyte was purged and blanketed with argon (Alphagaz, 5N5) and the electrochemical cell was located in an "atmos-bag" (Aldrich) as described in Chapter 3. Preliminary experiments with thermocouples attached to the perimeter of an electrode sample showed that the temperature difference between the electrode and the thermostated electrolyte amounted to ≈4°C after 1.5 minutes and to ≤ 1°C after 4.5 minutes. Therefore, the electrodes were immersed at 0.075 V into the methanol-free electrolyte for 1.5 minutes before the injection of deoxygenated methanol (0.5 M or 5.0 mM, Baker Analyzed) after which an additional 3 minutes at the same potential were allowed for the equilibration of both temperature and concentration gradients prior to electrochemical data acquisition.

Electrooxidation current densities were recorded potentiodynamically at 20 mV/s on an X/Y-recorder (Linseis), whereas potential step data were acquired on a PC using the Headstart Program (EG&G) to control a PAR 273 potentiostat. To avoid significant evaporation losses of methanol, 60°C was the upper temperature limit in potentiostatic experiments. All potentials will be referred to the reversible hydrogen electrode in the same solution (RHE).

3. RESULTS

3.1. CH_3OH Electrooxidation at 25°C

The electrooxidation of 0.5 M CH_3OH in 0.5 M H_2SO_4 at 0.5 V on sputter-cleaned Pt-Ru alloy electrodes and on pure Pt is shown in Figure 5-1a (Ru surface concentrations are indicated in the figure). The optimum Ru surface concentration under these conditions is fairly low, *viz* somewhere between ≈7 to ≈33 atomic%, leading to an approximately 30-fold higher current density than on pure Pt. As discussed in Chapter 2, changes in the relative activity displayed by alloys with different Ru surface concentrations reflect the balance between the two steps in the series reaction of methanol electrooxidation on these electrodes: the initial adsorption/dehydrogenation of methanol and the subsequent oxidative removal of adsorbed methanol dehydrogenation fragments *via* oxygen-containing species preferentially adsorbed on Ru surface sites. The lower catalytic activity of the surface with a Ru concentration of ≈46 atomic% (Figure 5-1a) derives from its reduced ability to promote the adsorption and initial dehydrogenation of methanol, a fact which became more evident in 5.0 mM CH_3OH (Figure 2-10), where the initial adsorption step became rate-determining so that same surface showed no catalytic improvement over pure Pt at all.

As the electrode potential is reduced to 0.4 V, Figure 5-1b, the extent of nucleation of oxygen-containing surface species on Ru sites to promote the oxidative removal of methanol dehydrogenation species decreases. As a consequence, a larger Ru surface composition becomes more favorable in preventing the accumulation of adsorbed methanol dehydrogenation fragments at, however, reduced overall reaction rates. Thus, the surface with a Ru concentration of ≈7 atomic% exhibits a two times lower activity at 0.4 V if compared to the ≈33 atomic% Ru surface, and very little improvement over the

alloy with a Ru surface concentration of ≈46 atomic%. Qualitatively, the same behavior was observed on Raney-type [66] as well as on supported Pt-Ru alloy catalysts [90], namely an increase in the optimum Ru surface concentration with decreasing electrode potentials.

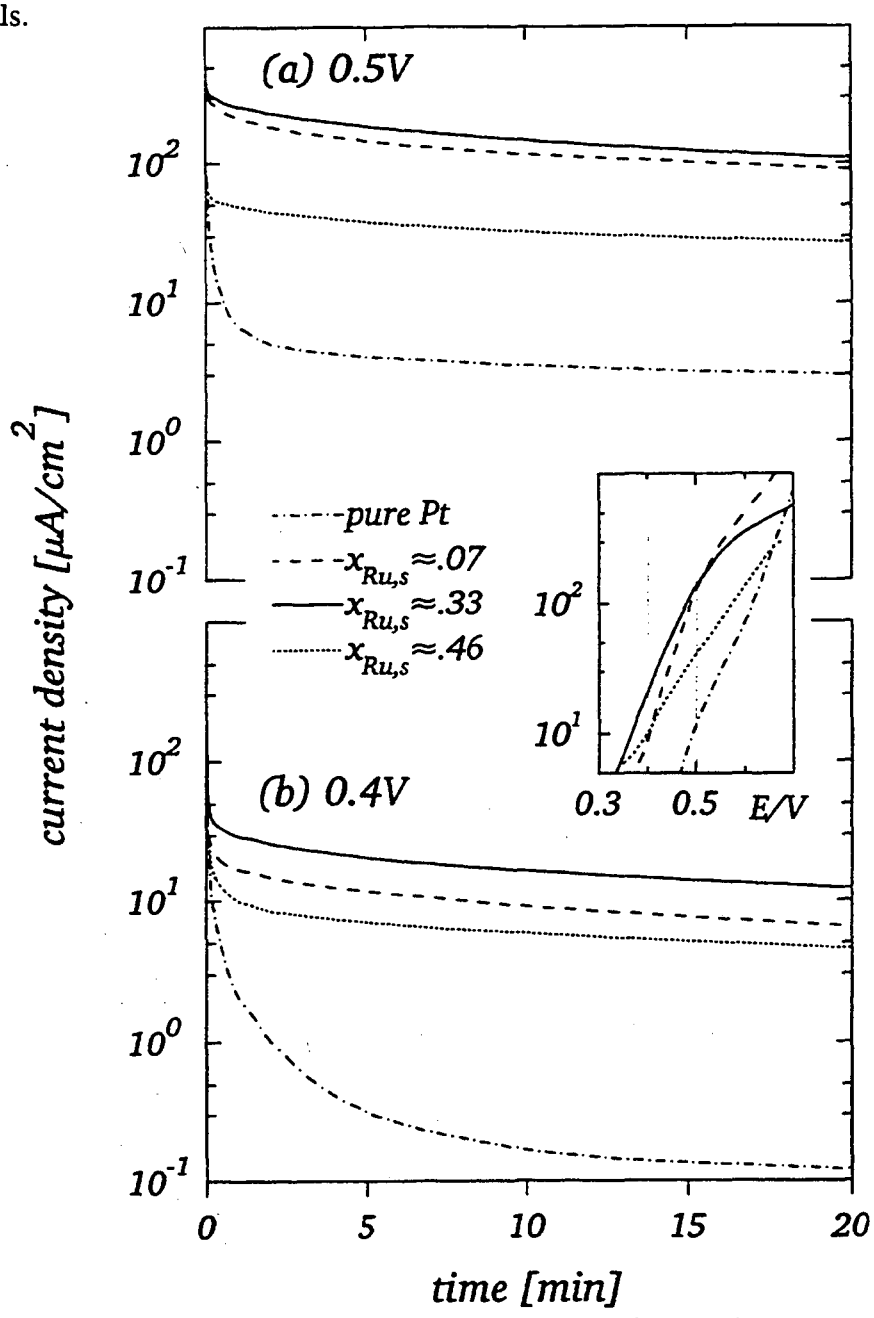

Figure 5-1. Potentiostatic oxidation of 0.5 M CH_3OH in 0.5 M H_2SO_4 at 25°C on sputter-cleaned Pt and Pt-Ru alloy electrodes (Ru surface compositions are indicated in the figure). Methanol was injected at 0.075 V three minutes before stepping the electrode potential to: (a) 0.5 V, and (b) 0.4 V. The insert shows the purely faradaic potentiodynamic current densities on the same surfaces for the 10th positive-going sweep at 20 mV/s.

The same trend is indicated in the insert of Figure 5-1, showing the purely faradaic potentiodynamic current densities (capacitive current densities were subtracted) of the 10th positive-going sweep for pure Pt and alloys with varying Ru surface concentrations: the highest relative activity at 0.4 V was observed for ≈33 atomic% Ru, with ≈7 and ≈46 atomic% Ru being roughly equal, whereas at 0.5 V the ≈7 and ≈33 atomic% Ru surfaces exhibited high activities compared to the much lower activity on the ≈46 atomic% Ru surface. At increasing electrode potentials the superior activity was found for the alloy with a Ru surface concentration of ≈7 atomic%, attesting to the reduced rate of methanol adsorption/dehydrogenation on Ru-rich surfaces.

3.2. CH_3OH Electrooxidation at Elevated Temperatures

It emerges from the discussion of Figure 5-1 that cyclic voltammetry of Pt-Ru alloy electrodes in methanol containing solutions may serve as a good indicator of their relative catalytic activity, even though it does not warrant a useful prediction of potentiostatic steady-state currents. For this reason, we will first describe the voltammetric response of different electrodes at 60°C before presenting potentiostatic activities.

3.2.1. Voltammetry at Elevated Temperatures

The most apparent difference between the cyclic voltammetry of pure Pt at 25°C (Figure 5-2a) and 60°C (Figure 5-2b) in 0.5 M CH_3OH is the approximately ten-fold increase in current density at potentials above 0.5 V for both the first and the tenth sweep. In the potential range more relevant for the design of a direct methanol fuel cell, *i.e.* ≤ 0.5V, the change of the activity of Pt with temperature is less striking. Thus, the essentially identical currents in the first sweep, where the turnover number (number of oxidized reactant molecules per surface atom) is less than one (reflecting an unpoisoned electrode surface), indicate the small influence of temperature on the initial adsorption/dehydrogenation reaction. However, in the tenth sweep, the onset of methanol

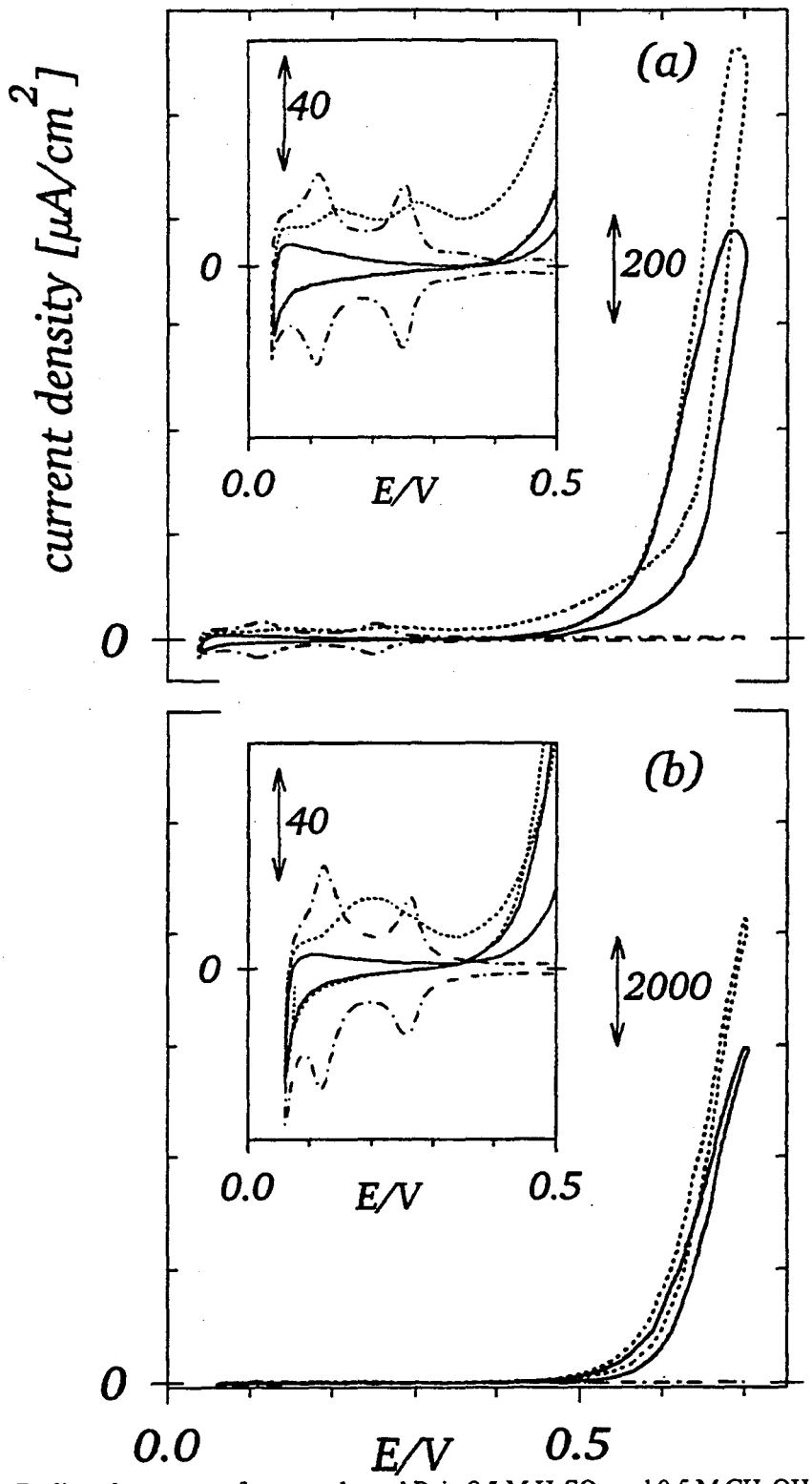

Figure 5-2. Cyclic voltammetry of sputter-cleaned Pt in 0.5 M H_2SO_4 and 0.5 M CH_3OH at: (**a**) 25°C, and (**b**) 60°C. (·-·-·-·-·) base voltammetry in 0.5 M H_2SO_4; (- - - -) first sweep after immersion at 0.075 V for 3 minutes; (——) 10th sweep. The inserts are a magnification of the potential region between 0 and 0.5 V. 20 mV/s.

oxidation at 60°C is shifted negatively by ≈50 mV if compared to room temperature, as is inferred from the change in the crossover-potential of purely capacitive currents in the methanol-free electrolyte and the currents recorded in 0.5 M CH_3OH. This is probably related to the negative potential shift for the onset of the nucleation of oxygen-containing species on Pt as the temperature is increased [164]. The accumulation of methanol dehydrogenation fragments on the electrode surface after the first sweep, evidenced by the small currents in the potential region between the negative potential limit and ≈0.3 V, indicates that the oxidative removal of these fragments rather than the initial adsorption/dehydrogenation of methanol is the rate-determining step at steady-state.

The cyclic voltammetry of a sputter-cleaned Ru electrode in 0.5 M H_2SO_4 and 0.5 M CH_3OH at 25°C was discussed in Chapter 2 and Figure 5-3a demonstrates the inert character of Ru towards the electrooxidation of methanol in this potential range. At 60°C (Figure 5-b) a small anodic peak is developed in the first, and less pronounced in the tenth positive-going sweep at ≈0.5 V. A similar feature, related to the oxidation of adsorbed CO is noticeable in the potentiodynamic oxidation of both CO (Chapter 3) and HCOOH (Chapter 4) on Ru at 25°C, albeit more positive by ≈0.1 V. A significant decrease in the pseudocapacitive currents at potentials below ≈0.2 V in conjunction with the clearly discernable faradaic currents at the positive potential limit clearly indicate that the interaction of CH_3OH with a Ru electrode is a strongly activated process, requiring elevated temperatures. At potentials positive of ≈0.2 V the adsorption of oxygen-containing species is known to occur on a Ru electrode, thus, its inert character towards CH_3OH at room temperature may be correlated with the exceptionally large energy of adsorption of oxygen on Ru (≈330 kJ/mole for atomic oxygen [135]), which in turn would predict comparably high activation energies for methanol oxidation. This is further corroborated by the sudden increase in anodic currents when the temperature is raised to 80°C, Figure 5-3c. Quite obviously, the reactivity of Ru towards the electrooxidation of

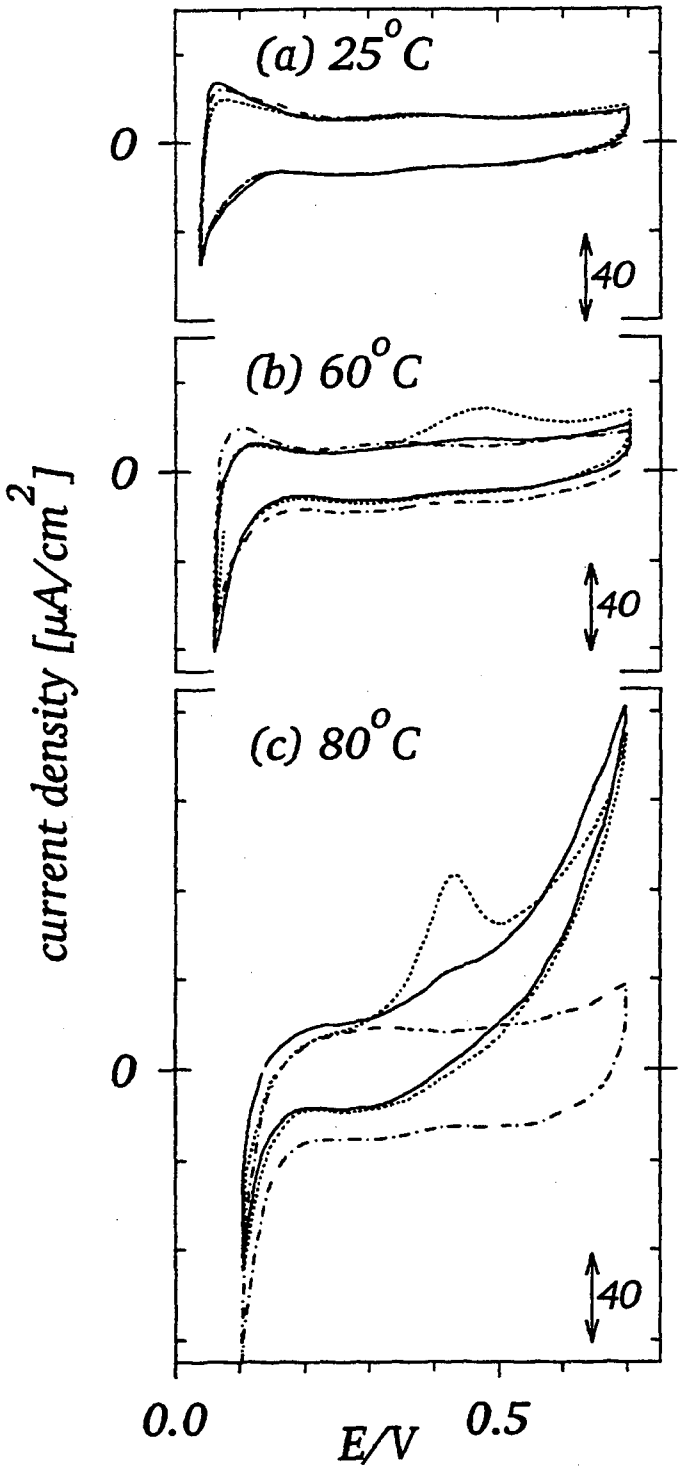

Figure 5-3. Cyclic voltammetry of sputter-cleaned Ru in 0.5 M H_2SO_4 and 0.5 M CH_3OH at: **(a)** 25°C, **(b)** 60°C, and **(c)** 80°C. (-·-·-·-) base voltammetry in 0.5 M H_2SO_4; (- - - -) first sweep after immersion at 0.075 V for 3 minutes; (——) 10th sweep. 20 mV/s.

CH_3OH is now substantial, as was similarly observed by Éntina *et al* [68] and by Binder *et al* [66]. The initial adsorption of methanol cannot anymore be assumed to proceed exclusively *via* Pt surface ensembles as was the case at room temperature; rather, the electrooxidation of CH_3OH on Ru does begin to resemble CO and HCOOH electrooxidation on this electrode (see Figure 4-3).

The tenth sweep in the cyclic voltammetry of an alloy electrode with ≈7 atomic% Ru in 0.5 M CH_3OH at 60°C, Figure 5-4a, closely resembles what was observed on pure Pt at potentials above ≈0.5 V, although the onset of the electrooxidation reaction is shifted negatively by ≈0.1V to ≈0.3 V (see insert). The increase in current density at the positive potential limit as the temperature is raised from 25 to 60°C, however, is much less on the alloy than on a pure Pt electrode, again pointing towards the slower methanol adsorption kinetics on Pt-Ru alloy electrodes, *i.e.* methanol adsorption becomes rate-limiting for potentials sufficiently positive to provide rapid oxidative removal of dehydrogenation fragments. This is even more apparent on a surface with ≈46 atomic%, Figure 5-4b, where the temperature effect at 0.7 V is minimal. The onset of methanol electrooxidation on this surface occurs at ≈0.2 V, nearly 0.1 V more negative than on the alloy with 7 atomic% Ru, indicating that the ability to oxidatively remove dehydrogenation fragments is inversely related to the Ru surface concentration for surfaces ≤50 atomic% Ru. The same conclusion may be reached by observing the much smaller reduction of hydrogen adsorption pseudocapacitive currents in 0.5 M CH_3OH in the potential region negative of ≈0.2 V for the surface with ≈46 atomc% *versus* ≈7 atomic% Ru. Conversely, our study on the electrooxidation of CO on Pt-Ru does lead us to expect that this trend will be reversed as the Ru surface concentration exceeds 50% due to a seemingly increasing adsorption strength of oxygen-containing species on Ru-Ru pair sites. In summary, the voltammetric behavior of Pt-Ru alloys in 0.5 M CH_3OH at 60°C follows the same trends as the data at 25°C shown in Figure 5-1: at successively

lower electrode potentials the optimum Ru surface concentration shifts from ≈7 atomic% towards ≈50 atomic% and *vice versa* at higher potentials.

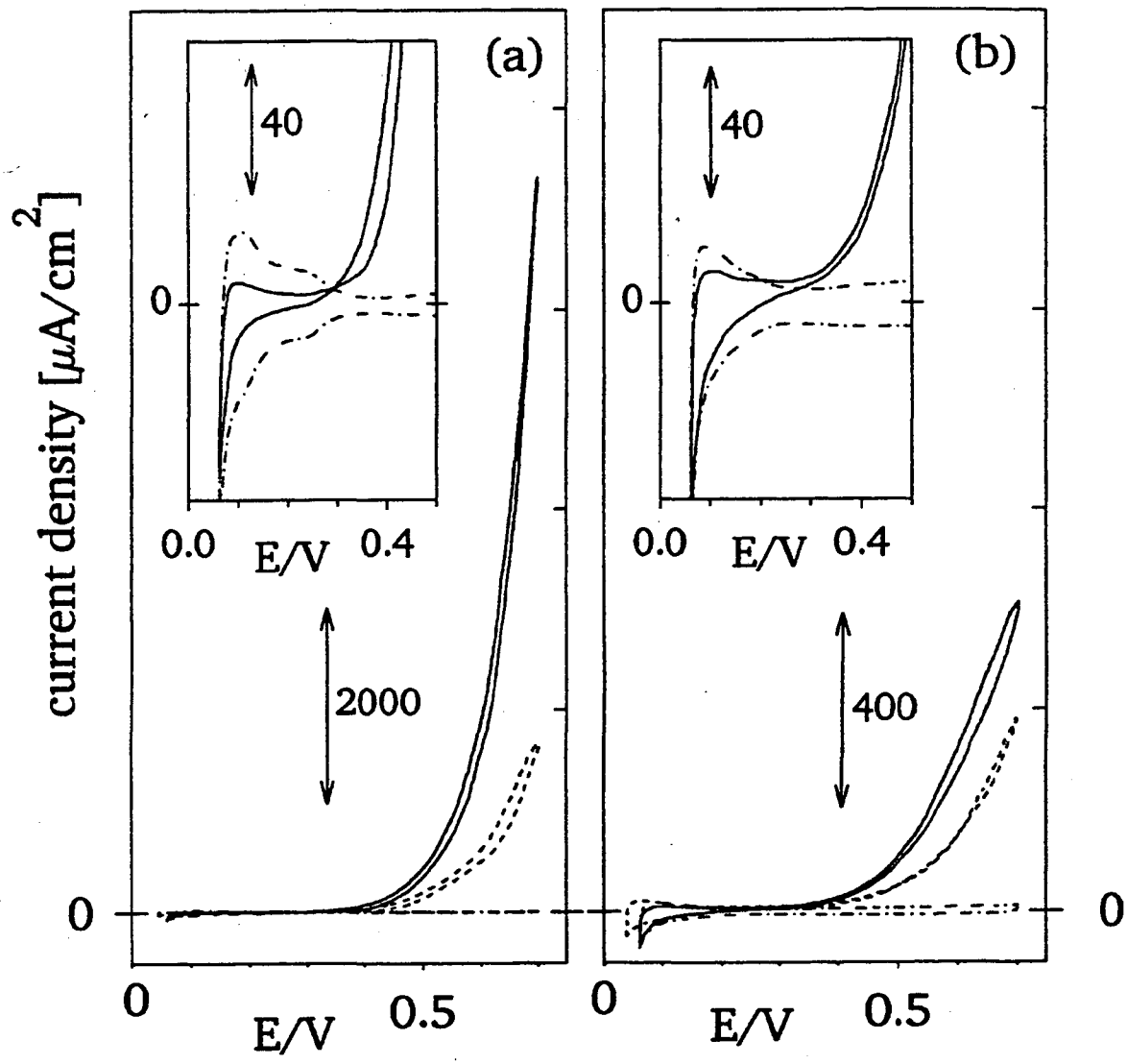

Figure 5-4. Cyclic voltammetry of sputter-cleaned Pt-Ru alloys in 0.5 M H_2SO_4 and 0.5 M CH_3OH at 60°C for various Ru surface compositions: **(a)** ≈7 atomic%, **(b)** ≈46 atomic%. (·-·-·-·-·) base voltammetry in 0.5 M H_2SO_4 at 60°C; (- - - -) 10th sweep at 25°C; (——) 10th sweep at 60°C. Immersion at 0.075 V for 3 minutes; 20 mV/s.

3.2.2. Potentiostatic CH_3OH Oxidation at Elevated Temperatures

The cyclic voltammetry of Ru in 0.5 M CH_3OH (Figure 5-3) demonstrates the highly temperature activated nature of the interaction of methanol with Ru, similarly evident from the potential-step experiments at 0.5 V in 0.5 M CH_3OH at 60°C, Figure 5-5a: the activity of Ru towards CH_3OH electrooxidation is only a factor of three smaller than on pure Pt, whereas no oxidation currents could be measured on Ru under the same conditions at room temperature. Within experimental error, the difference in activity between Pt and Ru at 60°C vanishes by lowering the electrode potential to 0.4 V (Figure 5-5b), or to rephrase this observation, the "Tafel slope" (change in overpotential per ten-fold change in current density) of Ru is apparently larger than of Pt.

The optimum Ru surface concentration at 60°C and 0.5 V is ≈33%, with a ten-fold electrocatalytic activity enhancement over pure Pt. In contrast to the same experiment at 25°C (Figure 5-1a) the difference in current density between the ≈33 atomic% and the ≈7 atomic% Ru surface now amounts to a factor of two; similarly, the difference between the ≈7 and the ≈46 atomic% Ru surface has diminished dramatically. It therefore seems that the thermal activation of Ru induces a more facile adsorption/dehydrogenation reaction on Ru-rich alloy surfaces, effecting an increase in the optimum Ru surface concentration with temperature.

At the lower electrode potential of 0.4 V (Figure 5-5b), the electrocatalytic activity of the most active alloy (≈33 atomic% Ru) is ≈50 times larger than that of pure Pt, closely followed by the alloy with a Ru surface concentration of ≈46 atomic%. The alloy with only ≈7 atomic% Ru on the surface is quite inactive compared to the Ru-rich alloys, as would be expected from the lower onset-potential of methanol oxidation on these surfaces as was discussed in Section 3.2.1 (Figure 5-4). In other words, the "Tafel slopes" between 0.4 and 0.5 V range from 80 mV/decade for pure Pt to 180 mV/decade for the Ru-rich alloy, with other surface concentrations in between. The term "Tafel

slope" in this context, however, does not carry its usual fundamental meaning, since straight lines of the logarithm of the current density *versus* the electrode potential are generally not observed for methanol electrooxidation [160, 162].

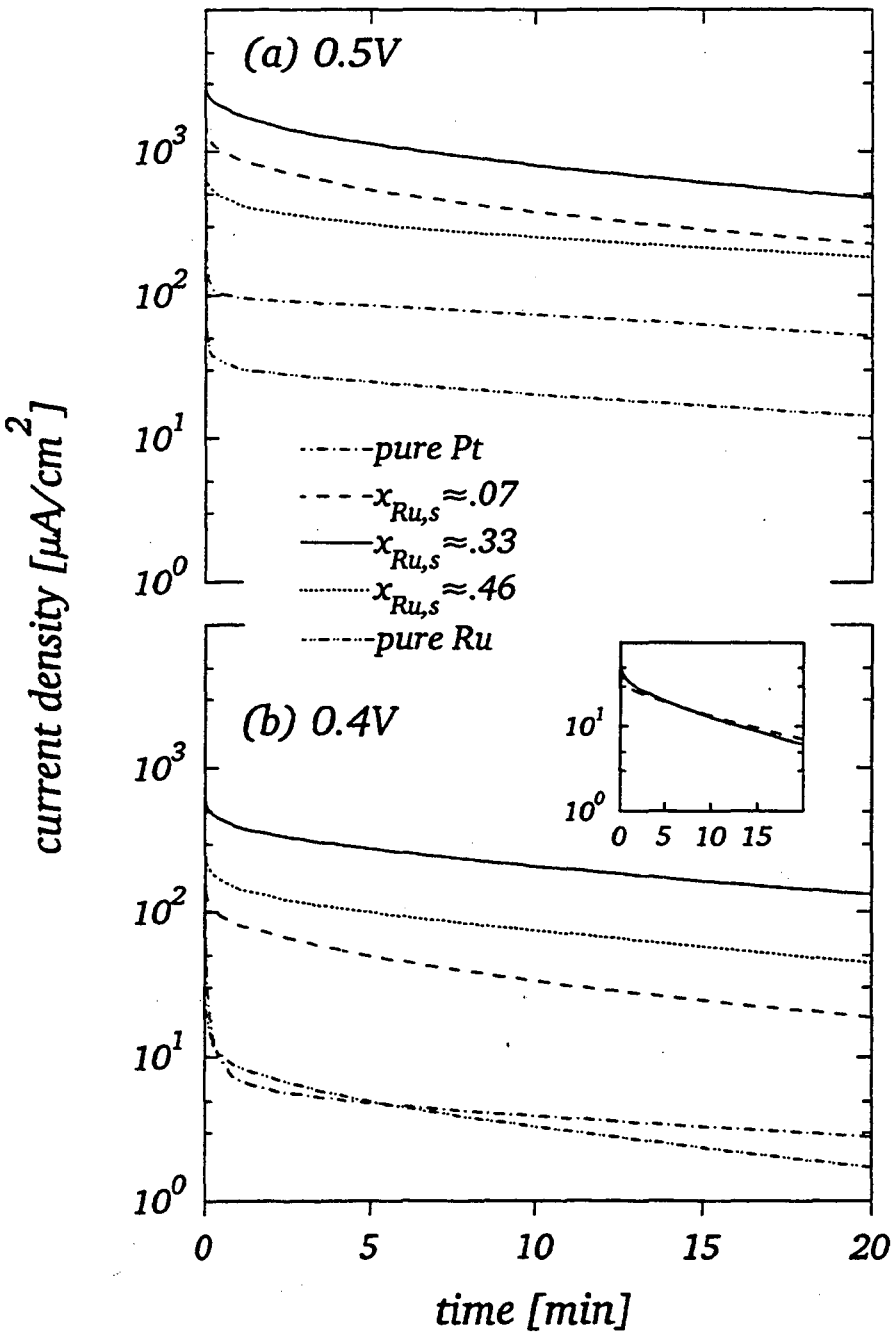

Figure 5-5. Potentiostatic oxidation of 0.5 M CH_3OH in 0.5 M H_2SO_4 at 60°C on sputter-cleaned Pt and Pt-Ru alloy electrodes (Ru surface compositions are indicated in the figure). Methanol was injected at 0.075 V three minutes before stepping the electrode potential to: (**a**) 0.5 V, and (**b**) 0.4 V. The insert in (b) shows the current densities at 0.4 V in 5.0 mM CH_3OH for the ≈7 and ≈33 atomic% Ru surfaces.

The high activity of the surface with a Ru concentration of ≈7 atomic% at room temperature in 0.5 M CH_3OH (Figure 5-1) is rationalized by fast adsorption on Pt ensemble sites coupled with facile oxidation on nearby Ru sites. Although the adsorption of CH_3OH at 60°C cannot be assumed to proceed exclusively *via* Pt atom ensemble sites, since adsorption occurs on Ru sites as well at this temperature, the almost one order of magnitude difference in current densities on the ≈7 atomic% *versus* the ≈33 atomic% Ru surface disappears when the CH_3OH concentration in the electrolyte is reduced to 5 mM, shown in the insert of Figure 5-5b (similarly at room temperature, see Figure 2-10a). Thus, lowering the methanol concentration at 60°C still has the same effect that it has at 25°C, *i.e.* a shift from oxidative removal of dehydrogenation fragments to adsorption/dehydrogenation as rate-determining.

3.2.3. Activation Energies of Pt-Ru Alloys

Activation energies provide important information for both the elucidation of fundamental catalytic mechanisms and the projection of actual fuel cell performance. Therefore, we measured the catalytic activity of Pt-Ru alloy electrodes at 0.4 V in 0.5 M CH_3OH at 25, 41 and 60°C for the alloy with the most active Ru surface concentration at this potential, *viz* ≈33 atomic% (Figure 5-6). It is quite clear that the deactivation of the electrode catalyst proceeds rapidly over an initial period of approximately 5 minutes after which a slower, steady decay is observed without ever reaching a "steady-state". This may partially be due to the fact that long-term experiments with smooth electrodes, *i.e.* for a small ratio of surface area to electrolyte volume (*e.g.* $1cm^2/100cm^3$), are extremely sensitive to the effect of surface-active impurities in the electrolyte. A back-of-the-envelope calculation based on diffusion-limited transport (Cottrell equation) of surface-active substances to the electrode surface will serve to illustrate this detrimental effect: 0.1 ppm of any surface-active impurity in the electrolyte, which is assumed to block the catalyst surface *via* a diffusion-limited adsorption process would deactivate ≈7% of the

catalyst surface 10 minutes after its immersion and an additional ≈3% for the following 10 minute interval (estimate based on: $D \approx 10^{-5} cm^2/s$, M≈100g/mole, one surface atom per adsorbed molecule). These levels of deactivation are consistent with what we observed at 10 minutes and longer. An impurity level much below 0.1 ppm is not regularly achievable and therefore we attribute the slow decay after ≈10 minutes primarily to blocking of the electrode by surface-active impurities.

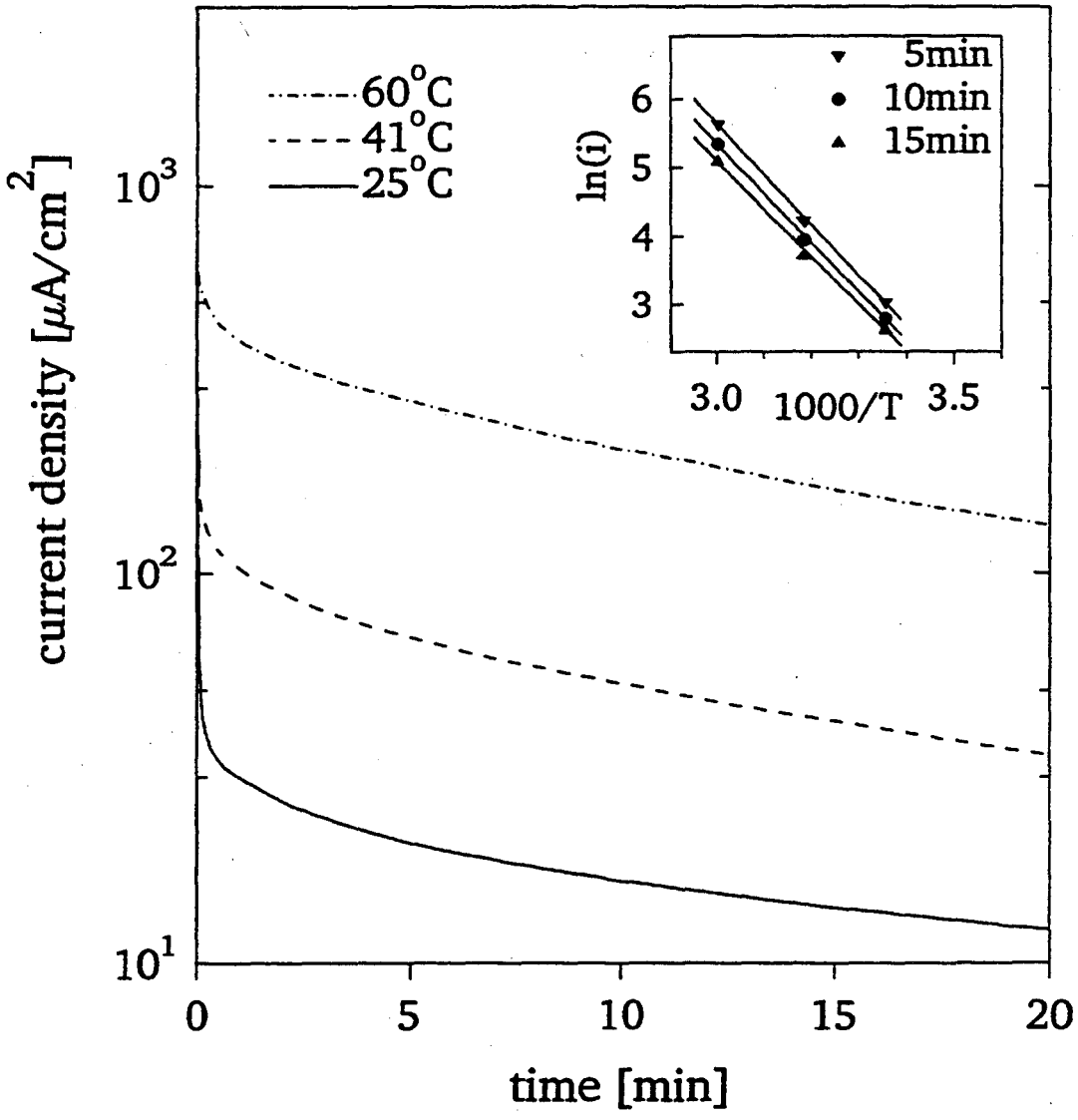

Figure 5-6. Potentiostatic oxidation of 0.5 M CH_3OH in 0.5 M H_2SO_4 at 25, 41 and 60°C on sputter-cleaned Pt-Ru alloy electrodes with a Ru surface composition of ≈33 atomic%. Methanol was injected at 0.075 V three minutes before stepping the electrode potential to 0.4 V. The insert is an Arrhenius plot of ln(i) vs 1/T after different times, with least-squares regression lines.

The apparent activation energy of the alloy with a Ru surface concentration of ≈33 atomic% is shown for various times after stepping the potential, yielding a value of 60 kJ/mole after 10 minutes, with a deviation of ±3% for longer or shorter time. A time of 10 minutes was used for evaluating activation energies, as it allows sufficient time to reach a "steady-state" for the methanol electrooxidation reaction while minimizing the effects of electrolyte impurities as well as methanol evaporation at longer times. Values in the literature for the activation energy of Pt-Ru alloy electrodes vary significantly, *e.g.* at 0.4 V from 50 kJ/mole (1 M CH_3OH, 3 M H_2SO_4 [162]) to 95 kJ/mole (2 M CH_3OH, 1 M H_2SO_4 [68]), and 84 kJ/mole at 0.35 V (2 M CH_3OH, 1.5 M H_2SO_4 [66]), a fact which may be attributed either to differences in the concentration of the electrolyte, which does assert a strong influence on measured current densities [162, 165], or to the variation in methanol concentration, or possibly to differences in the surface composition of catalysts having the same nominal bulk compositions.

An Arrhenius plot for all three alloy electrodes at 0.4 V in 0.5 M CH_3OH, Figure 5-7, yields activation energies of 60 kJ/mole for both the ≈33 atomic% and the ≈46 atomic% Ru surfaces, but only 30 kJ/mole for a Ru surface concentration of ≈ 7atomic%. This unusually low value for the Pt-rich alloy surface may be rationalized by postulating surface migration of adsorbed methanol dehydrogenation fragments as rate-determining, a hypothesis that will be discussed in detail in Section 4.3. On account of the very small activities of both Pt and Ru at 0.4 V we have not attempted to evaluate their activation energies at this potential.

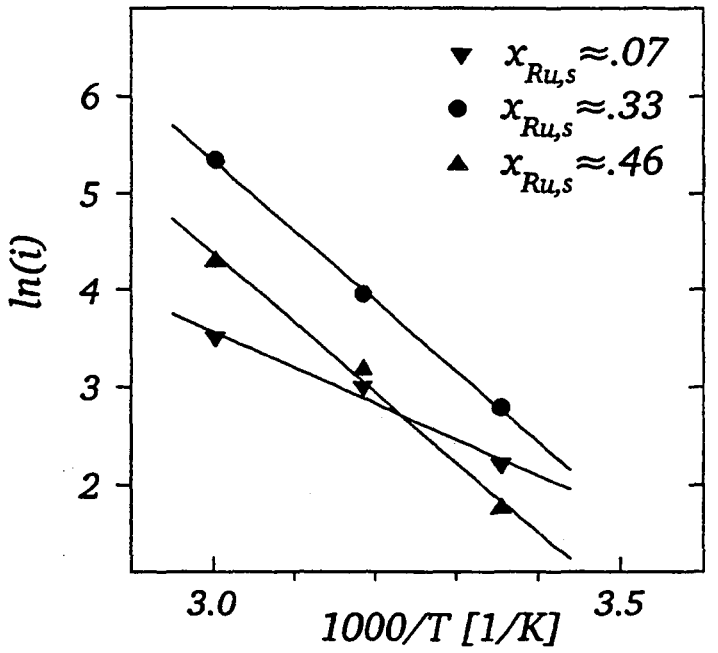

Figure 5-7. Arrhenius plot of ln(i) *vs* 1/T for different Pt-Ru alloys in 0.5 M CH_3OH and 0.5 M H_2SO_4 at 0.4 V (Ru surface compositions are indicated in the figure). Current densities were measured after 10 minutes.

4. DISCUSSION

In the following we will summarize the above description of our experimental results on the electrooxidation of methanol on Pt-Ru alloy electrodes at elevated temperatures in the context of a proposed reaction pathway based on both the findings of this and the previous chapters on CH_3OH, CO and HCOOH electrooxidation on the same alloy surfaces at room temperature. In addition we will discuss the activation energies found for Pt-Ru alloys with different Ru surface compositions and compare the performance we have measured on smooth electrodes with the literature data on high surface area fuel cell electrodes.

4.1. Formulation of the Reaction Pathway on Pt-Ru Alloy Surfaces

We proposed a major reaction pathway for the electrooxidation of CH_3OH on Pt-Ru alloy electrodes at room temperature, which we will sketch briefly in the following. It is primarily based on our observation that the balance between the initial adsorptive dehydrogenation of methanol and the subsequent oxidative removal of dehydrogenation fragments is a function of the Ru surface composition of the alloy electrodes. Since at room temperature no interaction between Ru and CH_3OH could be measured, the first step in the proposed series mechanism consists of the dehydrogenation of methanol on Pt surface ensembles, leading to the formation of adsorbed dehydrogenation fragments. These fragments are both inermediates and surface "poisons". In carefully reviewing the previous studies by IR (infra-red) and FTIR (Fourier transform IR) of the methanol electrooxidation reaction, which are available only for pure Pt, we reached the conclusion that linearly bonded CO would most likely be the most abundant surface intermediate for the time-scale of our experiments. Recent SPAIRS (single potential alteration IR spectroscopy) measurements did indeed confirm the predominance of linearly bonded CO on Pt-Ru electrodes (as well as the lack of CO_{ads} on Ru) during the methanol electrooxidation reaction [129], in close analogy to Pt electrodes, so that the first reaction step may be formulated as:

$$CH_3OH_{sol} \leftrightarrow CH_3OH_{ads} \xrightarrow{k_1} CO_{ads} + 4H^+ + 4e^- \qquad (5\text{-}1)$$

where CO_{ads} is used as an abbreviated notation for linearly bonded CO. The oxidative removal of CO_{ads} on a Pt surface in the gas-phase proceeds *via* a Langmuir-Hinshelwood mechanism [139], *i.e.* a reaction of chemisorbed CO with chemisorbed oxygen. On an electrode surface, an analogous mechanism is believed to occur, although the chemical nature of oxygen in this environment is most likely related to adsorbed hydroxyl species (OH_{ads}), which we have paraphrased so far as "oxygen-containing species". There is

strong evidence in the literature that the adsorption of oxygen-containing species on a Ru electrode occurs at significantly more negative potentials than on a Pt electrode, in correspondence to the higher affinity of Ru towards oxygen (Chapter 2):

$$Ru + H_2O \xleftrightarrow{E_{Ru}} OH_{ads} + H^+ + e^- \tag{5-2}$$

$$Pt + H_2O \xleftrightarrow{E_{Pt}} OH_{ads} + H^+ + e^- \tag{5-3}$$

where $E_{Pt} \approx 0.5$ V is significantly larger than $E_{Ru} \approx 0.2$ V (*e.g.* Reference 84). By means of providing OH_{ads} , Ru surface atoms in Pt-Ru alloy electrodes catalyze the oxidative removal of methanol dehydrogenation fragments formed on Pt atom ensembles at lower electrode potentials than on a pure Pt electrode:

$$CO_{ads} + OH_{ads} \xrightarrow{k_2} CO_2 + H^+ + e^- \tag{5-4}$$

The "seeding" of the electrode surface with OH_{ads} by Ru surface sites to remove adsorbed CO was demonstrated independently in experiments on the electrooxidation of adsorbed monolayers of CO on Pt, Ru and Pt-Ru alloy electrodes (Chapter 3). There, CO was found to adsorb with equal facility on both Pt and Ru surface atoms, and the voltammetric stripping of CO on an alloy with a Ru surface composition of ≈46 atomic% occurred at potentials ≈0.25 V more negative than on pure Pt. Furthermore, the onset of CO electrooxidation on Pt-Ru alloy electrodes did coincide with that of a pure Ru electrode, indicating the importance of bare Ru sites to initiate the nucleation of OH_{ads} . The optimum Ru surface composition for CO electrooxidation was ≈46 atomic%, attesting to a maximum of surface sites to "seed" the electrode with OH_{ads} and a reduced adsorption strength of OH_{ads} on Pt-Ru pair sites as compared to Ru-Ru pair sites.

4.2. Interpretation of Activity Data

4.2.1. CH_3OH Electrooxidation at 25°C

Current densities in potential-step experiments in 0.5 M CH_3OH on pure Pt drop by several orders of magnitude over a period of seconds, as for example seen at 0.4 V (Figure 5-8a, time resolution of 4 ms) where the current density (background corrected) on an initially clean electrode surface after 0.5 s amounts to ≈120 μA/cm^2 and decreases by nearly two orders of magnitude within one minute, with a total passage of charge of ≈650 μC/cm^2. It is well known that the dissociation of water on Pt (see Equation 5-3) does not occur to any appreciable extent at 0.4 V so that the oxidative removal of CO_{ads} (see Equation 5-4) becomes rate-limiting and a total charge of 650 μC/cm^2 would

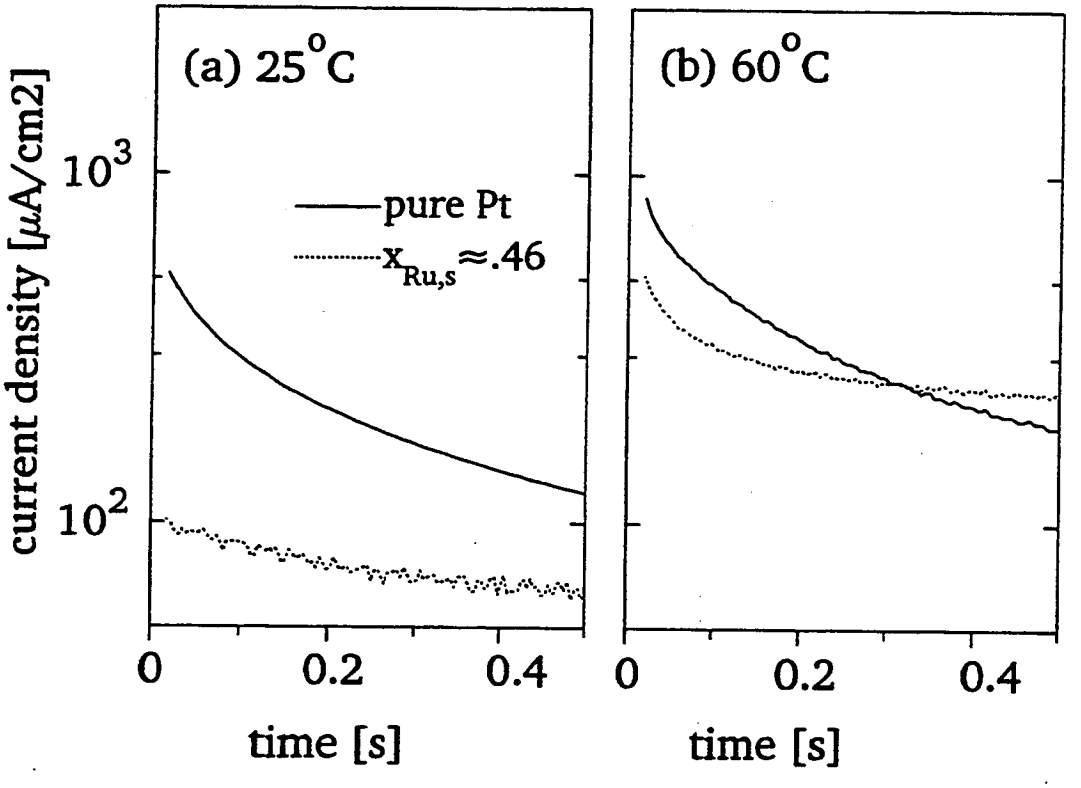

Figure 5-8. Potential-step experiment in 0.5 M CH_3OH in 0.5 M H_2SO_4 on sputter-cleaned Pt and a Pt-Ru alloy electrodes with a Ru surface composition of ≈46 atomic%: **(a)** 25°C, and **(b)** 60°C. CH_3OH was injected at 0.075 V three minutes before stepping the electrode potential to 0.4 V. Time resolution of 4 ms; background currents in 0.5 M H_2SO_4 were subtracted.

correspond to the formation of ≈75% of a saturated CO monolayer. Both the initially fast dehydrogenation reaction of CH_3OH and the accumulation of CO_{ads} are also apparent in the cyclic voltammetry of Pt (Figure 5-2a): in the first positive-going sweep with a turnover of less than one, fairly high currents can be observed at potentials ≤ 0.5 V, whereas the reduced pseudocapacitive currents in the potential region below ≈0.3 V in subsequent sweeps indicate the accumulation of CO_{ads} , now leading to largely diminished CH_3OH electrooxidation currents below ≤ 0.5 V. Even though the methanol dehydrogenation step (Equation 5-1) may be rate-limiting at very short times (ms scale) [102], and at high electrode potentials, as is evidenced by the disappearance of IR signals of CO_{ads} above ≈0.6 V [88], under our conditions (long-time, low electrode potentials) the oxidative removal of CO_{ads} in Equation 5-4 clearly represents the rate-limiting step on a Pt electrode.

A very different situation emerges for Pt-Ru alloy electrodes and may be understood by taking into account both the inert nature of Ru (Figure 5-3a) towards the initial dehydrogenation of methanol (Equation 5-1) and its high activity compared to Pt for the electrooxidation of CO_{ads} (Equation 5-4) due to of the early onset of water dissociation on the Ru surface (Equation 5-2). Therefore, the voltammetry of a Pt-Ru alloy electrode with a surface composition of ≈46 atomic% in 0.5 M CH_3OH indicates only a small degree of "poisoning" of the electrode surface with methanol dehydrogenation fragments, similarly verified by SPAIR measurements which demonstrated that the coverage of this electrode with CO_{ads} is very small compared to pure Pt or Pt-rich alloy surfaces [129]. But this lower rate of deactivation is accompanied by a much lower rate of methanol adsorption, as seen by the much lower current for the clean alloy surface at short times (Figure 5-8a) *versus* clean Pt. At long times, approaching steady-state, the lower rate of deactivation due to sustained oxidation of the methanol dehydrogenation product on the alloy surfaces produces a cross-over in rate,

such that the alloy surfaces are uniformly more active than Pt (Figure 5-1). The lower the potential is, the greater is the difference between the alloys and Pt and the larger is the optimum Ru surface composition due to the higher activity of Ru-rich surfaces for the oxidative removal of CO_{ads} *via* Equation 5-4, a trend which is shown qualitatively in the insert of Figure 5-1. The differences in steady-state activity between the alloys themselves are inversely proportional to the methanol concentration, which we attributed to the dehydrogenation reaction (Equation 5-1) becoming rate-determining at low concentration and to the greater facility of Pt-rich surfaces for this reaction.

4.2.1. CH_3OH Electrooxidation at 60°C

At 60°C the onset of methanol oxidation on a Pt electrode (Figure 5-2b) is shifted negatively by 50 mV, probably related to the enhancement in the nucleation of OH_{ads} (Equation 5-3) indicated by cyclic voltammetry in methanol-free electrolyte [164]. A more striking feature of the data at 60°C is the relatively high activity of pure Ru: whereas no oxidation currents in 0.5 M CH_3OH could be measured at room temperature, current densities at 60°C and 0.5 V are only a factor of three smaller than on pure Pt, and both metals are essentially equally active at 0.4 V (Figure 5-5). Similarly, the cyclic voltammograms of Ru at this temperature (Figure 5-3b) are reminiscent of both CO (Figure 3-3) and HCOOH (Figure 4-3) electrooxidation, indicating that the dehydrogenation reaction of methanol on Ru is a thermally activated process. The fact that the activity of Ru approaches the activity of Pt at lower electrode potentials may be related to a reduction of the adsorption strength of OH_{ads} which, at room temperature, prevents the dissociative adsorption of CH_3OH. Increasing the temperature to 80°C brings about an enormous activity enhancement (Figure 5-3c) supporting the hypothesis of a strongly activated adsorption process.

The ability of Ru to adsorb CO and HCOOH at room temperature was shown to result in an optimum Ru surface concentration of ≈46 atomic% on Pt-Ru alloy electrodes

for the catalysis of the electrooxidation of the respective reactants, and the thermal activation of Ru for the dissociatve adsorption of CH_3OH does indeed appear to produce a similar trend in the optimum composition for the electrooxidation of methanol at elevated temperatures. For a 0.5 M CH_3OH solution at 60°C, the alloy with a Ru surface composition of ≈33 atomic% is the most active (Figure 5-5a), whereas the ≈7 atomic% Ru surface has lost it's large activity enhancement over the Ru-rich alloy (≈46 atomic%) that occured at room temperature; the relative activities of these two surfaces are even reversed at 0.4 V (Figure 5-5b). The implication of these data is that the increased activity of pure Ru partially eliminates the requirement of Pt atom ensembles to facilitate the initial dehydrogenation of CH_3OH (Equation 5-1), a hypothesis supported by the five-fold increase in the initial oxidation currents on the clean Ru-rich alloy surface (≈46 atomic%) in 0.5 M CH_3OH at 0.4 V (Figure 5-8b), which now approach the large initial oxidation rates on a pure Pt electrode. According to our reaction pathway analysis, if methanol adsorption is facile on both Ru and Pt sites, the optimum surface composition should approach ≈50 atomic%, the composition which maximizes the oxidative removal of CO_{ads} (Equation 5-4). This trend, however, appears to be reversed even at 60°C as the methanol concentration is reduced, and the rate of the overall reaction is again limited by the adsorption reaction (Equation 5-1), such that the large difference in activity between the surfaces with ≈7 and ≈33 atomic% Ru vanishes in 5 mM CH_3OH solutions as is shown in the insert of Figure 5-5b.

4.3. Interpretation of Activation Energies

Although interpreting experimental activation energies of complex reactions can be difficult and not always useful, there appears to be some additional information gained by analyzing the activation energies in terms of the postulated reaction pathway. The alloy electrodes with a Ru surface composition of ≈33 and ≈46 atomic% yielded an activation energy of 60 kJ/mole, in fairly good agreement with other results with Pt-Ru

alloys in the literature (see Section 3.2.3). For these Ru-rich surfaces cyclic voltammetry (Figure 5-4) as well as SPAIRS data at room temperature [129] indicate a low coverage with CO_{ads} and as discussed above the rate-determining step was hypothesized to be the initial dissociative adsorption of CH_3OH (Equation 5-1). An activation energy of 60 kJ/mole is also reasonable for a reaction like dissociative adsorption.

The activation energy of the alloy with a Ru surface composition of ≈7 atomic%, however, differs by a factor of two from the other two surfaces, yielding a value of 30 kJ/mole. Based on other experimental data we expected the oxidative removal of CO_{ads} (Equation 5-4) to be the rate-determining step on Pt-rich alloys, because of the pronounced accumulation of CO_{ads} on this surface in contrast to Ru-rich electrode surfaces. An activation energy of 30 kJ/mole seems rather low for a chemical reaction like that in Equation 5-4. In order to rationalize this low an activation energy, it is instrumental to reexamine the electrooxidation of CO_{ads} on the alloys with a Ru surface composition of ≈7 and ≈33 atomic% Ru, respectively. Figure 5-9 shows the CO stripping voltammetry of preadsorbed saturated monolayers of CO on these two surfaces together with a schematic view of the distribution of Pt and Ru atoms at the surface. The quite narrow stripping peak characteristic of Ru-rich alloy surfaces (*viz* ≈33, ≈46 and ≈55 atomic% Ru, see Figure 3-4) reproduced in Figure 5-9b for the alloy with a Ru surface compositon of ≈33 atomic% is in stark contrast to the wide CO stripping peak displayed by the alloy with a Ru surface composition of ≈7 atomic%, although the potential for the onset of CO oxidation does coincide for all alloys. The schematic representation of the distribution of Pt and Ru sites conveys the idea that surface diffusion may be the rate-limiting elementary step in the CO electrooxidation reaction on the Pt-rich electrode, since CO adsorbed on a large fraction of the available Pt sites would need to migrate to Ru sites where the nucleation of OH_{ads} occurs; this situation does not arise on the Ru-rich alloys (schematic in Figure 5-9b).

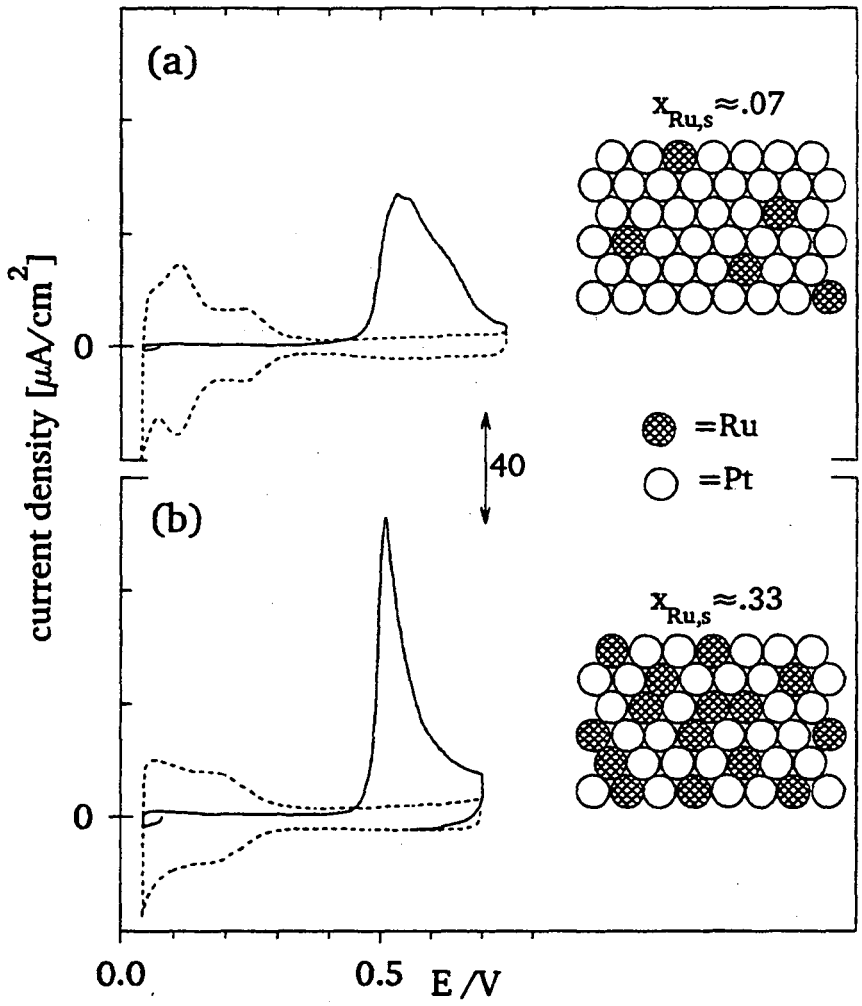

Figure 5-9. CO stripping voltammetry of sputter-cleaned Pt-Ru alloy electrodes (Ru surface compositions, $x_{Ru,s}$, are indicated in the figure). (——) stripping of a monolayer of CO in the first positive-going sweep; (- - - -) second positive-going sweep. 20 mV/s; 0.5 M H_2SO_4; adsorption and immersion from a saturated solution of CO at 25 mV.

Numerous studies on the activation energy for CO surface diffusion can be found in the gas-phase literature for both single-crystal and polycrystalline substrates: 25 kJ/mole [166], 29 kJ/mole [167], 17 kJ/mole [168] and 53 kJ/mole [108] for Pt(111)/CO, 26 kJ/mole for Ru(001)/CO [169], and 23 kJ/mole for Ru(polycrystalline)/CO [170]. With the exception of the very high value reported by Kwasniewski *et al* [108] measured by LITD laser-induced thermal desorption, activation

energies for CO surface diffusion are in the range of 20 to 30 kJ/mole, and therefore quite similar to the activation energy which we measured for the alloy with a Ru surface composition of ≈7 atomic% Ru.

4.4. Comparison With Fuel Cell Electrodes and Performance Projections

At the closure of this study it seems appropriate to provide a connection between our activity measurements on smooth electrodes and those on high surface area supported Pt-Ru alloy catalysts published in the literature and suggest, by extrapolation, what levels of activity might be possible by further optimization of real catalysts. For "steady-state" activity we will in the following use the current densities measured after 10 minutes (see discussion in Section 3.2.3).

Since most performance data in the literature are quoted in terms of mA/mg_{metal} we will first seek to convert the current densities measured on our smooth electrodes in units of $\mu A/cm^2$ real surface area into $mA/mg_{Pt\text{-}Ru}$. For a polycrystalline Pt or Ru electrode surface the density of surface atoms is in the order of 2.3 nmole/cm^2, which translates into ≈230 $m^2/g_{Pt\text{-}Ru}$ for a 7 atomic% Ru alloy, ≈260 $m^2/g_{Pt\text{-}Ru}$ for a 33 atomic% Ru alloy and ≈290 $m^2/g_{Pt\text{-}Ru}$ for a 46 atomic% Ru alloy, respectively. Noble metal dispersions for state-of-the-art fuel cell electrodes are usually in the order of 80 [64] to 100 m^2/g_{metal} [171] with particle sizes from 3 to 1 nm in diameter, so that activities measured on smooth alloy surfaces should be divided by a factor of 3 in order to allow a fair comparison. Applying the above conversions to our experimental data at 0.4 V and 60°C (including the factor of ≈3, taking account of realistic catalyst dispersions) results in an activity of ≈25, ≈180 and ≈70 $mA/mg_{Pt\text{-}Ru}$ for alloys with a Ru surface composition of ≈7, ≈33 and ≈46 atomic%, respectively.

For example, Watanabe *et al* [64] report a maximum activity of 65 $mA/mg_{Pt\text{-}Ru}$ at 0.4 V and 60°C on codeposited Pt-Ru supported on carbon black (1.5 M H_2SO_4 , 2 M

CH_3OH). Their catalyst with a dispersion of 80 m^2/g_{metal} had an overall composition of 50 atomic% Ru and was well-characterized by TEM (Transmission Electron Microscopy). Cameron *et al* [162] quote a maximum activity for carbon supported Pt-Ru (33 atomic% Ru, bulk) of 35 mA/mg_{Pt-Ru} at 0.4 V and 60°C (3 M H_2SO_4 , 1 M CH_3OH) and 100 mA/mg_{Pt-Ru} for less concentrated sulfuric acid (0.5 M H_2SO_4 , 1 M CH_3OH), whereas Hamnett *et al* [65] give 22 mA/mg_{Pt-Ru} (2.5 M H_2SO_4 , 1 M CH_3OH) at the same potential and temperature for their carbon supported catalyst (50 atomic% Ru, bulk).

The agreement between the activity measured on the smooth electrodes in our study and activities on high surface area electrodes, suggests that there is no fundamental difference between these two types of catalysts, *i.e.* that there is no significant particle-size effect or metal-support interaction. Since both methanol adsorption kinetics and its equilibrium coverage are essentially zero order for ≥ 0.5 M CH_3OH [85, 86], existing differences can be attributed to variations in the sulfuric acid concentration (see above), and to differences between bulk and surface composition of the catalysts depending on their preparation (*e.g.* precursor effects, thermal annealing, see Chapter 1). In particular it should be pointed out that the usual pretreatment of Pt-Ru fuel cell electrodes in electrolyte, namely their extended potential cycling to ≥ 1.2 V effects the preferential dissolution of Ru, thereby creating relatively Pt-rich alloy surfaces with reduced activity at high-temperatures. Nevertheless, the above comparison suggests that an optimization of Pt-Ru fuel cell electrodes might only produce small improvements over fuel cell performances already achieved by Watanabe *et al* [64] and Cameron *et al* [162].

5. CONCLUSIONS

It was shown that the activity of Ru towards the dissociative adsorption of methanol is a strong function of temperature. This produced an increase in the optimum

Ru surface composition with temperature, since the rate-determining step for methanol electrooxidation on Ru-rich Pt-Ru alloy surfaces was found to be its initial dissociative adsorption. The optimum Ru surface composition at 0.4 V and 60°C was ≈33 atomic% (0.5 M CH_3OH, 0.5 M H_2SO_4).

The activation energy at 0.4 V on Pt-Ru alloys with a Ru surface composition of ≈33 atomic% and ≈46 atomic% was 60 kJ/mole, reflecting the activation of the dissociative adsorption of methanol. The alloy with a Ru surface composition of ≈7 atomic% had an activation energy of only 30 kJ/mole, which was hypothesized to be a measure of the rate-limiting elementary step of surface migration of CO_{ads} on Pt-rich surfaces.

A comparison of the electrocatalytic activity of smooth electrodes with high surface area fuel cell catalysts gave no indication of particle-size effects or metal-support interaction effects for Pt-Ru alloy electrodes.

Conclusions

The aim of this study, "die Fragestellung", was to elucidate the fundamental aspects of methanol electrocatalysis on Pt-Ru alloys and to understand how ruthenium would modify the catalytic action of pure platinum. In approaching this problem we resorted to surface analytical tools available in ultra high vacuum in conjunction with traditional electrochemical techniques, a methodology which enabled us to shed some light on an old problem. What is it then, that we have learned and what are its ramifications?

At the onset of this project it was of prime importance to develop a procedure which would allow a definitive determination of the outermost layer composition of Pt-Ru alloy electrodes by means of low energy ion scattering. It showed that an equilibrated, *i.e.* annealed, alloy surface was strongly enriched in Pt consistent with ideal solution thermodynamics, whereas the naturally non-equilibrium process of sputter-cleaning produced electrode surfaces which closely resembled the bulk structure of the alloys. This essentially reinforced the widely hypothesized dependence of the alloy's surface composition on their "activation" treatment, be it high-temperature reduction in hydrogen or heating in air.

After having established a reliable transfer procedure from ultra high vacuum into an electrochemical cell, it was possible to measure electrocatalytic activities towards methanol as a function of a well-defined Ru surface composition. Thus, at room temperature it could be shown that the initial adsorption/dehydrogenation of methanol

was rate-limiting on Pt-Ru alloy electrodes, particularly at low methanol concentrations, leading to an optimum Ru surface composition of ≈10 atomic%; on the contrary, pure Ru electrodes and to a lesser extent Ru-rich surfaces acted as surface "poisons". The bifunctional character of Pt-Ru alloys emerged quite clearly from measurements of their activity towards the main intermediate of the methanol electrooxidation reaction, namely CO. It was shown that the nucleation of oxygen-containing species on bare Ru surface sites significantly enhanced the electrooxidation rate of adsorbed CO analogous to a Langmuir-Hinshelwood surface reaction, effecting a catalytic shift of 0.25 V for the alloy with the optimum Ru surface composition for this reaction (≈50 atomic%). The strongly synergistic effect observed for this surface was attributed to a reduced adsorption strength of oxygen-containing species on Pt-Ru pair sites in comparison to Ru-Ru pair sites. In the case of methanol electrooxidation the initial dissociative adsorption of methanol seemed to proceed *via* Pt surface atom ensembles, and the oxidative removal of methanol dehydrogenation fragments appeared to be catalyzed by oxygen-containing species nucleated on Ru atoms. Based on this hypothesized bifunctional nature of Pt-Ru alloy electrodes, it was proposed that the most active surface ensemble should consist of multiple Pt sites to facilitate the adsorption of methanol, adjacent to a Ru site to promote the nucleation of oxygen-containing species. A statistical model on the probability of creating this most active surface ensemble *versus* the Ru surface composition yielded a good representation of the experimental data, congruent with the proposed mechanistic reaction pathway.

The electrooxidation of formic acid on Pt-Ru alloy electrodes and on pure Ru resembled the oxidation of CO on these electrodes and was catalyzed most actively on a Ru surface of ≈50 atomic%. Since formic acid was shown to adsorb dissociatively on Ru as well as on Pt sites, its adsorption on alloy electrodes was not rate-limiting, in contrast to methanol adsorption, thereby increasing the optimum Ru surface composition as would

be expected. The same trend was then observed for the methanol electrooxidation reaction as the interaction of methanol with Ru was activated by raising the reaction temperature. At 60°C, the Ru content of the most active Pt-Ru surface increased to ≈30 atomic%, with a ten-fold enhancement over the ≈10 atomic% Ru surface. The activation energies for Ru-rich surfaces were interpreted as a measure of the activation of the dissociative methanol adsorption on Ru, whereas the very low activation energy of the Pt-rich surface was correlated to the effect of temperature on CO surface migration.

In sulfuric acid at 60°C and 0.4 V, methanol oxidation current densities on a catalyst weight basis for our model-catalysts were in the order of 500 $\mu A/mg_{metal}$, and are not a viable economic basis for electrochemical energy conversion. These current densities are rather similar to rates reported for supported high-surface area alloy catalysts, if their dispersion was considered properly. Slight variations were most likely due to different electrolyte concentrations and to differences in their surface *versus* bulk composition; the latter, however occurs to a lesser extent for the high dispersions achieved on state-of-the-art fuel cell electrodes due to mass balance restrictions governing the surface segregation thermodynamics. In essence, these comparisons revealed the lack of metal-support interaction effects and the above conclusions based on model-catalysts (atomically smooth) should apply equally well to fuel cell electrodes. It also indicates that a further optimization of fuel cell electrodes in terms of their alloy composition will not produce any significant enhancement of their catalytic activity towards methanol electrooxidation.

At the very end of this study one might *marvel* at the implications of the above conclusions as far as the "design" of an improved electrocatalyst for this reaction is concerned. Platinum, especially in acidic solutions is the most reactive surface towards the adsorption of methanol and the initial adsorption step was demonstrated to be crucial for the overall electrooxidation rate. The modification of Pt with elements which display

a large affinity towards oxygen was shown to positively effect the further oxidative removal of dehydrogenation fragments, while generally reducing the rates of the necessary initial adsorption step. Besides methanol adsorption, a crucial part in its catalysis on alloy electrodes is the adsorption of oxygen-containing species under reducing conditions, *i.e.* at low potentials. This idea is by no means novel, and many alloys of Pt with metals like Sn, Mo, other platinum-metals, *etc.* have been tested, unfortunately without any significant success. One key factor, however, which has never been considered, is the rather important role of the initial adsorption step, which in most cases probably behaves similar to what was observed in this study, namely that it proceeds predominantly *via* ensembles of multiple Pt sites, so that very low concentrations of the alloying component in a Pt alloy may exhibit high catalytic activity whereas high concentrations of the same element may altogether inhibit the reaction. This may be especially true at room temperature, where usually most initial activity screenings are carried out. With not clearly defined compositions of the electrode surface it is quite possible that catalytically active combinations may have been overlooked.

References

[1] Williams, F.L.; Nason, D. *Surf. Sci.* **1974**, *45*, 377.

[2] Murr, L.E.; *Interfacial Phenomena in Metals and Alloys*; Addison-Wesley Publishing Company, Reading (Massachusetts), 1975.

[3] Sachtler, W.M.H.; Van Santen, R.A. *Appl. Surf. Sci.* **1979**, *3*, 121.

[5] King, T.S.; in: *Surface Segregation Phenomena*; Eds. Dowben, P.A.; Miller, A.; CRC Press, Boca Raton (Florida), 1990; pp 27.

[6] J.H. Sinfelt *Bimetallic Catalysts*; Wiley, New York, 1983.

[7] McNicol, B.D.; Short, R.T. *J. Electroanal. Chem.* **1977**, *81*, 249.

[8] Bouwman, R.; Toneman, L.H.; Boersma; Van Santen, R.A. *Surf. Sci.* **1976**, *59*,72.

[9] Powell, C.J.; Seah, M.P. *J. Vac. Sci. Technol.* **1990**, *A 8* ,735.

[10] Smith, D.P. *J. Appl. Phys.* **1967**, *38*, 340.

[11] Brongersma, H.H.; Mul, P.M. *Surf. Sci.* **1973**, *35*, 393.

[12] Suurmeijer, E.P.; Boers, A.L. *Surf. Sci.* **1973**, *43*, 309.

[13] Leger, J.-M.; Lamy, C. *Ber. Bunsenges. Phys. Chem.* **1990**, *94*, 1021.

[14] Hultgren, R.; Desai, P.D.; Hawkins, D.T.; Gleiser, M.; Kelley, K.K.; Wagman, D.D., in: *Selected Values of the Thermodynamic Properties of the Elements*; American Society for Metals, Ohio, 1973.

[15] Smithells, C.J.; Brandes, E. A., *Metals Reference Book*; Butterworths, London, 1976.

[16] *Physical Electronics Product Bulletin P8301*; Perkin-Elmer, Eden Prairie MN, 1983.

[17] Rivière, J.C.; *Surface Analytical Techniques*; Oxford University Press, Oxford, UK, 1990.

[18] Rosenberg, D.; Wehner, G.K. *J. Appl. Phys.* **1962**, *33*, 1842.

[19] Laergreid, N.; Wehner, G.K., *J. Appl. Phys.* **1961**, *32*, 365.

[20] Beuken, J.-M.; Bertrand, P. *Surf. Sci.* **1985**, *162*, 329.

[21] Young, V.Y.; Hoflund G.B.; Miller, A.C. *Surf. Sci.* **1990**, *235*, 60.

[22] Kittel, C.; *Introduction to Solid State Physics*; Wiley, New York, 1986.

[23] Tanuma, S.; Powell, C.J.; Penn, D.R. *Surf. Interface Anal.* **1991**, *17*, 911.

[25] Baun, W.L.; in: *Quantitative Surface Analysis of Materials*; ASTM STP 643; Eds. N.S. McIntyre; American Society for Testing and Materials, Ohio, 1978; pp 150.

[26] Ackermans, P.A.J.; Krutzen, G.C.R.; Brongersma, H.H. *Nucl. Instr. and Meth.* **1990**, *B45*, 384.

[27] Everhart, E.; Stone, G.; Carbone, R.J. *Phys. Rev.* **1955**, *99*, 1287.

[24] *Non-Linear Curve-Fitting Software PeakFit 3.1.*, Jandel Scientific, 1991.

[28] Bingham, F.W.; *Sandia National Laboratory Report*; SC-RR-66-506; National Bureau of Standards, Springfield (Virginia), 1966.

[29] Hoffmann, F.M.; Weisel, M.D.; Peden, C.H.F. *Surf. Sci.* **1991**, *253*, 59.

[30] Oechsner, H. *Appl. Phys.* **1975**, *8*, 185.

[31] Beck, D.B.; DiMaggio, C.L.; Fisher, G.B. *General Motors Research Publication*; GMR-7798, 1992.

[32] Strohl, J.K.; King, T.S. *J. Catal.* **1989**, *118*, 53.

[33] Hutchinson (Jr.), J.M. *Platinum Met. Rev.* **1972**, *16*, 88.

[34] Foiles, S.M.; in: *Surface Segregation Phenomena*; Eds. Dowben, P.A.; Miller, A.; CRC Press, Boca Raton (Florida), 1990; pp 103.

[35] King, T.S.; Donnelly, R.G. *Surf. Sci.* **1985**, *151*, 374.

[36] Seah, M.P.; in: *Practical Surface Analysis*; Eds. Briggs, D.; Seah, M.P.; Wiley, New York, 1983, p. 181.

[37] Seah, M.P.; Dench, W.A. *Surf. Interface Anal.* **1979**, *1*,2.

[38] Jablonski, A.; Tougaard, S. *J. Vac. Sci. Technol.* **1990**, *A8*, 106.

[39] Davis, L.E.; McDonald, N.C.; Palmberg, P.W.; Riach, G.E.; Weber, R.E.; *Handbook of Auger Electron Spectroscop*; Physical Electronics Industries, Eden Prairie (Minnesota), 1976.

[40] Hilaire, L.; Guerrero, G.D.; Légaré, P.; Maire, G.; Krill, G. *Surf. Sci.* **1984**, *146*, 569.

[41] Ticanelli, E.; Berry, J.G.; Paffett, M.T.; Gottesfeld, S. *J. Electroanal. Chem.* **1989**, *258*, 61.

[42] Tsong, T.T.; Ren, D.M.; Ahmad, M. *Phys. Rev.* **1988**, *B38*, 7428.

[43] Ng, Y.S.; Tsong, T.T. *Surf. Sci.* **1978**, *78*, 419.

[44] Miura, H.; Suzuki, T.; Ushikubo, Y.; Sugiyama, K.; Matsuda, T.; Gonzales, R. D. *J. Catal.* **1984**, *85*, 331.

[45] Alerasool, S.; Boecker, D.; Rejai, B.; Gonzales, R.D.; *Langmuir* **1988**, *4*, 1083.

[46] Alerasool, S.; Gonzales, R.D. *J. Catal.* **1990**, *124*, 204.

[47] Butler, J.A.V. *Proc. R. Soc. London* **1932**, *135*, 348.

[48] Schuchowitzky, A.; *Acta Physicochim. URSS* **1944**, *19*, 176.

[49] Guggenheim, E.A. *Trans. Faraday Soc.* **1945**, *41*, 150.

[50] Defay, R.; Prigogine, I. *Trans. Faraday Soc.* **1950**, *46*, 199.

[51] Swalin, R.A.; *Thermodynamics of Solids*; Wiley, New York, 1962.

[52] Van Santen, R.A.; Sachtler, W.M.H. *J. Catal.* **1974**, *33*, 202.

[53] Wynblatt, P.; Ku, R.C. *Surf. Sci.* **1977**, *65*, 511.

[54] Miedema, A.R. *Z. Metallkde.* **1978**, *69*, 455.

[55] Overbury, F.H.; Bertrand, P.A.; Somorjai, G.A. *Chem. Rev.* **1975**, *75*, 547.

[56] Tyson, W.R.; Miller, W.A. *Surf. Sci.* **1977**, *62*, 267.

[57] Mezey, L.Z.; Giber, J. *Surf. Sci.* **1982**, *117*, 220.

[58] Kelley, M. *J. Catal.* **1979**, *57*, 113.

[59] Tyson, W.R. *Can. Met. Quart.* **1975**, *14*, 307.

[60] Miedema, A.R. *Philips Tech. Rev.* **1976**, *36*, 217.

[61] Parsons, R.; VanderNoot, T. *J. Electroanal. Chem.* **1988**, *257*, 9.

[62] Leger, J.-M.; Lamy, C. *Ber. Bunsenges. Phys. Chem.* **1990**, *94*, 1021.

[63] Goodenough, J.B.; Hamnett, A.; Kennedy, B.J.; Manoharan, R.; Weeks, S.A. *J. Electroanal. Chem.* **1988**, *240*, 133.

[64] Watanabe, M.; Uchida M.; Motoo, S. *J. Electroanal. Chem.* **1987**, *229*, 395.

[65] Hamnett, A.; Weeks, S.A.; Kennedy, B.J.; Troughton, G.; Christensen, P.A. *Ber. Bunsenges. Phys. Chem.* **1990**, *94*, 1014.

[66] Binder, H.; Köhling, A.; Sandstede, G. In *From Electrocatalysis to Fuel Cells*; Sandstede, G., Ed.; University of Washington Press: Seattle, 1972; pp 43-58.

[67] Iwasita, T.; Nart, F.C.; Vielstich, W. *Ber. Bunsenges. Phys. Chem.* **1990**, *94*, 1034.

[68] Éntina, V.S.; Petrii, O.A. *Élektrokhimiya* **1968**, *4*, 678.

[69] Watanabe, W.; Motoo, S. *J. Electroanal. Chem.* **1975**, *60*, 267.

[70] Beden, B.; Kadirgan, F.; Lamy, C.; Leger, J.M. *J. Electroanal. Chem.* **1981**, *127*, 75.

[71] McNicol, B.D.; Short, R.T. *J. Electroanal. Chem.* **1977**, *81*, 249.

[72] Landsman, D.A.; Luczak, F.J *Investigation of the In-Situ Oxidation of Methanol in Fuel Cells*, U.S. Army Mobility Equipment Research and Development Command Report #FCR-3463; United Technologies Power Systems: South Windsor (Connecticut), 1981.

[73] Miura, H.; Suzuki, T.; Ushikubo, Y.; Sugiyama, K.; Matsuda, T.; Gonzales, R.D. *J. Catal.* **1984**, *85*, 331.

[74] Alerasool, S; Gonzales, R.D. *J. Catal.* **1990**, *124*, 204.

[75] Hadzi-Jordanov, S.; Angerstein-Kozlowska, H.; Vuković, M.; Conway, B.E. *J. Phys. Chem.* **1977**, *81*, 2271.

[76] Hadzi-Jordanov, S.; Angerstein-Kozlowska, H.; Vuković, M.; Conway *J. Electrochem. Soc.* **1978**, *125*, 1471.

[77] Kötz, R.; Stucki, S. *J. Electroanal. Chem.* **1984**, *172*, 211.

[78] Vuković, M. *J. Chem. Soc. Faraday Trans.* **1990**, *86*, 3743.

[79] Kinoshita, K.; Ross, P.N. *J. Electroanal. Chem.* **1977**, *78*, 313.

[80] Marković, N.;Hanson, M.; McDougall, G.; Yeager, E. *J. Electroanal. Chem.* **1986**, *214*, 555.

[81] Conway, B.E.; Angerstein-Kozlowska, H.; Sharp, W.B.A. *J. Chem. Soc. Faraday Trans.I* **1978**, *74*, 1373.

[82] Bagotzky, V.S.; Vassilyev, Y.B. *Electrochim. Acta* **1967**, *12*, 1323.

[83] Vuković, M.; Angerstein-Kozlowska, H.; Conway, B.E. *J. Appl. Electrochem.* **1982**, *12*, 193.

[84] Ticanelli, E.; Beery, J.G.; Paffett, M.T.; Gottesfeld, S. *J. Electroanal. Chem.* **1989**, *258*, 61.

[85] Bagotzky, V.S.; Vassilyev, Y.B. *Electrochim. Acta* **1966**, *11*, 1439.

[86] Kazarinov, V.E.; Tysyachnaya, G.Y.; Andreev, V.N. *J. Electroanal. Chem.* **1975**, *65*, 391.

[87] Horányi, G.; Wieckowski, A. In *Proceedings of the Workshop on Direct Methanol-Air Fuel Cells*; Landgrebe, A.R.; Sen, R.K.; Wheeler, D.J., Eds.; The Electrochemical Society: Pennington (N.J.), 1992, volume 92-14; pp 70-97.

[88] Kunimatsu, K. *Ber. Bunsenges. Phys. Chem.* **1990**, *94*, 1022.

[89] Franaszczuk, K.; Sobkowski, J. *J. Electroanal. Chem.* **1992**, *327*, 235.

[90] Goodenough, J.; Manoharan, R. *Chemistry of Materials* **1989**, *1*, 391.

[91] Krausa, M.; Iwasita, T.; Vielstich, W. *Dechema* **1993**, *128*, 161.

[92] Wilhelm, S.; Iwasita, T.; Vielstich, W. *J. Electroanal. Chem.* **1987**, *238*, 383.

[93] Éntina, V.S.; Petrii, O.A. *Élektrokhimiya* **1967**, *3*, 1237.

[94] Beden, B.; Hahn, F.; Juanto, S.; Lamy, C.; Léger, J.-M. *J. Electroanal. Chem.* **1987**, *225*, 215.

[95] Chang, S.-C.; Ho, Y.; Weaver, M. *Surf. Sci.* **1992**, *265*, 81.

[96] Kunimatsu, K.; Kita, H. *J. Electroanal. Chem.* **1987**, *218*, 155.

[97] Willsau, J.; Heitbaum, J. *Electrochim. Acta* **1986**, *31*, 943.

[98] Iwasita, T.; Vielstich, W.; Santos, E. *J. Electroanal. Chem.* **1987**, *229*, 367.

[99] Lopes, M.I.; Fonseca, I.; Olivi, P.; Beden, B.; Hahn, F.; Léger. J.M.; Lamy, C. *J. Electroanal. Chem.* **1993**, *346*, 415.

[100] Sexton, B.A. *Surf. Sci.* **1981**, *102*, 271.

[101] Attard, G.A.; Chibane, K.; Ebert, H.D.; Parsons, R.*Surf. Sci.* **1989**, *224*, 311.

[102] Franaszczuk, K.; Herrero, E.; Zelenay, P.; Wieckowski, A.; Wang, J.; Masel, R.I. *J. Phys. Chem.* **1992**, *96*, 8509.

[103] Hrbek, J.; De Paola, R.; Hoffmann, F.M. *Surf. Sci.* **1986**, *166*, 361.

[104] Deckert, A.A.; Brand, J.L.; Mak, C.H.; Koehler, B.G.; George, S.M. *J. Phys. Chem.* **1987**, *87*, 1936.

[105] Ertl, G.; Neumann, M.; Streit, K.M. *Surf. Sci.* **1977**, *64*, 393.

[106] Marković, N.; Ross, P.N. *J. Electroanal. Chem.* **1992**, *330*, 499.

[107] Hoffmann, F.M.; Weisel, M.D.; Peden, C.H.F. *Surf. Sci.* **1991**, *253*, 59.

[108] Kwasniewski, V.J.; Schmidt, L.D. *Surf. Sci.* **1992**, *274*, 329.

[109] Lamy, C.; Léger, J.-M. *J. Chim. Phys.* **1991**, *88*, 1649.

[110] Niedrach, L.W.; McKee, D.W.; Paynter, J.; Danzig, I.F. *Electrochem. Technol.* **1967**, *5*, 318.

[111] McKee, D.W.; Scarpellino, A.J. *Electrochem. Technol.* **1968**, *6*, 101.

[112] Ross, P.N.; Kinoshita, K.; Scarpellino, A.J.; Stonehart, P. *J. Electroanal. Chem.* **1975**, *63*, 97.

[113] Castro Luna, A.M.; Giordano, M.C.; Arvia, A.J. *J. Electroanal. Chem.* **1989**, *259*, 173.

[114] Kazarinov, V.E.; Andreev, V.N.; Shlepakov, A.V. *Electrochim. Acta* **1989**, *34*, 905.

[115] Kunimatsu, K.; Shimazu, K.; Kita, H. *J. Electroanal. Chem.* **1988**, *256*, 371.

[116] Zurawski, D.; Wasberg, M.; Wieckowski, A. *J. Phys. Chem.* **1990**, *94*, 2076.

[117] Love, B.; Lipkowski, J. in *Electrochemical Surface Science. Molecular Phenomena at Electrode Surfaces*; Soriaga, M.P., Ed.; ACS Symposium Series: Washington DC, 1988, volume 378, pp 484-496.

[118] De Becdelièvre; de Becdelièvre, J.; Clavilier, J. *J. Electroanal. Chem.* **1990**, *294*, 97.

[119] Palaikis, L.; Zurawski, D.; Hourani, M.; Wieckowski, A. *Surf. Sci.* **1988**, *199*, 183.

[120] Beden, B.; Lamy, C.; Tacconi, N.R.; Arvia, A.J. *Electrochim. Acta* **1990**, *35*, 691.

[121] Kunimatsu, K. *J. Electroanal. Chem.* **1986**, *213*, 149.

[122] Leung, L-W.; Weaver, M.J. *Langmuir* **1990**, *6*, 323.

[123] Kunimatsu, K.; Seki, H.; Golden, W.G.; Gordon, J.G.; Philpott, M.R. *Langmuir*, **1986**, *2*, 464.

[124] Gutiérrez, C.; Caram, J.A.; Beden, B. *J. Electroanal. Chem.* **1991**, *305*, 289.

[125] Leung, L.-W.H.; Weaver, M.J. *Langmuir* **1988**, *4*, 1076.

[126] Feliu, J.M.; Orts, J.M.; Fernandez-Vega, A.; Aldaz, A. *J. Electroanal. Chem.* **1990**, *296*, 191.

[127] Weaver, M.J.; Chang, S.-C.; Leung, L.-W.H.; Jiang, X.; Rubel, M.; Szklarczyk, M.; Zurawski, D.; Wieckowski, A. *J. Electroanal. Chem.* **1992**, *327*, 247.

[128] Corrigan, D.S.; Weaver, M.J. *J. Electroanal. Chem.* **1988**, *241*, 143.

[129] Jiang, X.; Villegas, I.; Weaver, M.; Marković, N.; Ross, P.N. (Jr.) to be published.

[130] Santos, E.; Leiva, E.P.M.; Vielstich, W.; Linke, U. *J. Electroanal. Chem.* **1987**, *227*, 199.

[131] Vurens, G.H.; Van Delft, F.C.M.J.M.; Nieuwenhuys, B.E. *Surf. Sci.* **1987**, *192*, 438.

[132] Chang, S.-C.; Weaver, M.J. *Surf. Sci.* **1990**, *238*, 142.

[133] Hayden, B.E.; Bradshaw, A.M. *Surf. Sci.* **1984**, *125*, 787.

[134] Pfnür, H.; Menzel, D. *Surf. Sci.* **1980**, *93*, 431.

[135] Engel, T.; Ertl, G. *Adv. Catal.* **1979**, *28*, 1.

[136] Lee. H.-I.; Praline, G.; White, J.M. *Surf. Sci.* **1980**, *91*, 581.

[137] Gland, J.L.; Kollin, E.B. *Surf. Sci.* **1985**, *151*, 260.

[138] Kostov, K.L.; Rauscher, H.; Menzel, D. *Surf. Sci.* **1992**, *278*, 62.

[139] Campbell, C.T.; Ertl, G.; Kuipers, H.; Segner, J. *J. Chem. Phys.* **1980**, *73*, 5862.

[140] Derry, G.N.; Ross, P.N. *J. Chem. Phys.* **1985**, *82*, 2772.

[141] Madey, T.E.; Engelhardt, A.H.; Menzel, D. *Surf. Sci.* **1975**, *48*, 304.

[142] Mortensen, K.; Klink, C.; Jensen, F.; Besenbacher, F.; Stensgaard, I. *Surf. Sci.* **1989**, *220*, L701.

[143] Pfnür, H.; Held, G.; Lindroos, M.; Menzel, D. *Surf. Sci.* **1989**, *220*, 43.

[144] Fisher, G.B.; Sexton, B.A. *Phys. Rev. Lett.* **1980**, *44*, 683.

[145] Iwasita, T.; Vielstich, W. *J. Electroanal. Chem.* **1986**, *201*, 403.

[146] Ota, K.-I.; Nakagawa, Y.; Takahashi, M. *J. Electroanal. Chem.* **1984**, *179*, 179.

[147] Belgsir, E.M.; Huser, H.; Leger, J.-M.; Lamy, C. *J. Electroanal. Chem.* **1987**, *225*, 281.

[148] Capon, A.; Parsons, R. *J. Electroanal. Chem.* **1973**, *44*, 239.

[149] Capon, A.; Parsons, R. *J. Electroanal. Chem.* **1973**, *45*, 205.

[150] Wieckowski, A.; Sobkowski, J *Roczinki Chemii* **1974**, *48*, 1351.

[151] Kunimatsu, K.; Kita, H. *J. Electroanal. Chem.* **1987**, *218*, 155.

[152] Kazarinov, V.E.; Tysyachnaya, G.Y.; Andreev, V.N. *J. Electroanal. Chem.* **1975**, *65*, 391.

[153] Wolter, O.; Willsau, J.; Heitbaum, J. *J. Electrochem. Soc.* **1985**, *132*, 1635.

[154] Jensen, M.B.; Myler, U.; Thiel, P.A. *Surf. Sci.* **1993**, *290*, L655.

[155] Lamy, C.; Leger, J.M.; Clavilier, J.; Parsons, R. *J. Electroanal. Chem.* **1983**, *150*, 71.

[156] Columbia, M.R.; Thiel, P.A. *Surf. Sci.* **1990**, *235*, 53.

[157] Sun, Y.-K.; Weinberg, W.H. *J. Chem. Phys.* **1991**, *94*, 4587.

[158] Marković, N.; Ross, P.N. Jr. *J. Phys. Chem.* in press.

[159] Aramata, A.; Kodera, T.; Masuda, M. *J. Appl. Electrochem.* **1988**, *18*, 577.

[160] Méli, G.; Léger, J.-M.; Lamy, C.; Durand, R. *J. Appl. Electrochem.* **1993**, *23*, 197.

[161] Hamnett, A.; Kennedy, B.J. *Electrochim. Acta* **1988**, *33*, 1613.

[162] Cameron, D.S.; Hards, G.A.; Thompsett, D. *Proceedings of the Workshop on Direct Methanol-Air Fuel Cells*, edited by A.R. Landgrebe, R.K. Sen and D.J. Wheeler, The Electrochemical Society: Pennington, N.J. (1992), volume 92-14; pp 10-23.

[163] Watanabe, M.; Uchida, M.; Motoo, S. *J. Electroanal. Chem.* **1985**, *199*, 311.

[164] Raicheva, S.N.; Christov, M.V.; Sokolova, E.I. *Electrochim. Acta* **1981**, *26*, 1669.

[165] McNicol, B.D. *J. Electroanal. Chem.* **1981**, *118*, 71.

[166] Croci, M.; Félix, C.; Vandoni, G.; Harbich, W.; Monot, R. *Surf. Sci. Lett.* **1993**, *290*, L667.

[167] Poelsema, B.; Verheij, L.K.; Coms, G. *Phys. Rev. Lett.* **1982**, *49*, 1731.

[168] Reutt-Robey, J.E.; Doren, D.J.; Chabal, Y.J.; Christman, S.B. *J. Chem. Phys.* **1990**, *93*, 9113.

[169] Deckert, A.A.; Brand, J.L.; Arena, M.V.; George, S.M. *Surf. Sci.* **1989**, *208*, 441.

[170] Duncan, T.M.; Thayer, A.M.; Root, T.W. *J. Chem. Phys.* **1990**, *92*, 2663.

[171] Wilson, M.S.; Garzon, F.H.; Sickafus, K.E.; Gottesfeld, S. *J. Electrochem. Soc.* **1993**, *140*, 2872.

LAWRENCE BERKELEY LABORATORY
UNIVERSITY OF CALIFORNIA
TECHNICAL INFORMATION DEPARTMENT
BERKELEY, CALIFORNIA 94720